Partitioning of cytochrome c in multicomponent lipid membranes

vorgelegt von
Salome Pataraia, M.Sc
Georgia, Tbilisi

Von der Fakultät II - Mathematik und Naturwissenschaften
der Technischen Universität Berlin
zur
Erlangung des akademischen Grades

Doktor der Naturwissenschaften
(Dr. rer. nat.)

genehmigte Dissertation

Vorsitzender: Prof. Dr. Reinhard Schomäcker
1. Berichter: Dr.habil. Rumiana Dimova
2. Berichter: Prof. Dr. Peter Hildebrandt

Tag der wissenschaftlichen Aussprache: 05.10.2012

Berlin 2012
D 83

Acknowledgment

It is my pleasure to thank those who made this thesis possible.

I am especially grateful to my advisor Dr.habil. Rumiana Dimova, group leader of the “Biophysical Lab”-group at Max Planck Institute of Colloids and Interfaces and guide for my work. This thesis would not have been possible without her constant and continues helpfulness for discussions, support and patience to me. I would like to thank her for advices not only for my work, but also concerning, in general, life. Thank you.

I am very thankful to my advisor Prof. Dr. Peter Hildebrandt, professor and group leader at Technical University Berlin. I thank him for helpful advices during my work and supporting me financially. Thank you.

I would like to thank IGRTG program and DFG-german research foundation for granting and giving me opportunity to perform this work and grow professionally. I would like to thank especially Prof. Dr. Martin Schoen, chairman of IGRTG program, Dr. Daniela Fliegner, managing director and Petra Erdmann, administrative assistant, for their financial, moral and administrative support. Thank you.

I also would like to thank Prof. Reinhard Lipowsky for useful discussions and for providing pleasant work environment. I am very grateful to my group members at Max Planck Institute of Colloids and Interfaces especially Dr. Roland Knorr and Dr. Pavel Shchelokovskyy for their helpful discussions and support. Thanks to Dr. Yonggang Liu who developed the program I used for my data analyzes and for provided help concerning the subject. Thanks to Carmen Remde for introducing me all the lab issues. Thank you.

Furthermore, I would like to thank the people of the MPI-KG theory department for the pleasant working atmosphere.

Lastly, I would like to thank my family for encouraging me to improve myself and for support, without them I would not be able to accomplish this work.

Thank you!

Zusammenfassung

Die Wechselwirkung von dem wasserlöslichen Proteinen Cytochrome c (Cyt c) mit Lipidmembranen spielt in einer Reihe von biologischen Prozessen eine wichtige Rolle. Cyt c ist ein positiv geladenes Hämprotein, das sich in der inneren Membran der Mitochondrien befindet. Funktionell ist dieses Protein für die Synthese von Adinosintriphosphat (ATP) mitverantwortlich, das beim Elektronentransport der Atmungkette entsteht. Desweiteren ist Cyt c ein pro-apoptotisches Protein. Cyt c kann eine Reihe von Cystein-Proteasen aktivieren, die schließlich zum Absterben von Zellen führen können. Auf diese Weise ist Aktivität von Cyt c und seine Wechselwirkungen mit Membranen auf verschiedenen Ebenen im Leben von Zellen beteiligt. Vorherige Untersuchungen *in vitro* haben gezeigt, dass in Puffern mit niedrigen Ionenstärken Cyt c in Membranen eingebaut wird, hingegen führen höhere Ionenstärken lediglich zu einer Bindung an die Membran. Außerdem ist bekannt, dass niedrige Lipid-Protein-Verhältnisse für das Einbauen von Cyt c in geladene Lipidmembranen erforderlich sind. Wir untersuchten die Bindung dieses Proteins an multikomponente Membranen. Wir bestimmten den Einfluss von Cyt c auf das Phasenverhalten von Membranen und untersuchten dabei die Rolle von Oberflächenladung und Zusammensetzung der Membranlipide. Als Modellsystem wurden unilamellare Riesenvesikel (GUVs) genutzt. Um die Zusammensetzung der mitochondrialen Membran nachzuahmen, setzten wir Mischungen aus geladenem dioleoylphosphatidylglycerol (DOPG), Sphingomyelin (SM) und Cholesterol ein. Im ersten Schritt charakterisierten wir das Phasenverhalten dieser Mischungen mit dem confokalen Mikroskop und fluoreszent markierten GUVs. Nachfolgend studierten wir die Änderung des Phasenverhaltens der ternären Lipidmischungen durch Zusatz von 0.6 mM Cyt c. Die Konzentrationen des Proteins und des negativ geladenen Lipids DOPG entsprachen denen des biologischen Systems. Im Anschluss konzentrierten wir uns auf die Region im Phasendiagramm die für Lipid-Rafts relevant sind und in der zwei flüssige Membranphasen coexistieren: Flüssig-geordnete (Lo) „Raft-Domänen“ und flüssig-ungeordnete (Ld) „Non-Raft-Domänen“. Wir untersuchten die Verteilung von Cyt c in Vesikeln mit beiden Flüssigphasen. Die Analysen von Fluoreszenz-Intensitätsprofilen der Protein-Verteilung in den beiden Phasen ergaben unterschiedliche Verteilungen von Cyt c in beiden Domänen. Unsere Ergebnisse zeigen, dass Cyt c die DOPG-reichen Ld-Domänen bevorzugt, allerdings ist auch ein geringer Anteils von Cyt c in den Lo-Domänen zu finden. Die spezifische Affinität des Proteins zu den beiden flüssigen Phasen und die thermodynamische Charakterisierung dieser Wechselwirkungen wurden mittels isothermischer Titrations-Kalorimetrie gemessen. Wir fanden eine bevorzugte Bindung von Cyt c zu ternären Lipidmembranen sowohl in der Lo-, als auch in der Ld- Phase. Parallel dazu wurde der Einfluss von Cyt c auf die Oberflächenladung und die Größe von Vesikeln mit Messungen der elektrophoretischen Mobilität bzw. mittels dynamischer Lichtstreuung kontrolliert.

Abstract

The interaction of water soluble proteins like cytochrome c (cyt c) with lipid membranes plays an important role in a number of biological processes. Cyt c is a positively charged heme protein located at the inner membrane of mitochondria. The main function of this protein is related to electron transport trough the respiratory chain during adenosine triphosphate (ATP) synthesis. cyt c is also one of the pro-apoptotic proteins, which activates the chain of cysteine proteases upon apoptotic stimuli, causing cell death. Thus, the activity of cyt c and the related interactions with membranes are involved at many levels of cell life.

Previous studies have shown that at low ionic strength, cyt c inserts into the membrane, while at high ionic strength only a binding process takes place. It has been also demonstrated that insertion of cyt c into charged lipid membranes is stipulated for low lipid-protein ratios.

Here we characterized the binding of this protein to multicomponent lipid membranes and resolved the influence of cyt c on the phase state of membranes as well as role of the bilayer surface charge and lipid composition. As a model system, giant unilamellar vesicles (GUVs) were used. To mimic the membrane composition of the inner mitochondrial membrane we employed lipid mixtures of the charged dioleoylphosphatidylglycerol (DOPG), sphingomyelin (SM) and cholesterol. As a first step, we characterized the phase behavior of this mixture from confocal microscopy observations on fluorescently labeled GUVs.

Afterwards, we have investigated the alteration of phase behavior of the lipid ternary mixture induced by 0.6 mM Yeast cyt c. The protein concentration as well as the negatively charged lipid component, DOPG were chosen to mimic biologically relevant systems. After characterizing the membrane phase diagram in the presence of cyt c, we focused on the two fluid phase coexistence region, biologically relevant to rafts, and its surrounding environment. We studied the partitioning of cyt c in vesicles which belong to the two fluid phases: liquid ordered (Lo) raft and liquid disordered (Ld), non-raft phases. Analyzes of intensity profiles from fluorescence from the protein partitioning in the two phases yielded partitioning ratios of cyt c in the different domains. Our results indicate that cyt c prefers the DOPG-rich Ld domains, however there is a weak partitioning of cyt c into the Lo domains indicating compositional complexity of the membrane. The specific affinity of the protein to each of the fluid phases and the thermodynamic characterization of these interactions were quantified with isothermal titration calorimetry. We resolved the preferential binding of cyt c to the ternary lipid membranes close either to the Lo or the Ld phases. In parallel, the influence of cyt c on the membrane surface charge and vesicle size was monitored with dynamic light scattering and electrophoretic mobility measurements.

Contents

1. Introduction

1.1. Role of cytochrome c in cellular processes

Interactions between water-soluble proteins and membranes play an important role in many biological processes, such as signal transduction [1] and transport processes. A good example for such a protein is the peripheral membrane protein cyt c, which is a spherical water soluble heme protein with a diameter of about 3.4 nm, carrying approximately 4 effective positive charges. With its well characterized structure and many important biological functions, cyt c is a suitable model protein for studying the association and interaction of peripheral proteins with lipid membranes. Cyt c is a mitochondrial inner membrane protein located at cristae-the internal compartments formed by the inner membrane of mitochondria. Cyt c has developed in early stages of evolution and it is found in all aerobic cells starting from east to multicellular organisms [2]. The structure of cyt c is shown below in Figure 1.1.1.

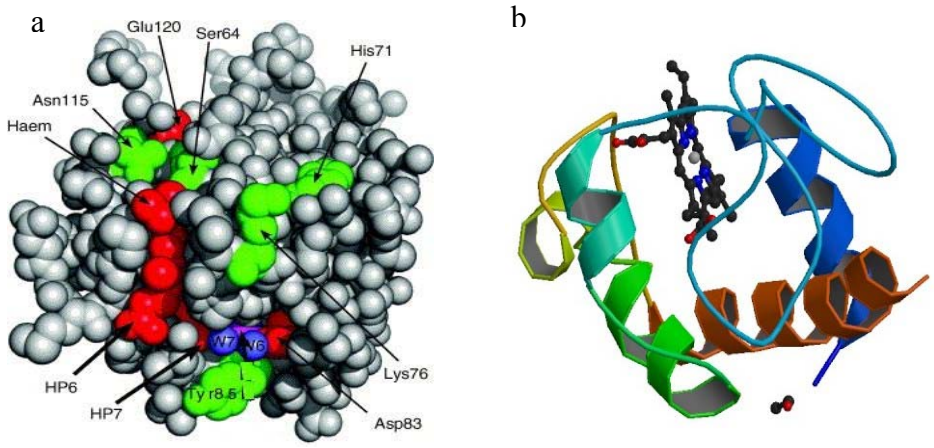

Figure 1.1.1 Surface view of cyt c (a) [3], in red is denoted the heme molecule, in blue water molecules and in green different amino acids. The 3D structure of cyt c with a heme molecule with iron atom in the center is presented in (b) [4].

The primary structure of cyt c consists of a single polypeptide chain containing 104 amino acid residues covalently attached to a heme group [5]. The view in Figure 1.1.1 (a, b) shows the protein backbone with α helices and β sheets with the single iron atom of the heme group in the center of the molecule. The heme group is surrounded by many tightly packed hydrophobic side chains and it is covalently linked to the protein by thioether links between the vinyl groups of the heme and

the sulphur atoms of two cysteine side-chains of the protein. The iron atom of the heme group is in the ferrous (Fe^{2+}) state when it is in the reduced form and in the Ferric (Fe^{3+}) state in its oxidised form [6]. The heme group is not readily accessible to the cytosol, most of it is well shielded by the side chains of hydrophobic amino acids. Only one edge of the planar heme ring is accessible to the surface, histidine (His_{18}) the iron ligand in the heme pocket of cyt c.

The primary function of cyt c is to transport electrons through the respiratory chain during the mitochondrial energy metabolism. It passes electrons between two transmembrane complexes in the inner membrane of mitochondria [7] in a manner that the positively charged cyt c stays in continuous contact with anionic lipids (see chapter 1.1.1). The second function of cyt c is related to the activation of a cysteine protease in response to pro-apoptotic stimuli, which are then responsible for cell death in the process of development, DNA damage or in response to infection [8] (see chapter 1.1.2).

The interaction of cyt c with zwitterionic and anionic lipids depends on a number of different factors. Several studies indicate that the peripheral or integral binding of cyt c to charged lipid membranes depends on the lipid-to-protein (L/P) ratio. It has been shown that at low L/P ratios (less than approximately 8), cyt c binds electrostatically to pure dioleoylphosphatidylglycerol (DOPG) vesicles, whereas at high L/P ratios (above approximately 18), partial penetration of cyt c into the lipid bilayer takes place [9]. Furthermore, the absorption of cyt c to negatively charged lipid membranes is highly dependent on the ionic strength of the solutions. On the one hand, at low ionic strength and high cyt c concentrations, the protein inserts into DOPG lipid bilayers [10, 11]. On the other hand, binding of cyt c to membranes containing a fraction of the charged lipid cardiolipin, was shown to decrease in solutions of low ionic strength, but also a collapse of cardiolipin-rich domains was observed [12]. Yet, another effect of cyt c on single-component membranes composed of anionic lipids relates to changes in the phase behavior of the lipids. Upon binding, cyt c lowers the phase transition temperature and broadens the transition of charged phosphatidylglycerol lipids [13]. Lateral lipid redistribution of two-component membranes made of anionic and neutral lipids has also been observed, see e.g. [14-16] and references therein. Large micrometer-sized domains in phosphatidylcholine vesicles containing a small fraction of phosphatidic acid were detected [14]. However, the effect of cyt c on the phase alteration of more complex ternary mixture lipid membranes undergoing phase separation has not been studied. In this thesis, we focus our efforts on studying the behavior of ternary lipid mixtures in the presence of cyt c.

1.1.1. ATP syntheses in mitochondria

Mitochondria are oval-shaped organelles found in eukaryotic cells, located outside the nucleus and known as a powerhouse of energy for the cells. It has an inner and outer phospholipid bilayer membrane with inter-membrane space in between where the inner membrane of mitochondria is folded forming internal ridges called cristae. The area bounded by the inner membrane is known as the mitochondrial matrix, where most of the reactions of the citric acid cycle and fatty acid oxidation occur. The outer membrane of mitochondria contains integral proteins, pores allowing molecules with 5000 Daltons or less in molecular weight to freely diffuse from one side of the membrane to the other [17]. Unlike the outer membrane the inner membrane of mitochondria does not contain pores and it is highly impermeable to all molecules. It is characterized by a high protein-to-phospholipid ratio (more than 3:1 by weight) and contains 1/5 of all mitochondrial proteins. The inter-membrane space and the matrix is the area where cyt c located generating most of the cell supply of adenosine triphosphate (ATP) [18]. The main biological function of cyt c is to transfer electrons between cyt c reductase and oxidase during the oxidative phosphorylation chain process in the inner mitochondrial membrane [19-22]. The inner membrane of mitochondria is folded in a way to increase the area of the surface and therefore enhancing its ability to produce ATP more efficiently.

During the oxidative phosphorylation chain the electrons are transferred across the membrane with the help of enzyme complexes within the inner membrane of the mitochondria. Complex I, called nicotinamide adenine dinucleotide (NADH) dehydrogenase removes two electrons from NADH and transfers them to a lipid-soluble carrier, ubiquinone (Q). As a result, Complex I translocates four protons (H^+) across the membrane creating proton gradient. In Complex II (succinate dehydrogenase) more electrons are delivered to quinone Q. In Complex III (cyt bc_1 complex) two electrons are transferred to two molecules of cyt c. Afterwards, in Complex IV (cyt c oxidase) four electrons are removed from four molecules of cyt c and transferred to molecular oxygen (O_2). As a result two molecules of water are produced and four protons are translocated across the membrane further increasing the proton gradient. In the electron transport chain Complex I, III and IV are proton pumps, while cyt c and Q are electron carriers.

Figure 1.1.2 shows the citric acid cycle and the electron transport chain driving proton gradient across the inner membrane of mitochondria and releasing the energy resulting for proton flow through the ATP synthesize enzyme for synthesizing ATP molecules.

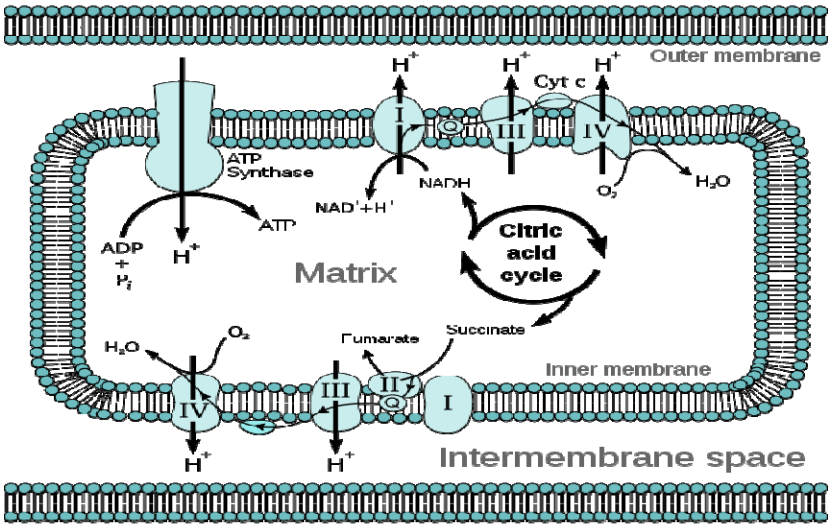

Figure 1.1.2 Citric acid cycle in the matrix of mitochondria of eukaryotic cells. Electron transport chain and proton flow through the ATP synthase releasing energy to synthesize ATP from ADP and Pi [23].

Cyt c as an electron transferring protein contains a heme group which readily accepts and releases an electron by undergoing oxidation and reduction process. As a result, a pH gradient is created across the inner membrane of mitochondria. This gradient is called proton-motive force and is responsible for protons to flow down their concentration gradient. Since the inner membrane of mitochondria is not permeable for ions, protons flow through the enzyme called ATP synthase. During the proton flow through the channel, energy is released which in turn is necessary for phosphorylation of ADP to ATP. ATP synthase is described as Complex V of the electron transport chain. ATP synthase is an enzyme that uses energy released during the proton flow across the membrane to promote synthesis of ATP from ADP and phosphate (P_i) [24, 25].

$$ADP + Pi + 4H^{+}_{intermembrane} \leftrightarrow ATP + H2O + 4H^{+}_{matrix}$$

1.1.2. Cellular apoptosis

Cellular apoptosis is a programmed cell death that occurs in the multicellular organisms and is essential for the organism's life cycle (Figure 1.1.3). In contrast to necrosis, which is the premature death of cells in living tissue almost always detrimental and fatal, apoptosis produces cell fragments called apoptotic bodies that are quickly removed by the phagocytic cells before the contents of the cell can spill out onto surrounding cells and cause damage [26]. Between 50 and 70 billion cells die in the average human adult each day due to apoptosis [27]. Defective apoptotic processes can cause various diseases such as atrophy and cancer.

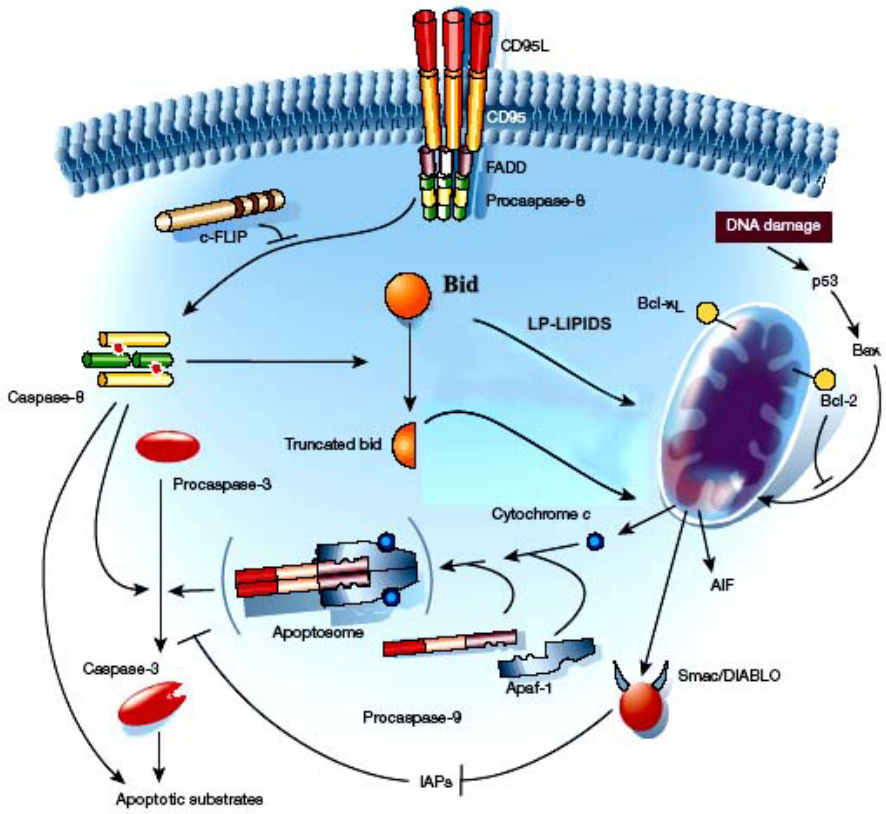

Figure 1.1.3 Mechanism of cell mediated apoptosis. Upon apoptotic stimuli, mitochondria releases proapoptotic molecules such as cyt c. Released cyt c in cytosol in the presence of ATP generates the complex called apoptosome, which is necessary for activation of caspase-9. In its turn caspase-9 initiates activation of caspase cascade driving the cell ultimately to the acquisition of the apoptotic morphology of the cell death [28].

The process of apoptosis is controlled by a diverse range of cell signals. It may originate either extracellularly by extrinsic inducers such as toxins, hormones, growth factors, nitric oxide or cytokines or intracellularly by irntinsic inducers [29, 30]. A cell initiates intracellular apoptotic signaling in response to stress, which may bring about cell suicide. Irntinsic signal inducers include the binding of nuclear receptors by glucocorticoids, heat, radiation, nutrient deprivation, viral infection, hypoxia and increased intracellular calcium concentration [31, 32]. Before the actual process of cell death targeting mitochondria the cell is precipitated by enzymes and apoptotic signals cause regulatory proteins to initiate the apoptosis pathway. This step allows apoptotic signals to cause cell death, or the process to be stopped by inhibiting or activating apoptotic processes.

Except being evolved in the electron transport, cyt c functions as an intermediate during apoptosis. Cyt c is released by the mitochondria in response to pro-apoptotic stimuli such as infection or DNA damage [33]. Cyt c release is initiated and sustained by increased calcium level in mitochondria. The release of small amounts of cyt c leads to an interaction with the IP3 receptor (IP3R) on the endoplasmic reticulum (ER), causing massive ER calcium release. The overall increase in calcium triggers a massive release of cyt c, which then acts as a positive feedback loop to maintain ER calcium release through the IP3Rs. Cyt c can be also released from mitochondria due to formation of a channel, the mitochondrial apoptosis-induced channel (MAC), in the cytosol [34]. Once cytochrome c is released, it binds with Apoptotic protease activating factor - 1 (Apaf-1) and ATP, which then bind to pro-caspase-9 to create a protein complex known as an apoptosome. The apoptosome cleaves the pro-caspase to its active form of caspase-9, which in turn activates the effector caspase-3 and eventually mediated biochemical and morphological features of apoptosis [35]. The apoptotic process is regulated by a variety of pro- and anti-apoptotic proteins. Such are the Bcl-2 family proteins that are able to promote or inhibit apoptosis by direct action on MAC/ Mitochondrial Outer Membrane Permeabilization Pore (MOMPP). Bax and/or Bak family proteins form the pore, while Bcl-2, Bcl-xL or Mcl-1 inhibit pore formation.

Recent results suggest that receptor-mediated apoptosis induce mitochondrial remodeling which appears to play a role in programmed cell death. In particular, a cascade of subcellular events provokes the movement of the pro-apoptotic protein Bax from the cytosol to the mitochondrial membranes [36, 37] where it is inserted into the outer membrane of mitochondria inducing escalation of the apoptotic pathway. Bax-type proteins have been shown to assist the initiation of cyt c release by forming of permeability pores in the lipid membrane [38]. A small amount of cyt c released triggers calcium level increase in the endoplasmic reticulum. High calcium level enhances massive cyt c release, which is an essential step in further activating the pathway responsible for destroying the cell from within. As a consequence, this causes lipid redistribution and raft-like domain formation in the

mitochondrial lipid membrane, which in turn recruits mitochondrial fission-associated proteins from the cytosol to the microdomains into the inner membrane [39]. These fission-associated proteins are then identified as a prerequisite for apoptosis [40, 41]. Even though the apoptotic pathway is well studied and characterized, the molecular mechanisms of many processes are still not clear. For example, not well defined are the identifying factors inducing lipid rearrangement in the mitochondrial membranes, which is the initial step for non-residential protein movement for apoptotic signaling. Thus, studying the effect of cyt c on raft-like membrane lipid mixtures is of high importance, which could give insights into the apoptotic pathway and signaling in mitochondria.

1.2. Cellular membranes

Biological membranes are involved in various steps of the cell life. They display complex compositions, containing hundreds of different lipids and proteins (Figure 1.2.1). The lipid composition of the membranes varies depending on the function of the cells and organelles; it is specific for different cell types and even for the different organelles of the same cell. The membrane acts as a selective barrier with low permeability to ions and large molecules. Channels and transporters are incorporated to control exchange of solutes. Gradients of ions, pH and electrical charge across the membrane are exploited to store energy and to allow fast responses to a signal. Membranes are also home to many enzymes catalyzing biochemical reactions, and they contain molecules that allow recognition between cells.

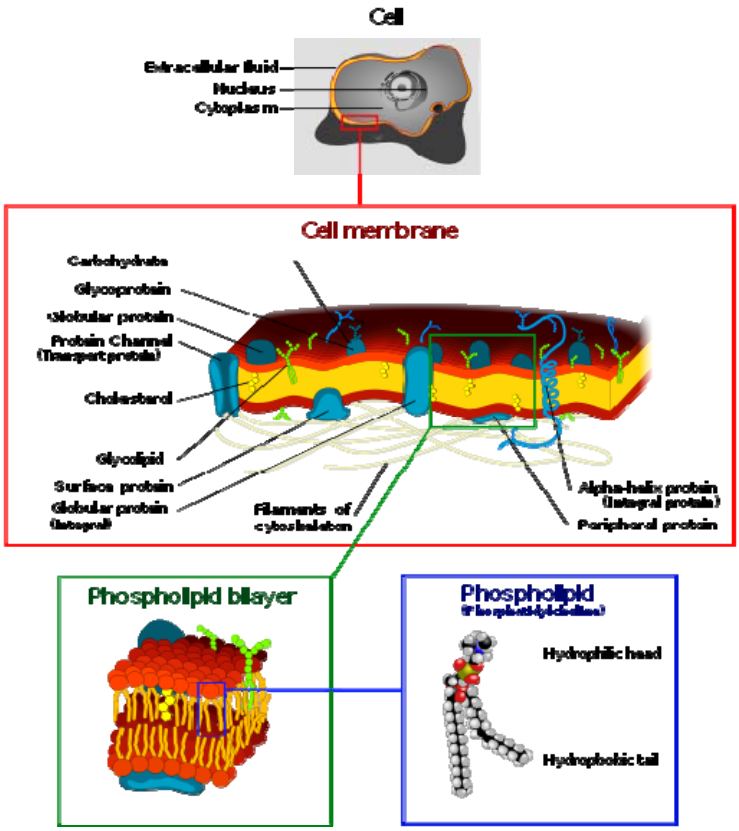

Figure 1.2.1 Schematic representation of the eukaryotic cell (a), the cell membrane (b), the phospholipid bilayer (c) and a phospholipid (d) [23].

Membranes enable cells and their internal compartments to adopt certain shapes, which can be dynamic for example when forming small vesicles for transporting a cargo between different compartments of the cell or when growing

of tubular structures. These processes require involvement of vesicle budding and fission, vesicle transport, recognition between membranes and membrane fusion.

The basic building block of membranes is the phospholipid bilayer, into which many more molecules are incorporated, such as cholesterol, proteins, integral membrane proteins etc. Unlike storage lipids (fats), which consist of a glycerol and three fatty acid chains, phospholipids contain only two fatty acids. They are derived from either glycerol or sphingosine. The headgroup is the sphingosine esterified to a phosphoric acid group, which is in turn ester-linked to a choline. The fatty acid chains usually contain an even number of carbon atoms between 14 and 24, where 16 and 18 are most common. They are normally unbranched and either saturated or contain one or more, non-conjugated double bonds in the cis-configuration. Lipids differ from each other by their head groups, hydrocarbon chain lengths and degree of saturation.

Since biological membranes are complex mixtures of many lipids with different melting temperatures, various phases simultaneously may coexist. Many of events in the cell membrane are related to the phase behavior of the membrane components. Lipid rafts have already been identified as functionally important components of cell membranes. A number of studies indicate their involvement in processes such as protein lipid sorting and signal transduction, cholesterol transport, membrane trafficking, cytoskeleton adhesion, fussion and fission, endocytoses and apoptosis [42-48]. A new development in molecular medicine called “membrane-lipid therapy” relies on the interaction of proteins with lipid domains as modulating the cell activity and thus presenting a way for treatment of human diseases [49, 50].

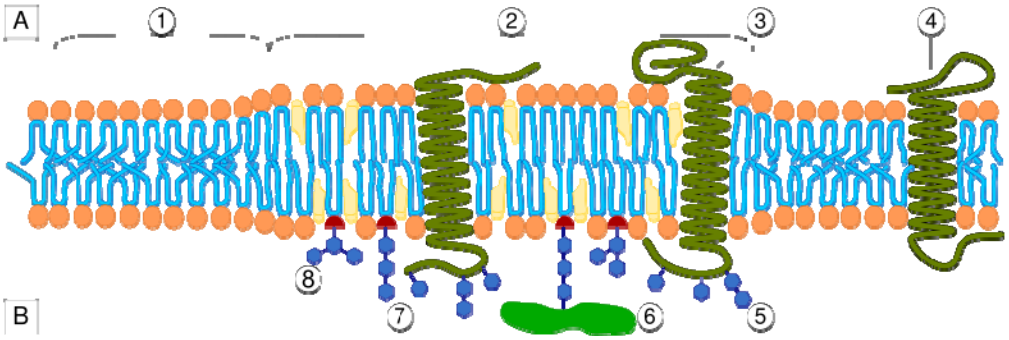

Figure 1.2.2 Schematic representation of lipid raft organization. Region (1) corresponds to standard lipid bilayer, region (2) corresponds to lipid raft. (3) Lipid raft associated transmembrane protein, (4) Non-raft membrane protein, (5) glycosylation modifications, (6) GPI-anchored protein, (7) Cholesterol and (8) Glycolipid [23].

1.3. Model membrane systems

Vesicles are enclosed by a lipid bilayer. They represent a powerful tool for studying biophysical properties of more complex biological cells. Many techniques have been developed for preparation of liposomes of different size. The largest ones called giant unilamellar vesicles (GUVs) have sizes several tens of microns comparable to the cell size and therefore allow direct visualization and manipulation under optical microscopy for studying membrane properties and behavior as in biological membranes. Model membrane systems are convenient as well, because can construct a membrane containing the lipid species of interest.

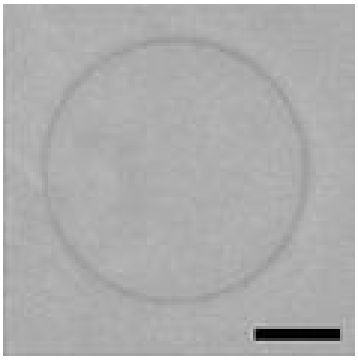

Figure 1.3.1 GUV under phase contrast microscopy. The scale bar corresponds to 10 μm.

Eukaryotic cell membranes are multicomponent systems containing proteins, glycerophospholipids (with low melting temperature), sphingolipids (with high melting temperature) and sterols. Naturally, both lipids and proteins display phase behavior forming domains and aggregates. Because of the resolution limitations of optical microscopy, it is still difficult to visualize nanometer scale membrane domains enriched in saturated lipids, cholesterol and specific proteins, which makes their existence in living cells controversial [51]. However, model systems such as GUVs [52] containing cholesterol and sphingolipids can serve as a powerful tool to visualize raft-like liquid ordered domains for characterizing biologically relevant phenomena, see e.g. references [53-55]. Upon mixing saturated and unsaturated lipids with cholesterol at room temperature one can observe phase separation and domain formation in a micron-scale range. Depending on the lipid composition and with the help of fluorescently labeled lipids one can then visualize domains in GUVs by confocal microscopy [56]. Recently, it has been demonstrated that phase separation and domain formation can be visualized not only in zwitterionic lipids but also in ternary mixtures containing anionic lipids [57], which in turn opens new possibilities for investigation of systems relevant for biological membranes. In particular, the

inner leaflet of the plasma membrane as well as the membranes of many cellular organelles exhibiting raft-like domains [58-60] contain charged lipids. The mitochondrial membrane also contains a number of charged lipids, such as phosphatidylinositols, fatty acids and cardiolipin, whose total fraction is of the order of a few ten weight percent [61].

1.3.1. Self assembly of lipid membranes

Aggregation of lipids is a self-assembly process, driven by lipid interactions such as van der Waals, hydrophobic, electrostatic interactions and hydrogen bonding. Membrane lipids have a polar, hydrophilic headgroup and two long hydrocarbon chains that are extremely hydrophobic. In general, the presence of an individual hydrophobic molecule in an aqueous environment is entropically highly unfavorable. The final shape of a lipid aggregate is mainly determined by the so-called shape factor of the constituting lipids:

$$v/al_c \qquad 1.3.1.1$$

where the optimal surface area occupied by the headgroup is a, the molecular volume of the hydrocarbon tail is v and the length of the hydrocarbon chains l_c.

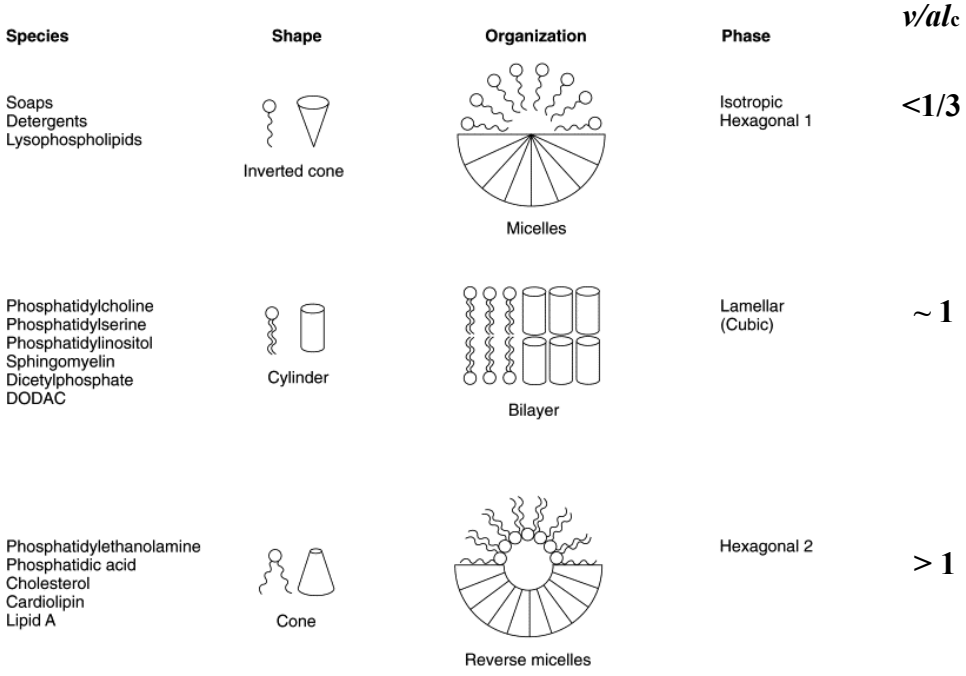

Figure 1.3.2 Schematic representation of phospholipid aggregates depending on their shape factor [62].

Self aggregation of polar lipid molecules depends on the temperature, the molecular shape of the lipids and the conditions in the lipid–water mixture (concentration and ionic strength). Lipid molecules may self assemble into different colloidal particles. The simplest lipid structures are spherical micelles with their chains pointing towards the center and their heads forming the sphere surface. For micelle structure formation, lipids must have the called cone-shape with a large headgroup area *a,* and a short hydrocarbon chain volume *v*. For bilayer structures, cylinder-shaped lipids are required with small head group areas and a bulky hydrocarbon chain. Bilayers are usually composed of lipids with two hydrocarbon chains. In a planar bilayer, the hydrophobic chains in the middle of the structure are well accommodated as they are in a hydrophobic environment and the hydrophilic heads face the aqueous interface. The structure tends to shield against the aqueous environment and connect open edges which results in forming the vesicles [63]. The corresponding shape factors are given in figure 1.3.2 For other lipid aggregate structures.

1.3.2. Lipid phases: Phase diagram of lipid ternary mixtures

Lipids can adopt a variety of phases. It is known that, when mixing low and high melting temperature lipids with cholesterol, phase separation and domain formation may be observed. This phenomenon is highly depended on lipid composition and is caused by immiscibility of the lipids. As a result, one can form membranes in different phase state such as, the fluid homogenous phase (Ld or Lo), the solid phase (So), two fluid phase coexistence (Ld/Lo, Ld/So or Lo/So) and the three phase coexistence (So/Ld/Lo) phase of the membranes (Figure 1.3.3).

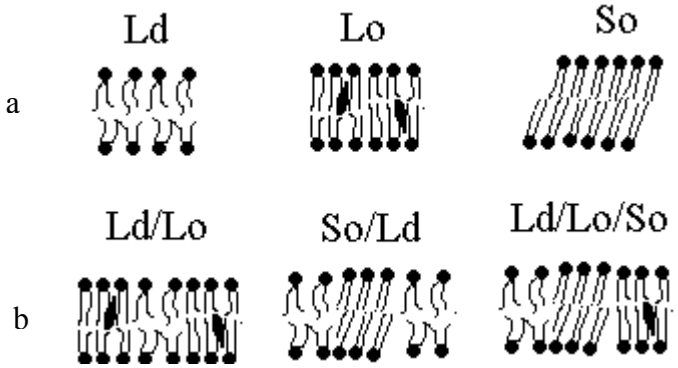

Figure 1.3.3 Schematic representation of possible lipid phase states (a). Phase separation driven by immiscibility when mixing low melting temperature unsaturated lipid with high melting temperature saturated lipid and cholesterol (b).

In the present study we characterized GUVs, which were composed of DOPG, a low melting temperature unsaturated lipid carrying a net negative charge, eSM, a high melting temperature saturated lipid, and cholesterol. The transition temperature of DOPG is 18 ºC which means that at room temperature DOPG is in the fluid phase. On the other hand, eSM at room temperature is still in gel phase. Thus, at room temperature membranes composed of this mixture can exhibit immiscibility depending on the specific membrane composition.

Lipid phase diagrams describe different phases existing in equilibrium for a combination of thermodynamic parameters, like temperature, pressure and composition. Binary lipid mixtures can already exhibit quite complex phase behavior and ternary mixtures even more so. The Gibbs phase rule is applied to determine the number of phases that can exist simultaneously in equilibrium for a given number of components. For a system with C components, containing P different phases the number of degrees of freedom F is:

$$F = C - P + 2. \qquad 1.3.2$$

The water is not counted as a component and there is no degree of freedom for the water concentration. Furthermore, pressure can usually be considered as given (except in monolayer systems), so that the number of remaining degrees of freedom is:

$$F = C - P + 1 \qquad 1.3.3$$

According to the Gibbs phase rule, a huge number of phases could be allowed, although it is impossible to produce a phase diagram of as complex a lipid mixture as found in native membranes.

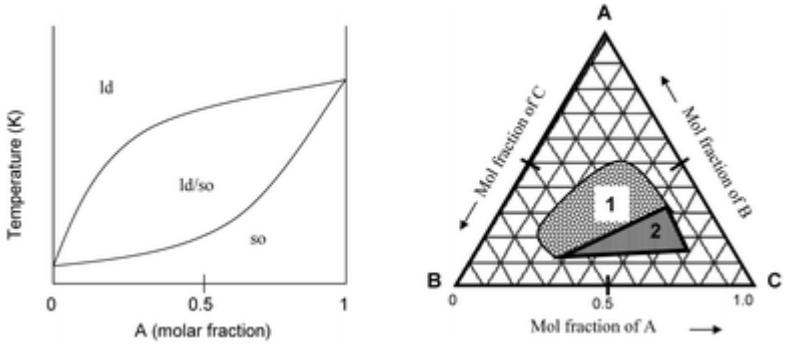

Figure 1.3.4 Representation of hypothetical phase diagram of binary (left) and ternary (right) lipid mixtures. In the generic ternary lipid mixture phase diagram (1) represents liquid disordered/liquid ordered and (2) solid ordered/liquid disordered/liquid ordered phase coexistence region [64].

A prerequisite for compiling a phase diagram is that there are distinguishable phases, and transitions between them are approximately first-order. Nevertheless, studying the simple systems with identifiable phases is hoped to give insight into phenomena that could be pertinent to real cell membranes. Even when there is no real cooperative phase transition over the whole membrane, there could be local ones, such as the formation of lipid phase domains or rafts which are though to be important components in biological membranes [65]. Therefore, ternary lipid mixtures of phosphatidylcholines, sphingolips and cholesterol have been intensively investigated in the last decade. Ternary lipid phase diagrams are difficult to investigate as in excess water and constant pressure four different phases can coexist simultaneously. The additional complication is how to apply the lever rule. The lever rule is a tool to determine weight percentages of each phase of a binary equilibrium phase diagram. To apply this rule the orientation of the levers along the tie-lines has to be known, which is an additional complication. The Gibbs triangle is an isothermal section of the phase diagram at given pressure for different concentrations of the components. The three components are found in the corners of the triangle with their corresponding mole fractions of 100%. Each point in the Gibbs triangle corresponds to a composition of the three component mixture, which may exist in one, two or three phases. These points form regions of different phases separated with boundaries from each other characterizing the phase behavior of the three component mixtures at constant temperature and pressure. Figure 1.3.4 represents the example of the hypothetical binary and ternary lipid mixture phase diagrams.

2. Materials and Methods

2.1. Materials

The lipids DOPG (1,2-dioleoyl-sn-glycero-3-phospho-[1'-rac-glycerol], sodium salt), eSM were purchased from Avanti Polar Lipids (Alabaster, AL). Cholesterol was purchased from Sigma-Aldrich (St. Louis, MO). The fluorescent labels 1,1'-dioctadecyl-3,3,3',3'-tetramethylindocarbocyanine perchlorate ($DiIC_{18}$) and 1,2-distearoyl-*sn*-glycero-3-phosphoethanolamine-N-[poly(ethylene glycol) 2000-N'-carboxyfluorescein] (DSPE-PEG2000-CF) were obtained from Molecular Probes (Eugene, OR) and Avanti Polar Lipids, respectively. Lipid and dye structures are shown on Figure. 2.1.1.

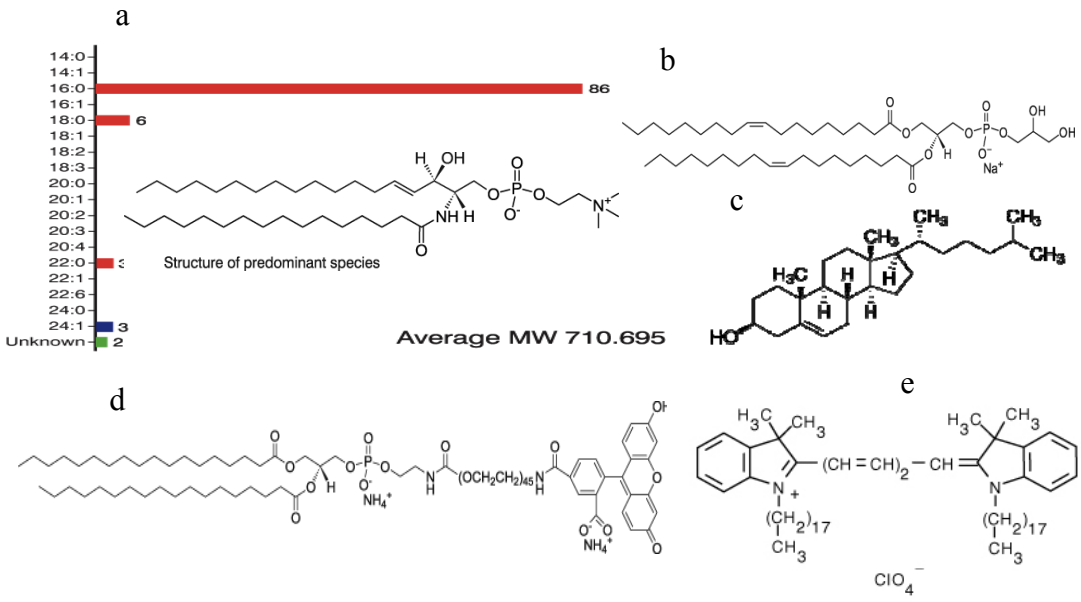

Figure 2.1.1 Structure of egg sphingomyelin fatty acid content and its predominant species (a)[23]. Structure of DOPG lipid (b)[23] and Cholesterol (c)[23]. DSPE-PEG2000-CF (d)[23] and $DiIC_{18}$ (e)[23] fluorescent dyes.

Yeast cytochrome c (*S. cerevisiae*), HEPES (4-(2-hydroxyethyl)-1-piperazineethanesulfonic acid) and EDTA (ethylenediaminetetraacetic acid disodium salt dehydrate) were purchased from Sigma Aldrich (Steinheim, Germany). Fluorescent label for cyt c was purchased from Invitrogen (Alexa Fluor 633 carboxylic acid, succinimidyl ester). PBS buffer (Phosphate-Buffered Saline, pH 7.4) sodium chloride (NaCl), potassium chloride (KCl), disodium phosphate (Na_2HPO_4), monopotassium phosphate (KH_2PO_4), sodium bicarbonate ($CHNaO_3$), sodium hydroxide (NaOH) and dimethyl sulfoxide (DMSO) were purchased from

Sigma-Aldrich (Steinheim, Germany). Gel filtration column filled with Sephadex G-25 was purchased as well from Sigma-Aldrich (Steinheim, Germany). All aqueous solutions were made in deionised water with 0.055 μS/cm conductivity (Purelab Plus).

THP-1 cell line expressing DC-SIGN was provided by NIH AIDS program (Virology, 318: 17-23, 2004). Recombinant Protein G, Sepharose® 4B, Silver Staining Kit, Bromophenol blue (BPB, 3',3",5',5" tetrabromophenolsulfonphthalein) and nitrocellulose membranes was purchased from Invitrogen, USA. Complete Protease Inhibitor tablets were obtained from Roche Diagnostics GmbH, Manheim, Germany. 10% Tris-HCl polyacrilamide gel was obtained from Bio-Rad, USA with Gel dimensions 8.6 x 6.8 cm (W x L) and Cassette dimensions 10 x 8 x 0.4 cm.

2.2. Vesicle preparation

Electroformation of giant unilamellar vesicles (GUVs)

GUVs composed of DOPG/eSM/Chol ternary mixtures were prepared by the method of electroformation [66] with some modifications [67]. 10 μl of 2 mg/ml of the ternary lipid mixtures in chloroform were spread on conductive glasses coated with indium tin oxide (ITO). Lipid coated ITO glasses were dried for several hours in the 60ºC oven under vacuum (Heraeus Vacutherm VT 6025, Thermo Electron GmbH, Langenselbold, Germany) to remove the traces of organic solvent. Afterwards, ITO glasses with lipid coated surfaces facing each other were separated with 2mm teflon frame and sealed. The frame is necessary to obtain the space for the vesicle solution. As a buffer, equilibrated at room temperature, 100 mM sucrose solution in 2 mM HEPES/1 mM EDTA (pH 7.5) was used. HEPES is a zwitterionic organic chemical buffering agent used to maintain physiological pH throughout the measurements, whereas EDTA is used to sequester free metal ions in the solution. Then the chamber was placed in the oven (TTI TG, 215, Thurlby Thandar Instruments; Fluke PM 5138A, Fluke, Germany) at 60 °C to ensure full miscibility and fluidity of the lipids. Vesicle swelling was accelerated by AC field with field strength of 1.0 V (peak-to-peak) and frequency of 10 Hz was applied using a function generator for 2 hours. Afterwards, the chamber was removed from the oven and left at room temperature (~25˚C) for equilibration. For observation under the microscope vesicle solution was transferred and diluted with 110 mM glucose solution in a 2 mM HEPES/1 mM EDTA buffer (pH 7.5) at room temperature.

The solution osmolarity inside and outside of the vesicles were measured with cryoscopic osmometer Osmomat 030 (Gonotec, Germany). The osmolarity of the sucrose to be 0.171 mOsm/kg and that of the glucose solution was 0.163

mOsm/kg. The slight asymmetry in sugar densities allows the vesicles to sit on the bottom of the chamber by gravity force, which in turn is essential for static state of the vesicles during the observation and scanning with the microscope.

In some experiments, the cover glasses were coated with a solution of the positively charged protein (10 mM concentration) to avoid adhesion of vesicles to the glass surface. The conductivity of the buffers were measured by conductivity meter SevenEasy (Mettler Toledo, Greifensee, Switzerland). The conductivity of glucose in 2 mM HEPES/1 mM EDTA buffer (pH 7.5) to be 257 μs/cm and sucrose was measured to be 268 μs/cm respectively.

Two fluorescent dyes $DiIC_{18}$ and DSPE-PEG2000-CF were used to label different types of vesicles. $DiIC_{18}$ is known to partition preferentially in the Ld phase being excluded from S_o and Lo phases, whereas DSPE-PEG2000-CF dye preferentially partitions in Lo phase [68, 69]. In all cases, the lipid mixtures contained 0.4 mol% of the fluorescent dye. Stock solutions of the dyes were prepared by dissolving dry powders into chloroform and were added during preparation of lipid mixtures just before applying solution on the conductive glass surfaces. A laser source at 561 nm was used to excite $DiIC_{18}$ and 488 nm for excitation of DSPE-PEG2000-CF dye.

During electroformation preparation of GUVs, many vesicles turned out to have inclusions or/and membrane tubes with interconnections. However, for observations, only isolated vesicles with diameter more than 10μm and with no visible defects were chosen.

Extruded large unilamellar vesicles (LUVs)

DOPG/eSM/Chol ternary mixtures in chloroform with desired lipid concentration (4 mM) were pipetted into a glass vial and dried under stream of nitrogen until the organic solvent evaporated completely leaving only lipid film at the glass surface. The flasks were placed in the oven at 60ºC under vacuum for 1 h for complete removal of organic solvent. Afterwards, a 2 mM HEPES/1 mM EDTA buffer (pH 7.5) was added to the dry lipid residues equilibrated at room temperature and shaken for several minutes. Large unilamellar vesicles were prepared by using LiposoFast pneumatic extruder (Avestin Otawa, Canada) and the desired size of the vesicles of around 100 nm was achieved by using sets of membrane filters (Avestin Europe, Germany) with different pore sizes. First, the vesicle suspension was passed through the 400 nm pore membrane and then the 200 nm pore membrane, each 20 times, after which through a 100 nm pore membrane 40 times. Just before performing the measurement, the vesicle solution was degassed for 8 minutes in a vacuum chamber ThermoVac (MicroCal, Northhampton, MA) at room temperature. Removing gas bubbles from the

solution is a necessary step for high quality measurement. Vesicle size distribution was checked with dynamic light scattering.

2.3. Labeling of cyt c

Cyt c was labeled with Alexa Fluor 633 carboxylic acid, succinimidyl ester. The labeling procedure of cyt c was performed by following the manufacturer's protocol. In detail, 5mg of cyt c powder was dissolved in 1ml of PBS buffer containing 0.2 M sodium bicarbonate solution with 2 M sodium hydroxide. Afterwards, 1.0 mg of dye N-HydroxySuccinimide (NHS)-ester was diluted in 200 µl of anhydrous amine-free DMSO and was added to the protein solution with the dye-to-protein ratio of 2, followed by gently shaking at room temperature. The reaction was incubated for 1 h under protection from light. NHS-ester is hydrolyzed during the labeling reaction that is why it is necessary to separate the unbound dye from the dye-protein conjugate which was done using Sephadex G-25 columns. First, the Sephadex G-25 column was equilibrated with the PBS buffer, and then the dye-protein conjugate was passed through the column. The first eluted colored and fluorescent zone was collected.

Purification of DC-SIGN

For DC-SIGN protein purification, first of all the Dentritic Cell 6 monoclonal antibody was purified (DC6 mAb). The DC6 mAb is produced from a hybridoma cell line ('hybrodoma' meaning fusion of cells, e.g. a lymphocyte cell which produces the monoclonal antibodies is fused with an immortal myeloma cell line, so that the fused cells continuously produces the antibodies as it becomes 'immortal' after fusion). DC6 is a monoclonal antibody that specifically binds to the carbohydrate recognition domain (CRD) of Dendritic Cell-Specific Intercellular adhesion molecule-3-Grabbing Non-integrin (DC-SIGN) therefore it is used for DC-SIGN purification. DC6 is being purified from DC6 cell supernatants using a Recombinant Protein G – Sepharose 4B affinity column.

First, the columns were assembled and equilibrated with PBS buffer. The total binding capacity of the column was calculated to be 0.1 ml/mg. The supernatant of DC6 hybridoma cells was applied to the guard column filled with Sepharose 4B beads. The guard column functions as a filter to remove bigger fractions of the cell lysate and prevent blocking the main affinity column. DC6 supernatant passes through the affinity column filled with protein G, from where DC6 antibodies are eluted facilitated by low pH buffer (0.1 M Glycine pH.3.0), collected in tubes containing high pH buffer (1 M Tris pH.9.0) for immediate pH neutralization and dialyzed against PBS buffer. As a next step a column was

constructed from the purified DC6 antibodies for the purpose of isolating DC-SIGN from the lysates of cells that express this receptor. THP is a human monocytic cell line infected with the target protein DNA, so that the cell expresses the target protein DC-SIGN continuously. THP-1 DC-SIGN cells were lysed using a Dounce homogenizer. Approximately $2x10^{10}$ cells were homogenized in PBS buffer containing 10% DMSO with 0.5% Igepal CA-630 to help dissolve hydrophobic parts.

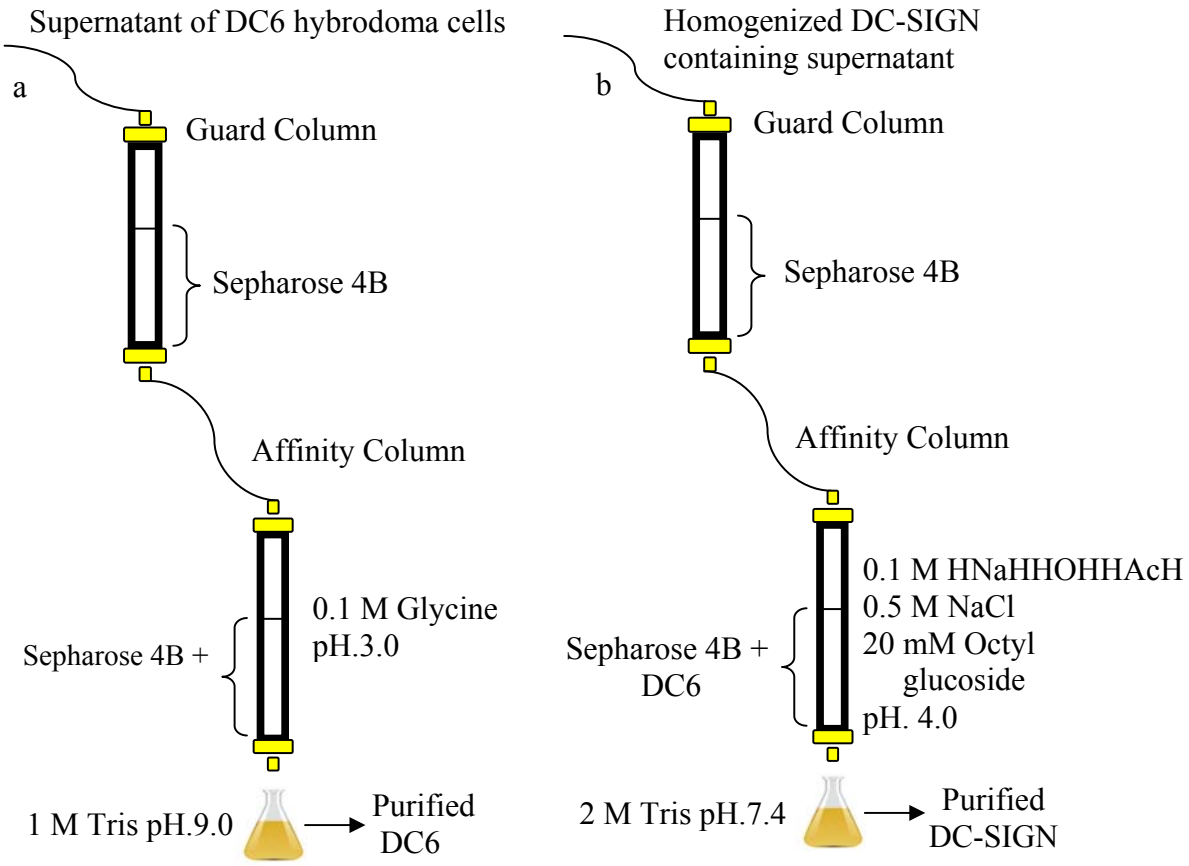

Figure 2.3.1 Schematic representation of the system assembled for protein purification. (a) Columns assembled for DC6 mAb purification: Guard column containing Sepharose 4B was connected to affinity column filled with Protein G. Elution buffer 0.1 M Glycine pH.3.0 was collected in tubes neutralized by 1 M Tris pH.9.0. (b) Columns assembled for DC-SIGN protein purification: Affinity column containing DC6 mAb was eluted with 0.1 M sodium acetate 0.5 M NaCl 20 mM Octylglucoside pH. 4.0 buffer. Samples were collected and neutralized with 2 M Tris pH.7.4 buffer.

Complete Protease Inhibitor tablet was added to prevent proteolysis. The homogenate was centrifuged to separate different cell compartments and

organelles prior to electrophoresis. It was centrifuged at 1600 g for 5 minutes and twice at 27 000 g for 1 h. Afterwards the clarified supernatant was applied to the DC6 affinity column equilibrated with PBS 0.5% Igepal CA-630 buffer. DC-SIGN was eluted using a low pH buffer (0.1 M sodium acetate, 0.5 M NaCl, 20 mM Octylglucoside, pH. 4.0) containing the detergents octylglucoside and triethylamine and immediately neutralized with 2 M Tris buffer pH.7.4. All procedures were carried out at 4°C (Figure. 2.3.1).

The concentration of protein was determined by measuring the absorbance at 280 nm and it was varied depending on the different cell patches. The purity of the purified DC6 and DC-SIGN protein was estimated with SDS-PAGE silver staining and Western-blot.

sodium dodecyl sulfate polyacrylamide gel electrophoresis (SDS-PAGE)

SDS-PAGE is a method widely used to separate proteins according to their electrophoretic mobility and the length of their polypeptide chain. The binding of SDS to the polypeptide chain of the protein causes an even distribution of charge per unit mass which in turn results in a fractionation by approximate size during electrophoresis. Non-reducing or reducing SDS-PAGE was used for visualization of the expected molecular weight of the purified protein. 20 µl of the sample to be analyzed was mixed with 20 µl Bromophenol blue (BPB, 3',3",5',5" tetrabromophenolsulfonphthalein), a tracking dye. Usually proteins are colorless, that is why anionic dye with known electrophoretic mobility is used to follow easily protein progress through the gel. This dye is colored at alkali and neutral pH and is a small negatively charged molecule that moves towards the anode. Being a highly mobile molecule it moves ahead of most proteins. As it reaches the anodic end of the electrophoresis medium electrophoresis is stopped. After mixing the sample with tracking dye plastic vials are boiled in water bath for 10 minutes to facilitate farther protein denaturation helping SDS to bind. In some cases 2µl of reducing agent (2 - Mercapteothanol) was added to the samples. It further denatures the proteins by reducing disulfide linkages, thus overcoming some forms of tertiary protein folding, and breaking up quaternary protein structure (oligomeric subunits). Thereafter, the chamber for electrophoresis was assembled. Ready 10% Tris-HCl polyacrilamide gel cassettes were placed into the electrode chamber and all together into the tank with Tris (tris(hydroxymethyl)aminomethane) running buffer. The samples were loaded from the top into wells within the gel in a way to avoid bubble formation. Molecular weight size marker of known molecular weight was placed in a separate lane in the gel, as well as mouse IgG 1B7.11 as a standard in order to calibrate the gel and determine the approximate molecular mass of unknown proteins by comparing the distance travelled relative to the marker. Then an electric field of

100 V was applied across the gel, causing the negatively-charged proteins to migrate across the gel towards the positive (+) electrode (anode). Depending on their size, each protein will move differently through the gel matrix, smaller proteins will have traveled farther down the gel, while larger ones will have remained closer to the point of origin. Following electrophoresis, the gel was stained with Coomassie Brilliant Blue R-250 for 30 seconds, allowing visualization of the separated proteins. After staining, different proteins will appear as distinct bands within the gel. In some cases more sensitive method such as silver staining was used for detecting the purified protein. Figure 2.3.2 shows the schematic representation of the SDS-PAGE electrophoresis process.

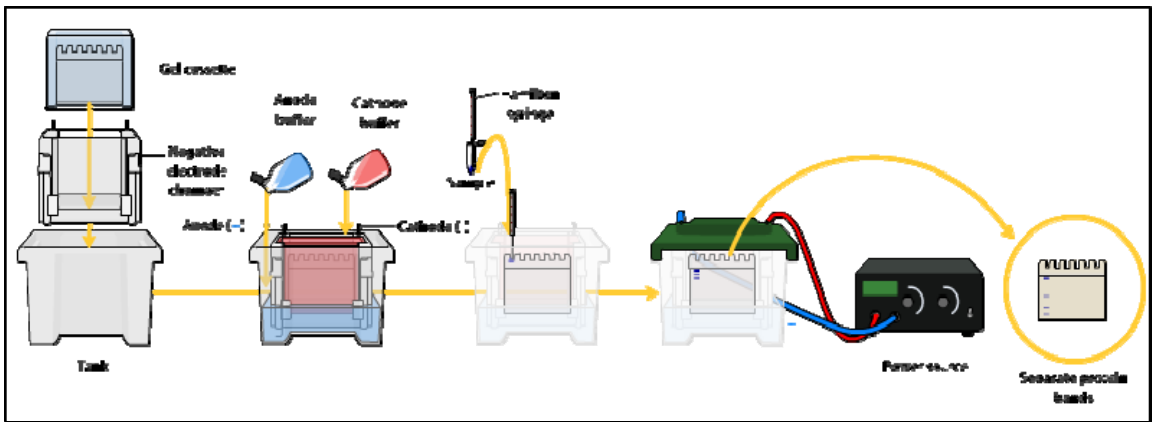

Figure 2.3.2 Schematic representation of SDS page electrophoresis process. Gel cassette placed into the chamber in the tank loaded with running buffer. 10 µl sample solution together with tracking dye was loaded into the well along with size marker in a separate well. Electric field applied for 1 h results in shift of a sample along the gel to the direction of the anode separating molecules according to their molecular weight [23].

Silver staining

Silver staining is a widely used method for protein and DNA staining. Classical Coomassie Briliant Blue staining can usually detect a 50 ng protein band, silver staining increases the sensitivity typically 50 times by using silver to selectively alter the appearance of the target. After electrophoresis, the gel was removed from the cassette, placed in a staining tray and rinsed with ultra pure water. The gel was fixed in 100 ml of fixative solution for 20 minutes with gentle rotation and washed afterwards in 30% ethanol for 10 minutes. The fixative reagent removes interfering ions and detergent from the gel and restricts the movement of proteins out of the gel matrix. Then the gel was incubated for 10 minutes in 100 ml of sensitizing

solution containing 0.02% sodium thiosulphate which increases sensitivity and contrast of the stain. After washing in 30% ethanol and water for 10 minutes, the gel was incubated for 15 minutes in 100 ml staining solution. During this step, silver ions bind to the protein and form a latent image. Upon completing staining, the gel was washed for 20 to 60 seconds and incubated in 100 ml of developing solution for 4-8 minutes which reduces silver ions to metallic silver at the protein positions resulting in development of the protein bands. Immediately after bands appear, 10 ml of stopper solution for 10 minutes was added to prevent further eduction.

Western blot

The western blot is a widely used technique to detect specific proteins in the given sample of tissue homogenate. It uses gel electrophoresis to separate native proteins by the length of the polypeptide. The proteins are then transferred to a membrane (nitrocellulose) based on hydrophobic and electrostatic interactions, where they are detected using antibodies specific to the target protein. The method for transferring the proteins into nitrocellulose membrane is called electroblotting and uses an electric current to pull proteins from the gel while maintaining the organization they had within the gel [70, 71].

A membrane with filters was placed in methanol for 10 minutes. Afterwards, it was equilibrated in a transfer buffer (Tris HCl with Glycine) for couple of minutes. The membrane was placed on top of the gel covered with filters form both sides. The entire stack was placed in a running buffer and the transfer was performed for 1 h at 350 mA keeping the system cooled with ice during the entire process. As a result, proteins were pulled on to the membrane from the gel. Figure 2.3.3 shows schematically the process described above.

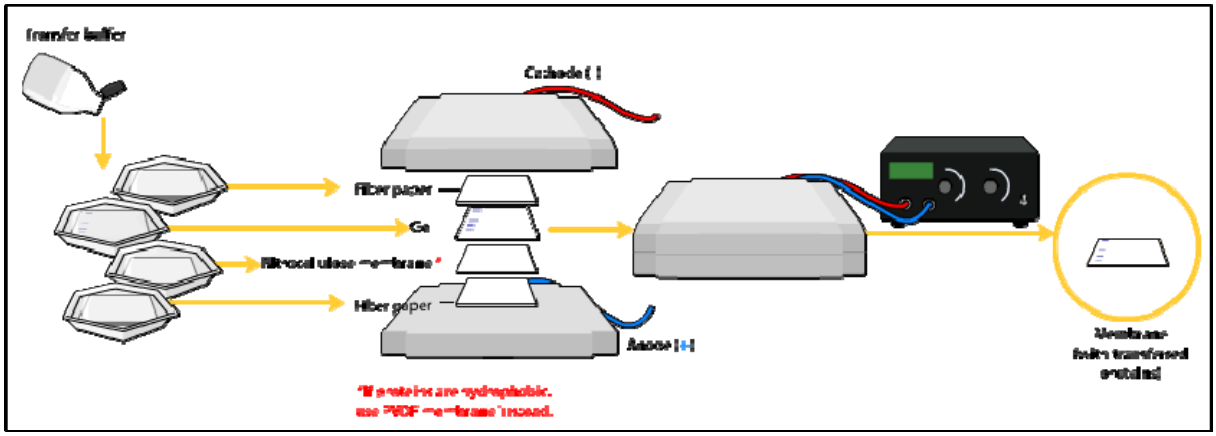

Figure 2.3.3 Schematic representation of protein transferring to the nitrocellulose membrane [23].

After protein transferring it was necessary to block the membrane in order to prevent farther binding of antibodies, which were used later for detection of the target protein. Blocking of non-specific binding was achieved by placing the membrane into the blocking buffer (Tris pH 7.5, 5 M NaCl, Tween 20, 5% non-fat dry milk) for 45 minutes at room temperature. Proteins from the blocking buffer attach to the membrane, except where target protein was bound. As a result, for the added antibody the only choice remains binding the target protein. After blocking, primary antibody mouse monoclonal Ab against human CD209 diluted in blocking buffer was added and incubated with the membrane over night gently rotating at 4°C. The membrane was rinsed 3 times with blocking buffer at 4°C and incubated with the secondary antibody anti mouse IgG diluted in blocking buffer at room temperature for 1 h. The secondary antibody was linked with biotinated streptavidin with a radioactive label attached containing a radioactive isotope of iodine. Other methods are safer, but an advantage of this approach is the sensitivity of auto-radiography based imaging, which enables highly accurate protein quantification. The membrane was exposed for 5 minutes and developed for 2 minutes in Chemiluminescence Detection solutions in dark. Afterwards, the membrane was developed for 15 to 30 seconds. Radioactive labels do not require enzyme substrates. By directly placing of medical X-ray film against the western blot it can be developed as it was exposed to the label and creates dark regions which correspond to the protein bands of interest. Figure 2.3.4 shows the chemiluminescence detection method.

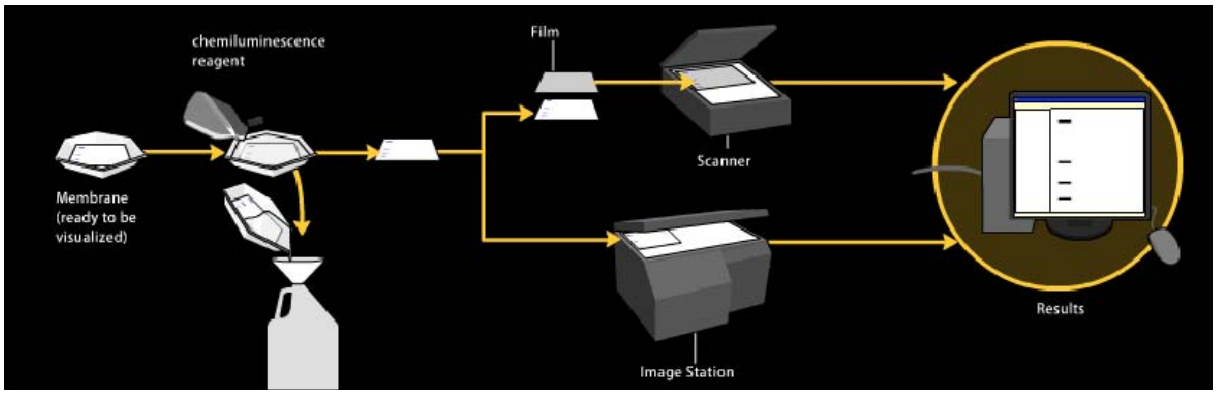

Figure 2.3.4 Schematic representation of western blot using chemiluminescence detection method [23].

2.4. Vesicle observation

2.4.1. Phase contrast microscopy

In the present work, GUVs were visualized for manipulating under phase contrast mode on a confocal laser scanning microscope (Leica DMI 6000, Leica Microsystems Heidelberg GmbH). The thickness of GUV membranes (approximately 4nm) is below the optical resolution limit; however phase contrast mode gives opportunity to observe unlabeled membranes by taking advantage of slight differences in the refractive indexes between membrane and the surrounding solution. Further contrast enhancement is achieved by using solutions inside and outside the vesicle, which also differ in their refraction index. This was obtained by preparing GUVs in 100 mM sucrose solution and diluted into 110 mM glucose solution which resulted in gradient difference inside and outside of the membrane. Phase contrast, using the optical devices, makes this tiny difference between refractive indexes visible by translating them into intensity difference.

Once the sample is illuminated by the light source (argon laser at 488 nm), light waves are shifted. The higher the refractive index of the solution, the smaller the speed of the light is, which in turn results in a lag behind or a phase shift of the light wave passing through the membrane compared to the surrounding solutions. The human eye is not capable of seeing such a phase shift under the microscope that is why the phase contrast technique uses ring system in the condenser and at the objective pupil to create visible phase contrast image. The first ring also called phase stop attenuates a bright light, whereas second ring adds constant phase shift to this light. The light is altered from the direct path while passing through the specimen containing vesicle membranes and different solutions. This partial light doesn't pass through the phase ring, but fuse and form the intermediate image. In the intermediate image the partial rays are superimposed where they amplify or attenuate each other and since the direct ray was strongly attenuated by the phase ring, much weaker diffracted light can become effective. This interference process results in bright and dark spots visible to the eye.

2.4.2. Confocal laser scanning microscopy

Observation of GUVs for characterization and manipulation were done by Confocal Lazer Scanning Microscopy (CLSM). The system of confocal LSM is composed of a fluorescent microscope with a confocal part, a scan head, several laser source combined with wavelength selection devices and the computer with software for image display, processing and storage. The principle of confocal LSM is schematically presented in Figure 2.4.1.

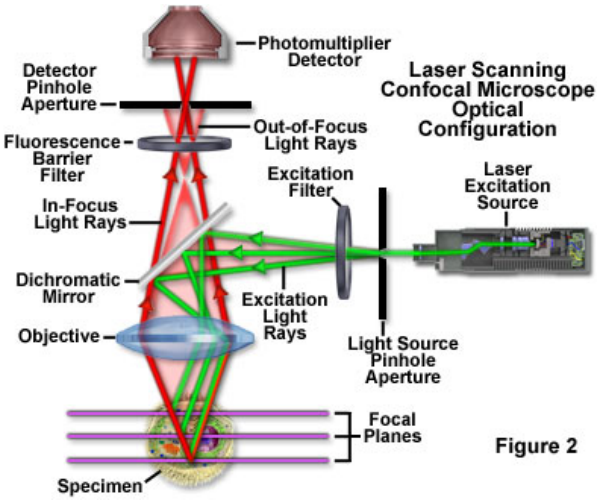

Figure 2.4.1 Schematic representation of optical pathway and contents of laser scanning confocal microscopy [72].

Coherent light emitted by the laser excitation source passes through the pinhole aperture located in a conjugate confocal plane. The laser beam is reflected by the dichromatic mirror and scanned at the chosen focal plane of the specimen. Secondary fluorescence emitted from the specimen passes back through the same dichromatic mirror, detector pinhole aperture and is focused as a confocal point. Significant amount of emitted fluorescence below and above the focal plane are out-of-focus light rays, however refocusing the objective shifts the excitation and emission points and a new plane on a specimen becomes confocal with the pinhole apertures and detector.

The point scanning method is one of the most important characteristic features of confocal microscopy. To obtain the information about the whole specimen the laser beam is guided across the specimen or the specimen is moved relative to the laser beam, a process known as point-probing scanning. Another important feature of confocal microscopy is the confocal aperture (called a pinhole). The detector, typically photo multiplier tubes (PMT), detects only the light that passed, through the pinhole. As the laser beam illuminates only a point of the object at a time, the illuminated point and the observed point (i.e. image and object points) are focused onto each other.

The result is what is called a confocal beam path. Ideally the pinhole is infinitely small, but varying the pinhole diameter the degree of confocality can be adjusted to specific requirements. The small confocal pinhole aperture is critical for obtaining thin optical sections of the specimen without any out-of-focus noise, providing clear focused optical sections over the whole depth of the specimen.

However, it is the reason for 25-50% loss of emission intensity. That is why PMTs are used for a high dynamic range and noise-free signal amplification. A PMT contains a photosensitive surface that captures incident photons and produces a stream of photoelectrons to generate an amplified electric charge, converts photons to electrons through the chain of electron multipliers, known as dynodes and outputs electrical impulse to the position logic circuits. In a majority of commercial confocal microscopes, the photomultiplier is located within the scan head, which is the main part of the confocal system. It contains fluorescence filter sets and dichromatic mirrors a scanning mirror system, variable pinhole apertures for generating the confocal image, and photomultiplier tube detectors for tuning different fluorescence wavelengths. The function of the scan head is rasterisation of an image (converting to pixels or dots) and collecting the photons from the specimen to assemble the final image. Detected intensity values are displayed then as gray levels by photomultiplier and for multi-channel- acquisition presented in pseudo-colors.

A combination of different laser types in confocal LSM can be used: Argon, Argon-Krypton, Helium- Neon, etc. providing laser lines of 458, 476, 488, 496, 514, 561, 594, 633, 705-980 (λ in nm). In the present work we have used the excitation source of 488 nm spectral line of the argon-ion laser and Diode-pumped solid-state (DPSS) laser with excitation source of 561 nm. Laser sources generate monochromatic light of discrete wavelengths. The spectral detection is determined by prisms, free adjustable barriers and tunable quartz crystals such as acousto-optic tunable filter (AOTF) within the microscope. The AOTF is an electro - optical device that is used to modulate simultaneously wavelength and the intensity of multiple laser lines from one or several laser sources (Figure. 2.4.2).

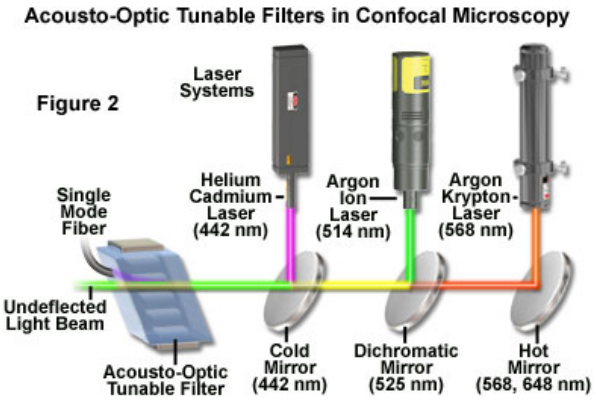

Figure 2.4.2 Schematic visualization of AOTF configuration for intensity control and laser wavelength selection in confocal microscopy [72].

The AOTF adjustable quartz filter works at frequencies as high as sound. Light, which passes the AOTF, is diffracted depending on its own wavelength and

the wavelength of the ultrasonic wave field. The ultrasonic wave field can be modulated, so that the intensities of the different laser lines can be changed by the software even during the scanning process.

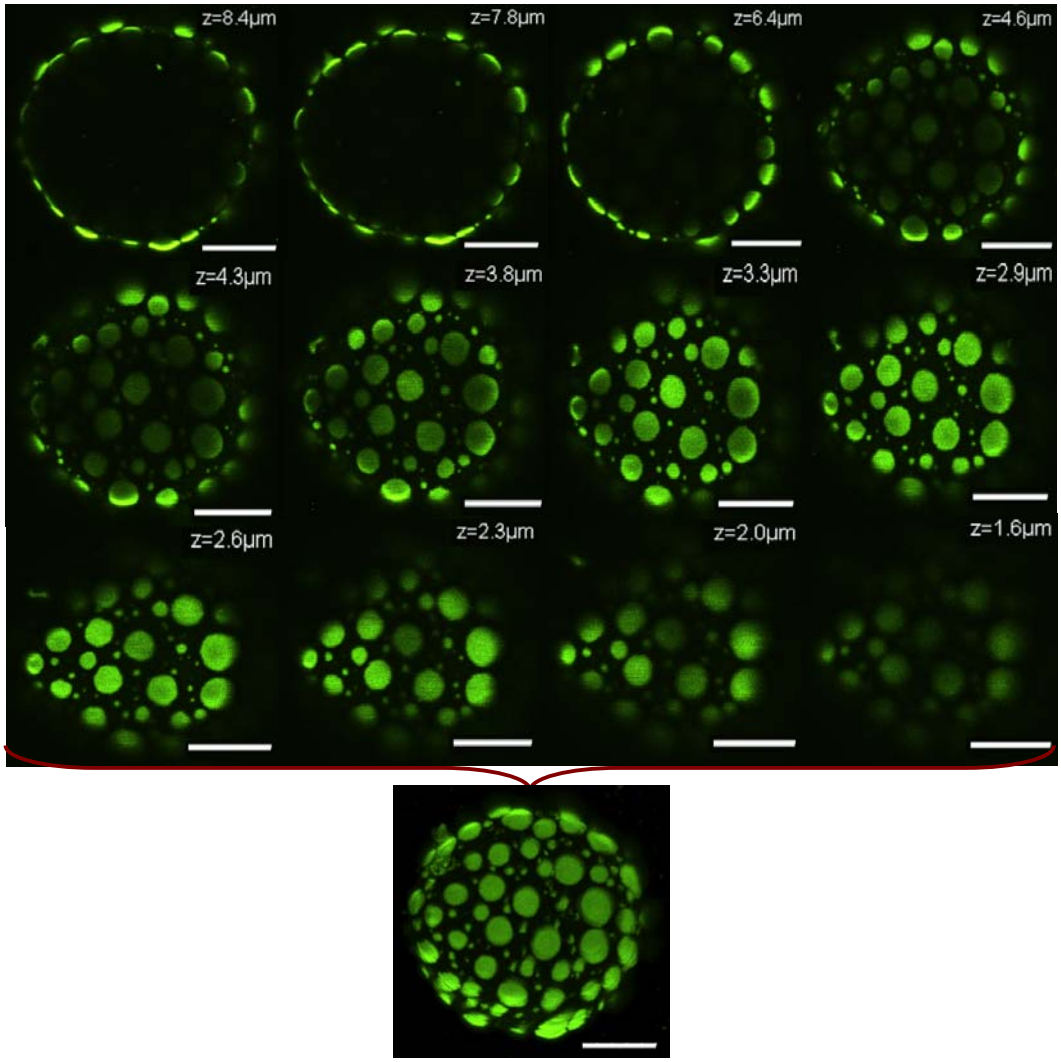

Figure 2.4.3 A representative set of GUV sections along with the computed 3D image (right). 12 optical sections were chosen from original data set containing 49 images. The slices are 0.1 µm apart. Only a hemisphere of the GUV was scanned to optimize the process duration, nevertheless obtaining necessary information. The object information is clearly seen to change with the z position. On the right, a projection enhancing the 3D structure of the GUV is shown, generated from the data set by computation. All scale bars correspond to 10 µm.

The method known as optical sectioning is the ability of confocal LSM to image a thin "optical slice" out of a "thick" specimen (typically, up to 100 µm). It gives the possibility to scan through the entire specimen providing a 3D data set,

i.e., information about the spatial structure of the object. In addition to the possibility to observe a single plane (or slice) of a "thick" specimen in good contrast, optical sectioning allows a great number of slices to be cut and recorded at different planes of the specimen, with the specimen being moved along the optical axis (z) by coordinating incremental changes in the microscope fine focus mechanism (using e.g. a stepper motor). Thereafter, by computation a 3D image of the specimen can be generated. A typical stack of optical sections (termed a z-series) through a GUV labelled with DiIC18 fluorescent dye together with the generated 3D structure is illustrated in Figure 2.4.3.

In the present work, various fluorescent dyes were implicated for visualization and characterization of GUVs. In general fluorophores are characterized by their absorption and fluorescence properties such as molar extinction coefficient and the quantum yield of a fluorophore. The first is characterizing the ability of a molecule to absorb light whereas the second describes the probability of a given excited fluorochrome to produce an emitted photon. The quantum yield of a fluorophore represents a quantitative measure of fluorescence emission efficiency, and is expressed as the ratio of the number of photons emitted to the number of photons absorbed. The quantum yield of fluorophores ranges topically between zero to one, however it largely varies depending on the environmental factors. In confocal microscopy, excitation of the fluorophores with a focused high power density laser beam increases the emission intensity up to the point of dye saturation. In the excited state, fluorophores are unable to absorb another incident photon until they emit a lower-energy photon through the fluorescence process. When the rate of fluorophore excitation exceeds the rate of emission decay, the molecules become saturated and the ground state population decreases. As a result, a majority of the laser energy passes through the specimen not contributing to fluorophore excitation. Therefore balancing fluorophore saturation with laser light intensity levels was essential for achieving the optimal signal-to-noise ratio in confocal experiments.

In the present work, GUVs where studied with confocal laser scanning microscopy. For visualization, the prepared vesicle solution was placed between two cover glasses 26 x 56 mm and 22 x 40 mm (Menzel GmbH, Germany) sealed with viscous silicon (Kurt Obermeier GmbH, Germany) to ensure hermetic closure of the vesicle solution and placed under the microscope for observations. The sample was left to rest in horizontal position for several minutes to let vesicles sediment to the lower cover glass due to gravity force driven by higher density of the sucrose inside the vesicles compared to the surrounding glucose solution. Two different fluorescent dyes $DiIC_{18}$ and DSPE-PEG2000-CF were used for visualization and characterization of the different phases in GUVs. One of them, DiIC18, is a positively charged molecule with fluorescent carbocyanine moiety located near the head group region of the bilayer and alkyl chains penetrating the lipid bilayer, which are known to preferentially partition into the Ld phase and to

be excluded from Lo and solid ordered (S_o) domains. Whereas DSPE-PEG2000-CF containing a hydrophylic molecule bound to the head group of a lipid, preferentially partitions into the Lo phase and is excluded from the Ld domains.

$DiIC_{18}$ was excited with the 561 nm diode-pumped solid-state (DPSS) laser line and the emission of the fluorescence was collected between 571 and 671 nm. DSPE-PEG2000-CF was excited with the 488 nm argon laser line, and the emission detected in 500 to 600 nm window. Filter cube 13 (Leica) consisting of BP 450-490, FT 510, LP 515 filters were used for distinguishing the dyes under the microscope. For visualization of cyt c protein binding to lipid membranes we used Alexa Fluor 633 carboxylic acid, succinimidyl ester. NHS-esters readily react with amino groups of proteins. Particularly lysine residues are highly reactive towards dye-NHS-ester. Excited by the 633 nm line of the He-Ne laser line, the Alexa Fluor 633 dye conjugated with cyt c is bright and photostable, with emission range between 643 to 700 nm. In the performed experiments using multiple channels, a combination of maximum two dyes was used. For those dyes isolation of emission spectra was distinct and was detected simultaneously without any interference (cross talk effect). The DiIC18 fluorescent dye was used separately and distinguishably for characterization of different phases to map the Gibbs triangle. The emission spectra of DiIC18, DSPE-PEG2000-CF and Alexa Fluor 633 dyes are presented in Figure 2.4.4.

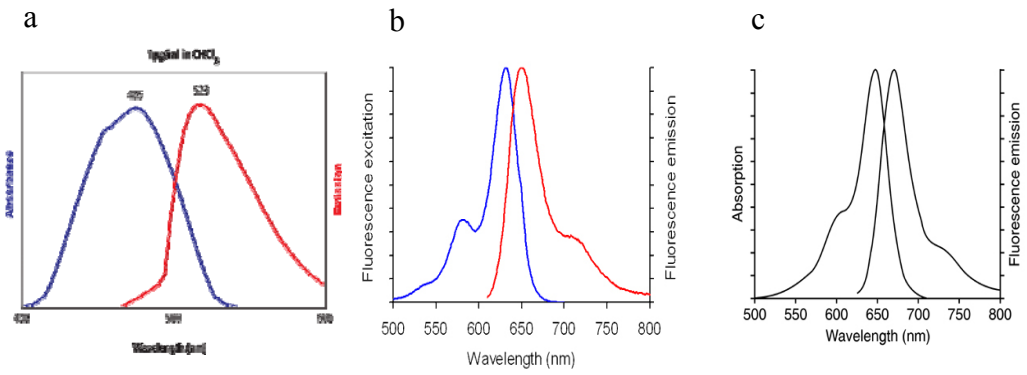

Figure 2.4.4 Absorption and fluorescence emission spectra of DSPE-PEG2000-CF fluorescent dye (a)[23]. Fluorescence excitation and emission spectra of Alexa Fluor® 633 (b)[23] and absorption/emission spectra of DiIC18 (c)[23].

2.5. Fluorescence spectroscopy

A Helios Gamma UV/VIS spectrophotometer (Fisher Scientific GmBH, Germany) was used to measure the absorbance spectra of yeast cyt c at various concentrations between 0.5 and 4.2 mM in a 2 mM HEPES/1 mM EDTA buffer (pH 7.5) in quartz cuvettes with pathlength of 1 cm. The absorption spectra were recorded in the wavelength range of 300 – 600 nm. Emission spectra of the same cyt c solutions were measured in the wavelength range of 530 – 700 nm on a Fluomax-4 Spectrofluorometer (Horiba Jobin Yvon, Japan).

2.6. Flow chamber experiments: domain area changes upon cyt c binding

Flow chambers allow dynamic fluid flow exchange in the system, herewith observing changes on the same object throughout the process. In the present work, flow chamber was used for single vesicle observation before and after binding of cyt c. The flow chamber used for experiments was home made and consisted of two teflon frames with holes on both sides for fluid exchange. The fluid enters from one side of the chamber and leaves from the opposite side. The teflon frames were sealed from above and below with glass slides and assembled in a way that the liquid does not leack to ensure optimal steady state. The buffer was injected into the chamber in a way to avoid bubble formations followed by adding the vesicle solution. In particular vesicles from two fluid phase coexistence region exhibiting two distinct domains were chosen, the chamber was left to rest under the microscope for allowing the vesicles to reach static state. Afterwards, cyt c solution was injected into the system with a programmable syringe pump (LAMBDA CZ s.r.o. Czech Republic) at sufficiently low speed not to disturb the system by fluid flow. Equilibrated for minimum 30 minutes after completely injecting the protein solution, changes in domain size influenced by cyt c partitioning into the membrane were recorded with confocal LSM. The recorded 3D images before and after injection of cyt c were analyzed and compared by calculating the area change of domains. The GUV was treated as a sphere, whereas the domain was a spherical cap, i.e., a portion of a sphere cut off by a plane. In Figure 2.6.1 as an example is shown computed 3D image recorded after injection of cyt c. The fluorescent dye DSPE-PEG2000-CF was used to visualize different domains. The dark green part, a spherical cap, corresponds to the Lo phase, and the lighter green part is the Ld phase.

If the radius of the sphere is r, the radius of the base of the cap is a, and the height of the cap is h, then the surface area of the spherical cap is:

2.6.1.

$$A = 2\pi rh$$

We measured the value of *r, a* and *h* and calculated the surface area for Lo spherical cap.

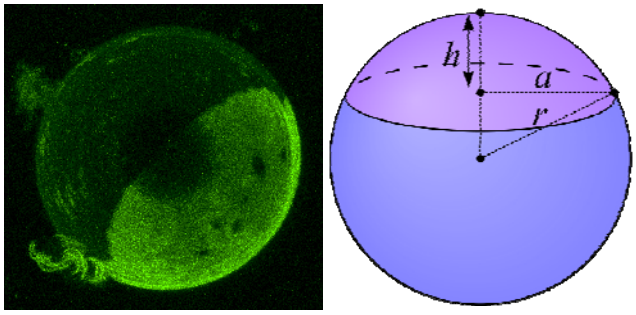

Figure 2.6.1 Left, 3D projection of GUV hemisphere after injection of cyt c. On the right side is shown schematic representation of spherical cap [23]. Lipids labeled with DSPE-PEG2000-CF dye. Dark green part corresponds to Lo phase and was treated as a spherical cap. Right, schematic representation of vesicle and domain along with characteristic parameters.

2.7. Isothermal titration calorimetry

Isothermal titration calorimetry (ITC) is a thermodynamic technique that directly measures interaction between the ligand and a receptor by detecting change in the energy levels during a molecular binding event at a fixed temperature [73]. ITC provides a whole thermodynamic profile of the molecular interaction in a single experiment providing values of parameters such as the binding constant K, reaction stochiometry N, the enthalpy change ΔH, the enthropy change ΔS and the free energy change ΔG.

Our measurements were performed with a VP-ITC microcalorimeter from MicroCal (Northhampton, MA) (Figure 2.7.1). The experiment is performed by placing two binding partners in the injection syringe and the ITC cell respectively. In our case, vesicle suspension as a titrant was injected into the ITC working cell filled with cyt c solution - titrand. The reference cell containing buffer 2 mM HEPES/1 mM EDTA (pH 7.5) and the working cell are placed in an adiabatic jacket chamber. However, the reference cell is kept at a tiny temperature difference compared to the working cell. When the titrant L is injected into the titrand P and the two components interact, heat release or absorption in the sample cell is measured in comparison to the reference cell filled with the buffer. Detected negative peaks denote exothermic process meaning that the heat is released during the interaction. Whereas positive peaks describe endothermic reaction when

external heat is needed to heat the cell. Calculation of the thermodynamic parameters is achieved by precise measurement of the energy required to maintain the temperature of the cell during several injections.

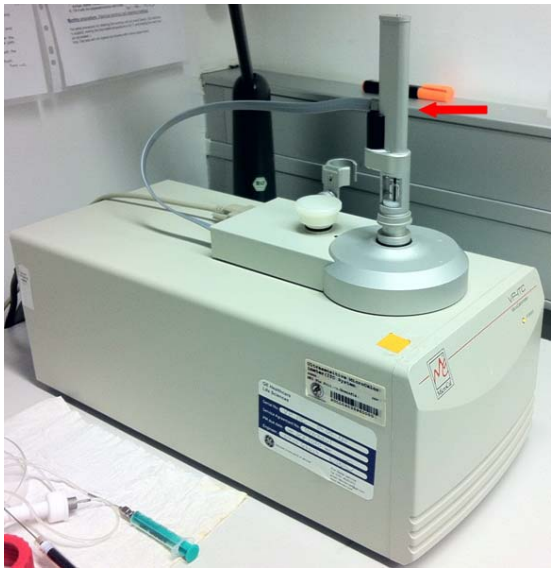

Figure 2.7.1 Isothermal titration calorimetry with the syringe pointed by red arrow, placed into the working cell.

In the performed experiments, a vesicle solution of 4mM lipid concentration with the total volume of 288 µl was injected stepwise into the 0.3 mM cyt c solution. The titrant was injected in 28 steps into the cell with the total volume of 1.442 ml. The first injection of titrant (2 µl) is discarded during the analyzes as dilution might occur during the equilibration process before the measurement. Then followed 10 µl injections spaced by time interval of 200 sec. The content of the working cell is constantly stirred at a stirring rate of 310rpm to ensure rapid mixing of the sample. Reference measurements, vesicle solution injected into the buffer and buffer injected into the cyt c solution, are always performed along with the experiment and the one with the highest impact subtracted during the data analyzes. The integrated heat change is plotted in µcal/sec against the titrant/titrand molar ratio of a raw data, from which then the reference measurement is subtracted. Integrated heat change with the respect to time leads to the apparent heat change $\Delta q_{i\ \mathrm{app}}$ between *i*-1 and *i* additions.

2.7.1

$$\Delta q_{i,\mathrm{app}} = q_i - q_{i\text{-}1}$$

where $\Delta q_{i,app}$ corresponds to the to the area of *i*th peak. $\Delta q_{i,app}$ is proportional to the calorimetric cell volume V_{cell} to the apparent molar enthalpy of association ΔH_{app} and to the concentration of the bound ligand $\Delta[L_i]_{bound} = [L_i]_{bound} - [L_{i-1}]_{bound}$. Taking in account the heat of ligand dilution $q_{i,dil}$ we can write

2.7.2

$$\Delta q_{i,app} = \Delta q_i + \Delta q_{i,dil} = \Delta[L_i]_{bound} * V_{cell} * \Delta H_{app}$$

ΔH_{app} is constant at fixed temperature, pressure and solvent conditions. V_{cell} is known and $\Delta q_{i,dil}$ is obtained from the titration of ligand into the buffer. ΔH_{app} and K are calculated from

2.7.3.

$$\Delta q_i = \Delta q_{i,app} - \Delta q_{i,dil} = N[P]_{tot}\, V_{cell}\, \Delta H_{app} * \Theta$$

$[P]_{tot}$ is a total concentration of protein in the sample cell and Δq_i effective heat change caused by the formation of the *PL* complex at the *i*th injection of the titration. Θ is the route of the quadratic equation [73]:

2.7.4

$$X^2_i - X_i * (1 + 1/NK[P]_{tot} + [L_i]_{tot}/N[P]_{tot}) + N[L_i]_{tot}[P]_{tot} = 0$$

where N is the number of independent binding sites for the ligand *L* on the macromolecule *P* in the cell. X_i is a degree of saturation defined as

2.7.5

$$X_i = \Delta[L_i]_{bound}/[P]_{tot}$$

$[L_i]_{tot}$ is the total concentration of *L* ligand added until injection *i*. Solving the quadratic equation (2.7.4) and substituting it into the equation (2.7.3) yields the thermodynamic parameters *N*, *K* and ΔH from a single titration experiment. The experimental data is plotted as a normalized heat change for injection *i*, in kcal/mole of injectant added, against the molar ratio of ligand to macromolecule after injection *i*.

2.8. Dynamic light scattering

We measured the size distribution of LUVs before and after each experiment, in all ITC measurements, on the one hand to confirm that vesicle preparation was done successfully, obtaining desired size LUVs, and on the other hand, to monitor size alterations during cyt c binding to the membranes. LUV sizes are below the optical resolution to be visualized with the microscope that is why we use dynamic light scattering (DLS) also called photon correlation spectroscopy performed by Zetasizer Nano – ZS (Malvern Instruments, Germany) (Figure 2.8.1).

Figure 2.8.1 Zetasizer Nano device with the cuevette shown enlarged in white frame. Zetasizer cuevette was used for measuring vesicle size and zeta potential.

The vesicle suspension was degassed to avoid bubble formation, sealed in a cuvette and placed into the temperature-controlled jacket for the cuvette at 25°C in the instrument. Afterwards, the vesicle solution is illuminated with a 4mW HeNe laser (632 nm) and the scattered light is monitored with a detector positioned at the scattering angle of 173°. Analyzing the fluctuation in scattering intensities is used then to calculate the size of particles within the sample [74, 75]. Particles in the suspension are constantly moving due to the Brownian motion - a random collision with the molecules of the surrounded liquid. When the vesicle suspension is illuminated by a light source, light will scatter in all direction and form a speckle

pattern. As the particles suspended into the liquid are constantly moving the speckle pattern will also appear to move – bright and dark areas will grow and diminish in intensity. The Zetasizer Nano system measures the rate of the intensity fluctuation to calculate the particle size. It is done by the digital correlator placed within the instrument by distinguishing the degree of similarity between signals over a period of time. The rate of decay for the correlation function occurs in milliseconds and depends on the particle size (Figure 2.8.2).

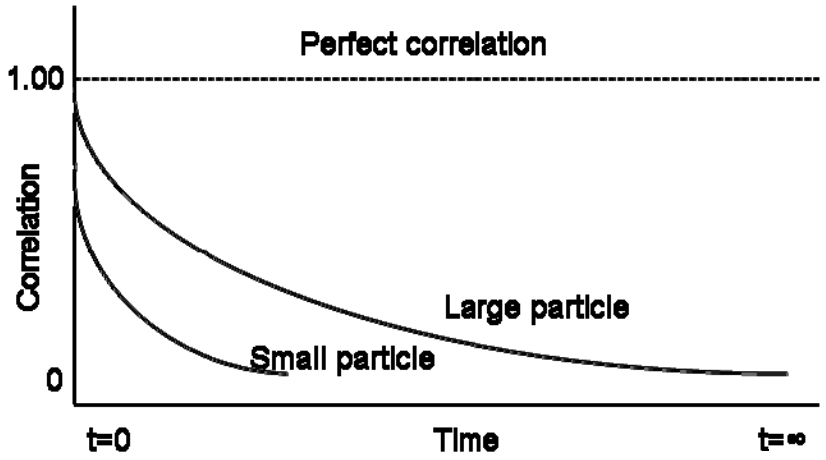

Figure 2.8.2 Correlation function for large and small particles. The rate of decay is correlated to the particle size- faster for the small particles compare to large ones.

The correlation function is calculated and related by the software to the particle size using the Stokes-Einstein equation

2.8.1

$$D = RT/N * 1/6\pi Zr$$

where D is the diffusion coefficient, R gas constant, T absolute temperature, N Avogadro's number, Z viscosity of the solution and r the radius of the diffusing particle.

2.9. Electrophoretic mobility and zeta potential

As DOPG lipids carry one net negative charge, vesicles made of the ternary mixture of DOPG/eSM/Chol exhibit a negative charge as well and it varies depending on the DOPG concentration in the membrane. To monitor the charge of the LUVs throughout the measurements was an initial step for characterizing of cyt c binding to the lipid membranes. For this reason we used the Zetasizer Nano which measures average electrophoretic mobility of the LUVs and converts it to zeta potential using the Smoluchowski - Hückel model [76].

The vesicle suspension was placed into the instrument where in a folded capillary an alternating electrical field was applied causing the directed motion of the vesicles and measuring the speed of the particle movement as a result. In our particular case, the negatively charged vesicles move towards the anode resulting in negative electrophoretic mobility. The negatively charged vesicles affect the distribution of the ions in the solution causing accumulation of the counter ions at the surface. The area where ions attach strongly to the particle is called the Stern layer which is followed by the outer diffusive area. When the electric field pulls the particle in one direction, ions within the Stern layer – beyond the boundary will move with the particle. That surface, which separates the bound charge from the diffuse charge around the particle, is called the surface of hydrodynamic shear or the slip surface. The electrostatic potential that exists on that surface is known as the zeta potential and it is that potential which is measured.

When electric field is applied to the vesicle solution, charged particles are attracted to the oppositely charged electrodes. Once equilibrium is reached the speed of the particles becomes constant. This velocity of a particle is referred to as its electrophoretic mobility. The technique that measures the speed is used within the Zetasizer Nano and is called Laser Doppler Velocimetry (LSD), a widely used method for fluid flow studies. The cell, where vesicle solution is placed has electrodes at both ends to which then potential is applied. The sample is illuminated by the laser beam (633 nm) and the scattered light at 17° combined with the reference beam detected by the receiving optics. This procedure produces fluctuating intensity which is proportional to the speed of the particles calculated by LSD. In its turn the velocity υ of the dispersed particle is proportional to the applied electric field E and defines the electrophoretic mobility with the following equation

$$\mu_e = \upsilon / E \qquad 2.9.1$$

The measured electrophoretic mobility is related to the zeta potential by the Henry equation:

2.9.2

$$\mu_e = 2\varepsilon z f(ka)/3\eta$$

where ε is the dielectric constant, z, the zeta potential, η the viscosity of solution and $f(ka)$ is the Henry function, with ka being the ratio of particle radius to the double layer thickness (the Debye length). For determination of $f(ka)$ function two general approximations are made. For systems with particles larger than 0.2 microns into 1mM salt solution, calculating the zeta potential is done according to the Smoluchowski model and $f(ka) = 1.5$. For smaller particles with low dielectric constant media $f(ka) = 1$ and is referred to as a Huckel approximation.

2.10. Image analysis

Fluorescence methods, because of their specificity and access to multiple simultaneous labels are well suited for membrane structure studies. Therefore, quantitative analysis allows obtaining information of differences between intensities across the phase boundary which can be related to the partition coefficient in the two phases. The following section describes the method to obtain membrane properties analyzed in terms of fluorescent dye partitioning behavior.
Confocal microscopy provides an image of a GUV, in which the intensity is linearly proportional to the concentration of fluorophore within the sample. Furthermore, dye partitioning is studied using linear methods in which ratios of intensities, corrected for difference in probe brightness, correspond to the partitioning coefficient of the two dyes in the two phases.

For the analysis of a confocal fluorescence image of the equatorial plane of a GUV, two algorithms (the maximum brightness (MB) and the least squares (LSQ) methods) can be used [77]. First of all, shape analysis of membrane equatorial sections, is performed which in turn relies on determination of the position and angle (orientation) of the membrane. From this slice, which is rotated to orient the symmetry (Z) axis in the vertical direction, the R-Z coordinates of the membrane as a function of arc length are determined. The angle of the membrane path θ (measured from the horizontal) and its derivative θ′ as a function of arc length S are then used for numerical analysis of physical shape parameters (Figure 2.10.1 a).

For determination of area fractions of Lo and Ld phases for an equatorial section of a phase-separated GUVs it is necessary to trace the shape of the membrane using the LSQ method the program written in MATLAB (The Mathworks, Inc. Natick, MA). The LSQ algorithm uses each pixel in the image as a data point, estimated as the square root of the number of photons in that pixel, and then fits by a second order polynomial through the data points. From the fit,

the position and curvature of the membrane can be estimated. For the tracing routine, the algorithm as the starting pixel value manually selects a coordinate, where membrane path is horizontal ($\theta = 0$) on the vesicle. Some of the parameters, such as the threshold value, the step size, and the maximum turn rate are used in MATLAB to optimize the trace. The output of the shape tracing routine provides x- and y-coordinates, membrane path angles, and pixel intensities (for each channel). After equatorial sections are traced, the fluorescence intensity can be quantified by averaging for all pixels within a region centered on the given pixel of the trace. The intensity in both channels is quantified separately and plotted as a function of arc length.

The partitioning of cyt c between Ld/Lo phases was characterized quantitatively by analyzing the intensity profiles of the fluorescence signal of the protein in confocal images of GUVs using the described method. The equatorial sections of the vesicles were traced by a LSQ algorithm, thereafter fluorescence intensities on the membrane of the vesicles extracted from the picture and the intensities of cyt c along the radial direction averaged over all the angles for both Ld and Lo phases (Figure 2.10.1).

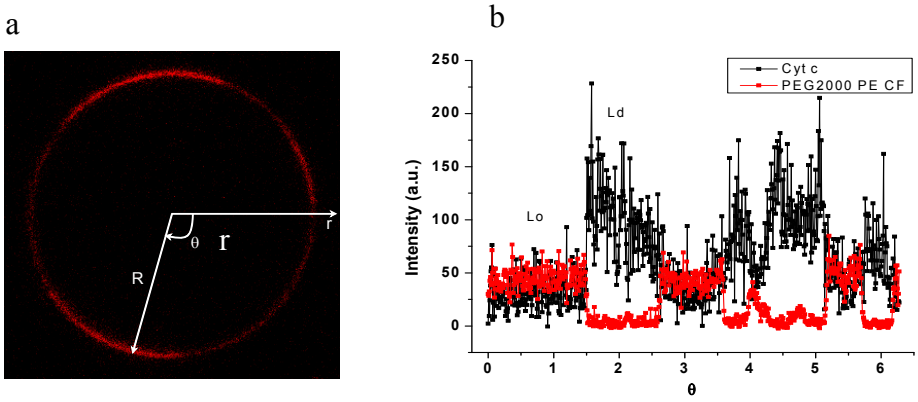

Figure 2.10.1 Top-view confocal images for a GUV composed of DOPG/eSM/Chol with fluorescent signal from labeled cyt c partition (a). Fluorescent intensities along the vesicle for labeled cyt c and DSPE-PEG2000-CF dye coming from Ld and Lo phases. Scale bar corresponds to 10 μm.

Finally the partitioning ratio of cyt c between Ld and Lo phases were obtained from the ratio of the areas under the radical intensity profile.

3. Results

In this chapter, we describe results about ternary mixture membrane phase states as a function of lipid composition and the effect of cyt c. GUVs composed of DOPG, eSM and Chol were characterized with confocal laser scanning microscopy. The main goal was to determine the thermodynamic phase diagram, and in particular, to locate the two fluid phase coexistence region (Ld/Lo) of the DOPG/eSM/Chol ternary mixture (see chapter 3.1). After mapping the phase diagram, we studied the interaction and partitioning of cyt c with the ternary mixture lipid membranes. The phase diagram of the DOPG/eSM/Chol lipid mixture was characterized in the presence of 0.6 mM cyt c and the influence of cyt c on the phase state of this ternary mixture was investigated (see chapter 3.2). Thereafter, partitioning of cyt c into multicomponent lipid membranes belonging to the two fluid phase coexistence region (Ld/Lo) was studied by calculating partitioning ratios between Lo and Ld phases (see chapter 3.3). In chapter 3.4, we describe the influence of cyt c on lipid demixing upon protein binding and characterize domain area changes depending on the different lipid compositions. Chapter 3.5 presents results from the protein purification procedure of the protein DC-SIGN. Isothermal titration calorimetry was used to investigate thermodynamic parameters of cyt c binding to DOPG/eSM/Chol lipid mixtures with different compositions. The enthalpy, entropy and stochiometry of the binding process were calculated (see chapter 3.6). In this chapter we also describe results about the effect of cyt c adsorption on the surface charge and size of large unilamellar vesicles made of DOPG/eSM/Chol investigated by Zetasizer Nano.

3.1. Characterization of the phase behavior of DOPG/eSM/Chol ternary lipid mixtures

In the present study we characterized GUVs, which are composed of DOPG, a low melting temperature unsaturated lipid carrying a net negative charge, eSM, a high melting temperature saturated lipid, and cholesterol. The transition temperature of DOPG is –18 ºC which means that at room temperature DOPG is in the fluid phase. On the other hand, eSM at room temperature is still in the gel phase. Thus, at room temperature membranes composed of this mixture can exhibit immiscibility depending on the specific membrane composition.

Confocal microscopy was used to explore in detail 75 different lipid compositions of GUVs in the Gibbs triangle characterizing the phase diagram of the DOPG/Chol/eSM mixture in buffer at room temperature (~ 25 °C) (Table 3.1.1). The examined compositions were classified according to the observed phase state of the membrane.

Our first aim was to locate the region of coexistence of liquid ordered (Lo) and liquid disordered (Ld) phases which is the biologically relevant one [78]. The fluorescently labeled lipid $DiIC_{18}$ used in our studies is known to preferentially partition into the Ld phase and to be excluded from Lo and solid ordered (So) domains [68]. DSPE-PEG2000-CF preferentially partitions into the Lo phase [69]. Vesicles belonging to So phase only have not been explored in the present study as this region is not biologically relevant. Our measurements suggested that it was sufficient to use only the dye $DiIC_{18}$ in order to characterize the phase diagram of DOPG/eSM/Chol from confocal images of GUVs as explained further.

In the same batch of GUVs one could observe a variety of domain sizes and area fractions. That is why the decision about the phase state of a particular membrane composition was set according to the behavior of the majority of GUVs in the sample. The following domain features were used to distinguish the various regions in the phase diagram. For vesicles in the single fluid phase (Lo or Ld) region, the fluorescent dye is homogenously distributed in the membrane and the vesicles appear smooth, quasispherical and with fluctuating membrane; see vesicle image in Figure 3.1.2 (a).

Table 3.1.1 The list of lipid compositions investigated for characterizing the phase diagram of the DOPG/Chol/eSM ternary mixture. Four different phase states were observed: fluid homogenous phase (Ld or Lo), two fluid phase coexistence (Ld + Lo), three phase coexistence region (Ld + Lo+ So) and gel-fluid phase coexistence (Ld + So or Lo + So).

Vesicle composition DOPG/Chol/eSM (molar ratios)				
Ld or Lo	Ld + Lo	Ld + Lo+ So	Ld + So or Lo + So	
7/2.3/0.7	5/2/3	6.3/1.7/2	6/1.3/2.7	5/1/4
7/3/0	5/1.7/3.3	7/1.7/1.3	4/0/6	4.8/1.2/4
6.3/3/0.7	5/1.3/3.7	7/1.3/1.7	5/0/5	5/0.7/4.3
6.7/3/0.3	4.7/2.3/3	6/2.7/1.3	6/0/4	5/0.3/4.7
5/2.3/2.7	5.3/1.7/3	6/1.6/2.4	7/0/3	5.3/0.7/4
5/2.7/2.3	4.6/1.4/4	6.7/1.5/2	4/1/5	5.7/0.3/4
4.3/2.7/3	4.3/1.7/4	6.4/2.3/1.3	8/0/2	7.3/1.7/1
3.5/2/4.5	4/2.3/3.7		7.7/0.3/2	7.7/1.3/1
6.3/2.7/1	4/2/4		7.3/0.7/2	8/1/1
6.7/2.3/1	4/1.7/4.3		7/0.7/2.3	3/1/6
7/2/1	5/2.3/2.7		7/0.3/2.7	4/1.3/4.7
3.3/1.7/5	4.5/2/3.5		6.7/0.3/3	4/1/5
3.5/2/4.5	6/2/2		6.3/0.7/3	4/0.7/5.3
3.3/2.7/4	5.5/2/2.4		6/0.3/3.7	4/0.3/5.7
3.7/2.3/4	5.7/2.3/2		6/0.7/3.3	3/1.3/5.7
3/2.7/4.3			7/1/2	3/0.7/6.3
3/2.3/4.7			6/1/3	3/0.3/6.7
2.7/2.3/5			5.7/1.3/3	

In the region of coexistence of the two fluid phases Lo and Ld, the domains have smooth borders see images in Figure 3.1.2 (b) and are free to move relative to each other. In regions of coexistence of one fluid phase and gel phase (Ld and So), the solid domains are depleted from fluorescent dye, appear dark, exhibit angular features and are rigid with fixed borders; see images in Figure 3.1.2 (c) These vesicles may also appear faceted. In GUVs in the three-phase coexistence region (Ld, Lo and So), three types of domains can be distinguished: angular, rigid and very dark So domains; weakly fluorescent Lo domains and strongly fluorescent Ld domains; see images in Figure 3.1.2 (d). All confocal snapshots of GUVs where made in 3D projection and only one hemisphere of the vesicle was captured, otherwise domains might overlap and it would be difficult to judge about the domain shapes. This is also necessary in order to avoid distortion of the images caused by membrane fluctuations. We did not detect vesicles with coexisting So and Lo domains in the studied compositions and because of no biological relevance we did not explore further.

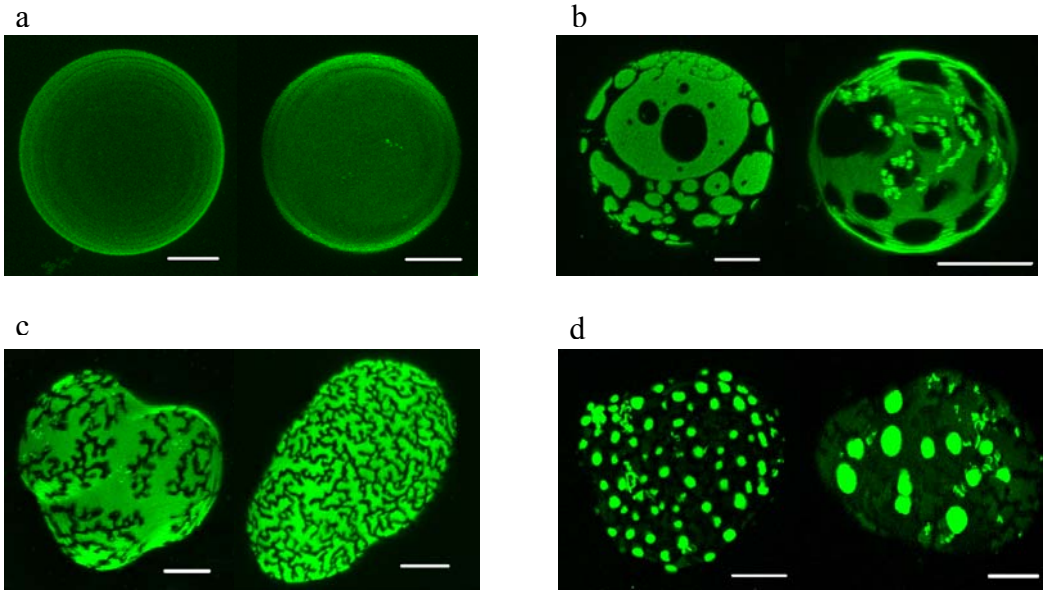

Figure 3.1.2 3D projections of GUVs composed of the DOPG/eSM/Chol ternary mixture obtained from confocal laser scanning microscopy observations at 25ºC. The bathing media used were 100 mM sucrose (inside)/110mM glucose solution (outside) in a 2 mM HEPES/1 mM EDTA buffer (pH 7.5). The vesicles were labeled with $DiIC_{18}$ which partitions preferentially in the Ld phase. Images representing homogenous fluid phase where no phase separation was apparent are shown in (a) corresponding to compositions 2/5.3/2.7 (left) and 3/4/3 (right), phase separated vesicles with coexisting two fluid Ld/Lo phases with compositions 4/4.3/1.7 (left) and 3/5.3/1.7 (right), are shown in (b). Vesicles with domains with angular shape and linear features (So phase) surrounded by Ld phase with compositions 5/4/1 (left) and 3/6/1 (right), are shown in (c). Vesicle images with composition 2/5.7/2.3 (left) and 1/6.5/2.5 (right) with coexisting three phases (Ld/Lo/So), are shown in (d). All scale bars correspond to 10 μm.

On the basis of these observations, we were able to partially construct the phase diagram of DOPG/eSM/Chol in buffer; see Figure 3.1.3. The phase diagram of DOPG/eSM/Chol in glucose/sucrose solutions has been partially characterized in reference [57]; see inset in Figure 3.1.3. Here, we observe that the area of the region with two fluid phase (Ld and Lo) coexistence is slightly expanded and shifted towards higher DOPG concentrations. Furthermore, we detect a three phase (Ld, Lo and So) coexistence region; see triangles in Figure 3.1.3 and the accompanying images.

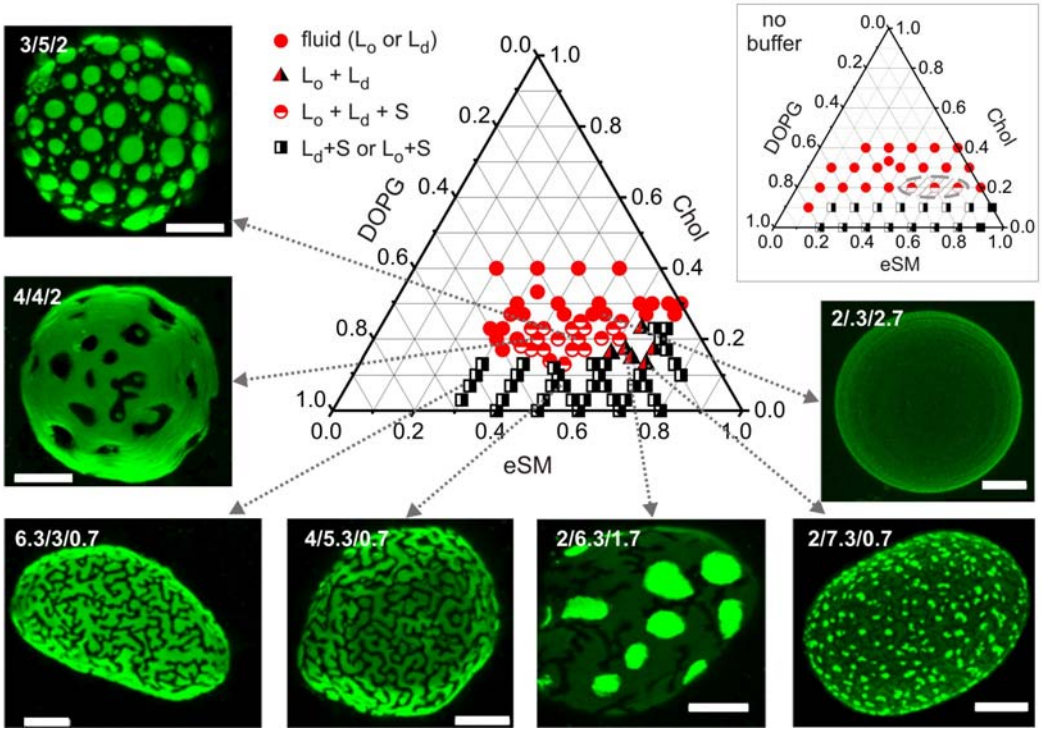

Figure 3.1.3 Phase diagram of the DOPG/eSM/Chol ternary mixture obtained from confocal laser scanning microscopy observations on GUVs at 25ºC. The GUV solutions and membrane labeling were the same as in Figure 3.1.2. The images, representing 3D projections, were used to identify different phase regions in the Gibbs triangle (see text for details). For clarity, only hemispheres of the vesicles are shown. For comparison, the inset in the upper right part shows the phase diagram of DOPG/eSM/Chol in buffer-free sugar solutions as obtained in Ref. [57]. The different symbols correspond to the notation in the main legend. The hatched area in the inset indicated the region of Lo-Ld phase coexistence.

The differences in the media bathing the membrane here and in the ref. [67] consist of the following: In reference [57], the investigated vesicles were prepared in 0.2 M sucrose solution and diluted in 0.2 M glucose solution. Here, the vesicles were prepared in 0.1 M sucrose solution and were diluted in 0.11 M glucose but in addition to this, we used 1 mM EDTA and 2 mM HEPES at pH 7.4. This suggests differences in the pH and the ionic strengths of the pure glucose and the buffered

solutions. We measured the pH of the 0.2 M glucose solution to be 6.1 and the solution conductivity is 1.8 mS/m, while that of the buffered glucose solution is 25.7 mS/m, i.e., more than ten fold higher. The small difference in the pH has presumably a negligible effect. The higher ionic strength of the buffered solution, however, could explain the observed changes in the phase diagram. Addition of salts, i.e. increased ionic strength, was already shown to stabilize the two-phase coexistence region of this ternary mixture, as expressed in an increase in the miscibility temperature [57].

3.2. The influence of cytochrome c on the phase behavior of DOPG/eSM/Chol ternary lipid mixtures

After characterizing the phase diagram of the DOPG/eSM/Chol ternary mixture in buffer, we studied the influence of cyt c on the membrane phase behavior. As already mentioned in section 1.1, cyt c influences the main phase transition of single-component PG lipids by broadening as well as lowering their gel to liquid-crystal phase transition temperature [13, 79]. In two-component membranes made of anionic and neutral lipids, cyt c was observed to induce lateral lipid redistribution [14-16] and, in some cases, formation of large micrometer-sized domains [14].

We investigated the phase state changes in DOPG/eSM/Chol vesicles brought into contact with solutions of cyt c at various concentrations in the range from 0.01 mM to 1.3 mM. At very low concentrations, less than 0.01 mM, no changes in the phase state of the membranes were detected under the microscope. At very high cyt c concentrations (starting from 1.3 mM) vesicle bursting was observed (data not sown). The choice for the final concentration at which we examined the effect on the ternary lipid membrane was 0.6 mM which corresponds to the biologically relevant system, namely, conditions in the cell [80]. It has been shown that the cyt c concentration in the intermembrane space vary considerably (0.5–5 mM) [81]. The vesicles were observed approximately 30 minutes after adding the protein solution to allow for equilibration and homogeneous distribution of cyt c in the chamber. The observations were limited to up to 1 h after mixing to avoid possible domain-induced budding in particular for membrane compositions close to the boundary of the two-fluid phase coexistence region.

Figure 3.2.1 summarizes the results describing the new phase region boundaries in the Gibbs triangle of the DOPG/eSM/Chol ternary mixture upon interaction with 0.6 mM cyt c. We first considered the vesicles from the two fluid phase coexistence (Ld/Lo) region. Upon the addition of 0.6 mM cyt c to the vesicles, membrane rearrangement was observed exhibited in changes in the domain sizes, however, without changing the phase state (Ld/Lo). We then explored vesicles with compositions from the single fluid phase region (Ld or Lo). In this case, cyt c induced phase separation and fluid Ld or/and Lo domain formation depending on the specific lipid composition of the vesicles (Figure 3.2.1).

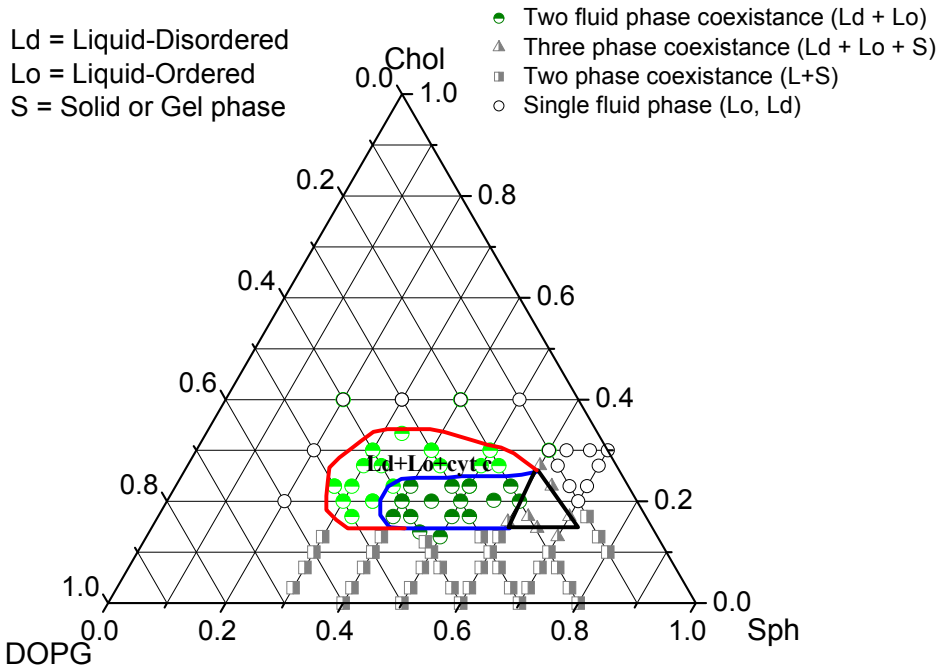

Figure 3.2.1 Change in the phase diagram of the DOPG/eSM/Chol ternary mixture in the presence of 0.6 mM cyt c at 25˚C. The area outlined with blue line denotes the region of two fluid phase coexistence in the absence of cyt c as displayed in Figure 3.1.3 this area is expanded (see red boundary) in the presence of 0.6 mM cyt c. The area located in the black triangle corresponds to the three phase coexistence region. The GUV solutions used were 100 mM sucrose (inside)/110mM glucose solution (outside) in a 2 mM HEPES/1 mM EDTA buffer (pH 7.5).

The detected changes are in accordance with the previous observations studying the phase state alteration and domain formations caused by interaction of oppositely charged lipid membranes, namely, when large unilamellar vesicles composed of DOPG/eSM/Chol were brought in contact with positively charged DOTAP vesicles [57]. We also examined the lipid compositions from Ld/So and Ld/Lo/So phases. In these regions of the phase diagram, cyt c was not observed to alter the phase states of the membranes. To conclude, in the presence of 0.6 mM cyt c with DOPG/eSM/Chol ternary mixture we observed enlargement of the region of two fluid phase coexistence, which is represented with the red border in Figure 3.2.1. Adding cyt c to the GUVs mainly influences the phase state of single fluid phase region by inducing phase separation and fluid phase domain formation.

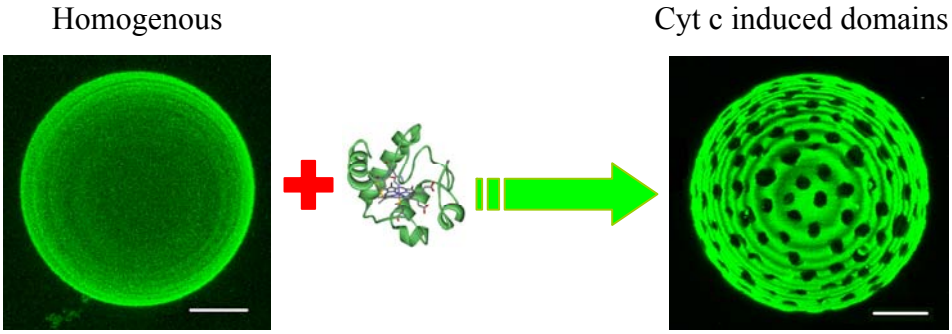

Figure 3.2.2 3D projections of GUVs composed of the DOPG/eSM/Chol ternary mixture obtained from confocal laser scanning microscopy observations at 25ºC. The GUV solutions used were 100 mM sucrose (inside)/110mM glucose solution (outside) in a 2 mM HEPES/1 mM EDTA buffer (pH 7.5). The vesicles were labeled with $DiIC_{18}$ which partitions preferentially in the Ld phase. On the left is a shown vesicle in homogenous fluid phase state with lipid composition 2/5.3/2.7 before adding cyt c. On the right a vesicle from the same batch after adding of 0.6 mM cyt c. Scale bars correspond to 10 μm.

In our observations domain formation induced by cyt c appear to occur in both leaflets simultaneously. We did not observe phase separation only in the outer leaflet of vesicles, as there was "registration" of the domains. In the opposite case one would expect difference of the fluorescence between inner and outer leaflets of vesicles.

We also investigated vesicles in different phase states in the presence of cyt c at lower concentration down to 0.01 mM. At such concentrations of cyt c we did not detect changes in the phase state of the membranes (data not shown). Considering our experience, phase state alteration of negatively charged ternary mixture membranes should strongly depend on the concentration of positively charged protein. At high concentrations of cyt c (1.3 mM and up), the changes induced on the membrane phase state are difficult to characterize because vesicles were observed to collapse similarly to events reported on GUVs containing cardiolipin [12]. The final lipid protein (L/P) concentration ratio by only taking in account total amount of the negatively charged DOPG is about 0.009 at cyt c concentration of 0.6 mM. Compared to previous studies about the L/P ratio dependence of cyt c interaction and partitioning into pure DOPG vesicles [9], the concentration ranges we explored fall in the range of dominant electrostatic interactions between the positively charged cyt c with membranes made of negatively charged PG lipids. However, when making such comparison one should take in account a number of factors, among which the low ionic strength in our measurements as compared to previous studies. Considerable amount of lipids are lost during the preparation of GUVs by the electroformation method this amount is difficult to estimate when calculating lipid concentrations. In the above estimate, we ignored this lost.

3.3. Partitioning of cytochrome c in DOPG/eSM/Chol membranes with fluid domains

Our next aim was to quantitatively characterize the partitioning of cyt c in vesicles which belong to the region of coexistence of two fluid phases: the raft-like Lo phase, and the non-raft like Ld phase. Preferential partitioning of positively charged cyt c was expected to occur into Ld domains, as they are mainly composed of negatively charged DOPG lipids. That is why we used the fluorescent dye DSPE-PEG2000-CF, which partitions preferentially into this phase and is excluded from the Ld phase. In this way we visualize the vesicle domains and avoid major interference between fluorescence of labeled lipids and protein.

Initially, we considered using the autofluorescence of cyt c to visualize the adsorption of the protein to the membrane. A number of studies in the last 50 years have been dedicated to the investigation and characterization of cyt c structure and spectroscopic properties. The intensity and wavelength of maximum absorption was found to be very sensitive to the solvent and pH, see e.g. references [66, 82, 83] Amino acid composition studies of the protein revealed that yeast cyt c contains the fluorescent residues tryptophan, tyrosine and phenylalanine [83-85], which can contribute to the intrinsic fluorescence of the protein. We measured the absorption and emission spectra of yeast cyt c under the conditions used in this work. Cyt c exhibits fluorescence in the wavelength region around 500nm. Presumably, this is due to the heme moiety. Figure 3.3.1 shows the spectra of the protein at different concentrations in 2 mM HEPES/1 mM EDTA buffer (pH 7.5).

Because of the week emission signal, as well as overlapping spectra with that of DSPE-PEG2000-CFT, it was not possible to perform intensity analyzes using only the intrinsic fluorescence of cyt c. Thus, for visualization and fluorescent intensity analyzes cyt c was labeled with Alexa Fluor 633. The procedure of protein labeling is described in chapter 2.3 of Materials and Methods section. The excitation and emission spectra of Alexa Fluor 633 fluorescent dye is given in Figure 2.4.4 (b) of Materials and Methods section.

To characterize the preferential partitioning of cyt c between Ld and Lo phases we chose three different lipid compositions from the two fluid (Ld/Lo) phase coexistence region in the Gibbs triangle. These lipid compositions were DOPG/eSM/Chol = 2/6/2, 3/5/2 and 4/4/2. Note that the cardiolipin (CL) concentration in the inner membrane of mitochondria in biological membranes is 18% to 24% by weight of total lipids (inner membrane (IM) and IM contact sites) [61].

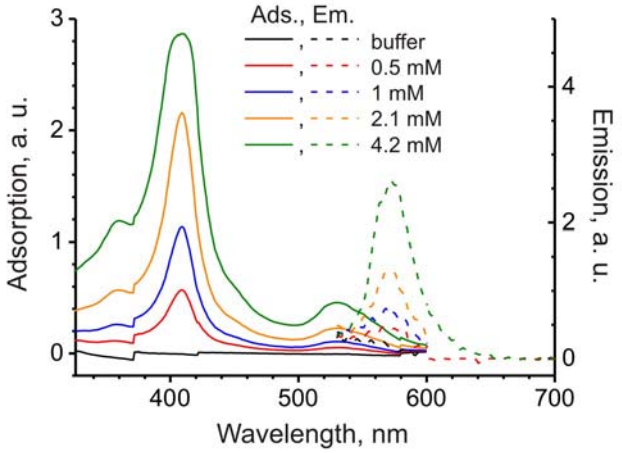

Figure 3.3.1 Absorption (left axis, solid curves) and emission (right axis, dashed curves) spectra of yeast cyt c in 2 mM HEPES/1mM EDTA (pH 7.5) buffer. Absorption in the visible range (relevant for the microscopy observations) occurs in the wavelength range of 500 nm – 580 nm, and emission is observed between 540 nm and 620 nm.

Taking in account that CL possesses two negative charges compared to PG which carries only one net negative charge, the studied lipid compositions are comparable in the biologically relevant charge amount. After preparing the GUV solutions, labeled cyt c was dropwise added to each of the vesicle solutions of different lipid composition separately and was examined with confocal scanning microscopy. Figure 3.3.2 shows representative cross section confocal images of a vesicle from the Ld/Lo phase coexisting region after adding 0.6 mM cyt c.

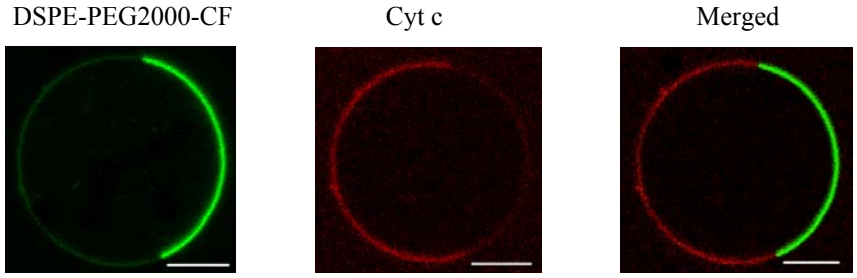

Figure 3.3.2 Equatorial cross section confocal images of a GUV composed of 4/4/2 DOPG:eSM:Chol, with fluorescent signals from DSPE-PEG2000-CF (green) partitioning mainly in the Lo phase (left), from labeled cyt c (red) adsorbing predominantly to the Ld phase (middle), and their merged image (right). Scale bars correspond to 10 μm.

As it is evident from the images, cyt c preferentially partitions into the Ld phase i.e. the DOPG rich domain. This result was expected as positively charged

cyt c would preferentially interact with the more negatively charged Ld domains. This is also in agreement with a recent study where authors have shown preferential partitioning of cyt c into CL rich domains [12]. However, our observations provide evidence for weak partitioning of cyt c also into the Lo domains. Observation of cyt c partitioning in Lo phase possibly results from the fact that even though the lipids phase separate, some amount of charged lipids are present in the raft like phase. The partitioning ratio between the two fluid phase domains for cyt c varies depending on the specific lipid composition which will be discussed in detail below.

3.3.1. Intensity profile analysis: quantitative characterization of the partitioning of cytochrome c between the Lo and Ld phases

The partitioning of cyt c between Ld/Lo phases was characterized quantitatively by analyzing the intensity profiles of the fluorescence signal of the protein in the confocal images of GUVs using a program written in Matlab.

Vesicles used for intensity profile analyzes were with the same lipid compositions as those used for preferential protein partitioning studies (2/6/2; 3/5/2; 4/4/2) (see previous section). Samples were observed following at least 30 minutes of equilibration after introducing cyt c in the chamber to make sure that the adsorption on the vesicle reached equilibration. Our studies suggest that approximately 15 to 20 minutes are sufficient for this equilibration process, see Figure 3.3.3. To evaluate this we have measured the fluorescence intensity of cyt c adsorbed in a selected vesicle throughout a period of 30 min after introducing cyt c in the chamber. The same vesicle was monitored during 30 minutes recording images every 5 min. The intensity values in the figure were measured then by analyzing images using the Matlab program. Error bars were obtained by analyzing the same image several times and calculated standard deviation. Thereafter, cross sections of vesicles were taken with confocal laser scanning microscopy. Beforehand we ensured that during capturing of images (requiring max 3min), bleaching of the fluorescent label of cyt c by laser exposure does not occur. Figure 3.3.4 below shows the intensity changes during 3 min of laser exposure for the fluorescent dyes of cyt c and the lipids. The intensity values in the figure below were obtained by analyzing the intensities from cross section images with Matlab separately for the fluorescent dye of the lipids partitioning into the Lo, Ld phases and for fluorescently labeled cyt c partitioning into the Ld, Lo phases. Error bars were obtained by analyzing the same image several times and calculated standard deviation. As it is seen from Figure 3.3.4, during the time necessary for image capturing, intensity of fluorescently labeled cyt c does not change. It means that evaluated values of intensity profile were not altered by bleaching of the dye. In contrast, the lipid dye bleaches dramatically during 3 minutes. However, it is not important in our case, as for calculation of partitioning ratios we use fluorescence intensity of labeled cyt c only.

The partitioning of cyt c into the membrane phases was quantitatively evaluated by analyzing the fluorescence intensity of cyt c in confocal images of GUVs. The analysis mainly involves the tracing of the equatorial sections of the vesicles by a least squares algorithm [77] and the subsequent statistics of the fluorescence intensity, see also section 2.10. The detailed procedure of such an analysis is illustrated in Figure 3.3.5. It includes the removal of background signal and finding the high intensity region along the membrane to locate the center of the vesicle and the membrane contour (Figure 3.3.5 (a,b)).

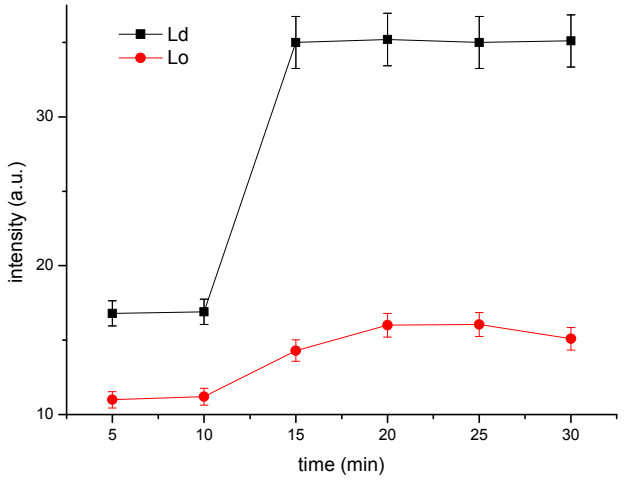

Figure 3.3.3 Saturation of 2/6/2 lipid compositional membranes with cyt c shown with intensities separately for Ld and Lo phases monitored during 30 min after introducing cyt c in the observation chamber.

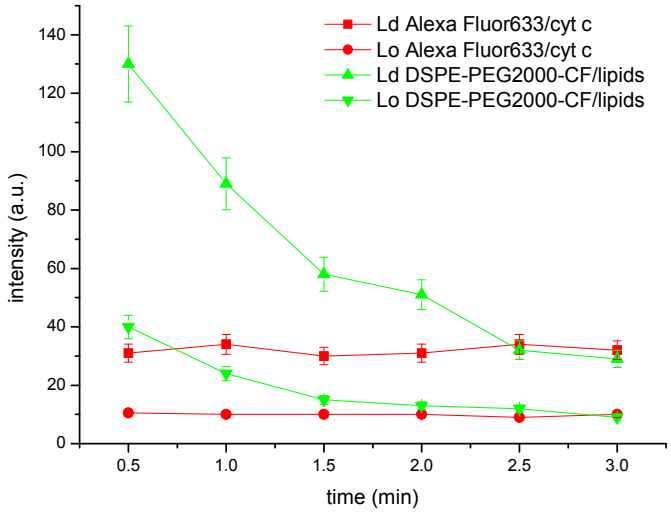

Figure 3.3.4 Intensity changes from fluorescent dyes during laser source exposure shown for labeled cyt c and lipids with composition 2/6/2, during 3 min measured separately for Ld and Lo phases.

Thereafter the fluorescence intensities on the membrane of the vesicles were extracted from the picture after changing from a Cartesian coordinate system to a polar one (Figure 3.3.5 (c)). The Ld and Lo phases were identified from the angular intensity profile of the signal from cyt c, which partitions more into the Ld phase. Then the intensities of cyt c along the radial direction were averaged over

all the angles for both Ld and Lo phases (Figure 3.3.5 (d,e)). Finally the partitioning ratio of cyt c between Ld and phases were obtained from the ratio of the areas under the radial intensity profile. The average partitioning ratio was found to be 3.4 for composition 2/6/2, 2.4-for composition 3/5/2 and 1.7 for 4/4/2 composition respectively.

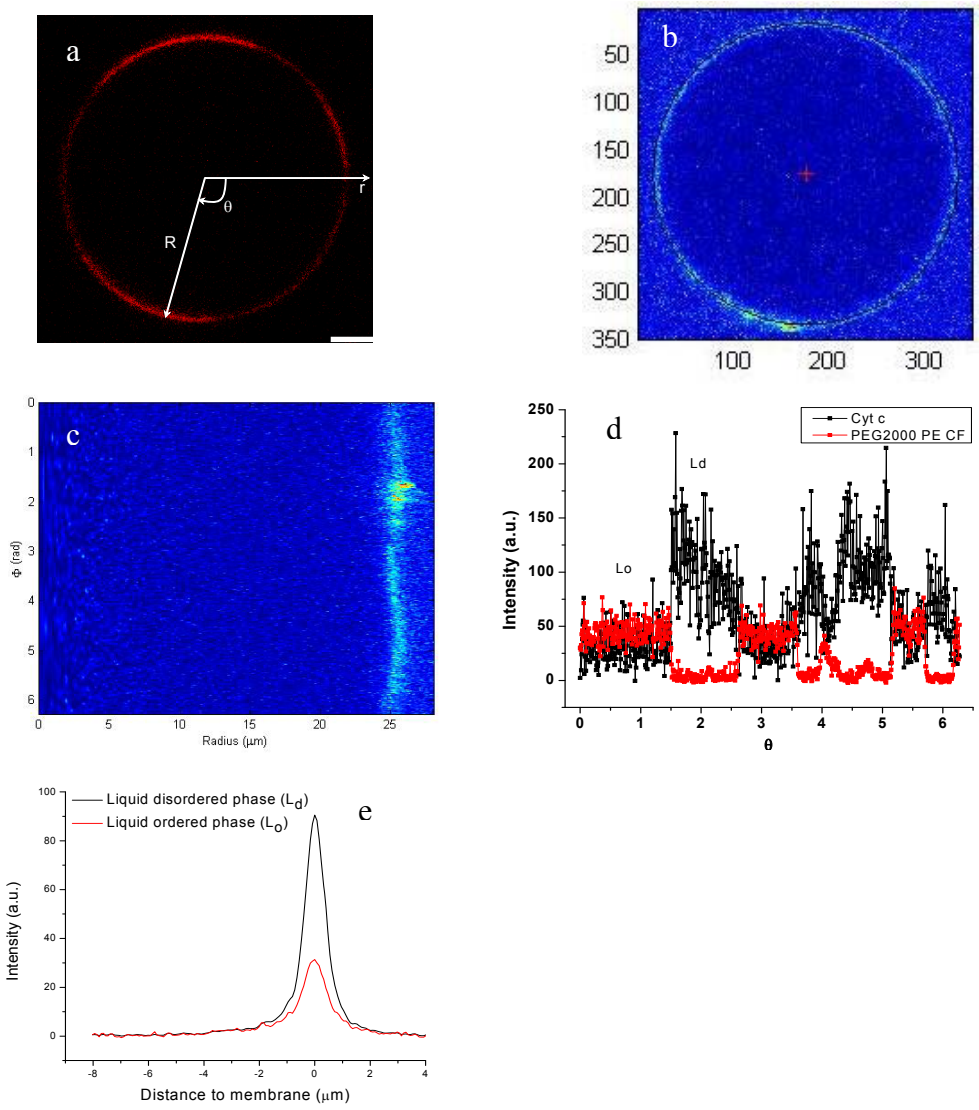

Figure 3.3.5 (a) Top-view confocal images for a GUV composed of DOPG/eSM/Chol = 4/4/2 with fluorescent signals from cyt c partition into the different fluid phases. (b) Background subtraction and localizing the center and a circular contour. (c) Fluorescence intensity on the membrane of the vesicles on a polar coordinate system. (d) Angular dependence of the fluorescent intensities along the vesicle for cyt c and DSPE-PEG2000-CF dye, which partition more into the Ld and Lo phases, respectively. (e) Averaged intensity profile of cyt c partitioning into the vesicle from Ld (black) and Lo (red) phases.

3.3.2. Partitioning ratios between domains in the liquid ordered and liquid disordered phase

In order to quantitatively characterize the partitioning of cyt c between the Lo and Ld phases, we separated the signal from the red (cyt c) and the green (Lo phase) channels. The signal in the green channel was used to localize the Lo and Ld phases. From the red channel data we measured the intensity profiles along the vesicle contour for the protein partitioning in the Lo and Ld phases (Figure 3.3.6) as described above. For each of the three compositions 2/6/2; 3/5/2; 4/4/2 at least 8 different vesicles from the same batch were collected and analyzed.

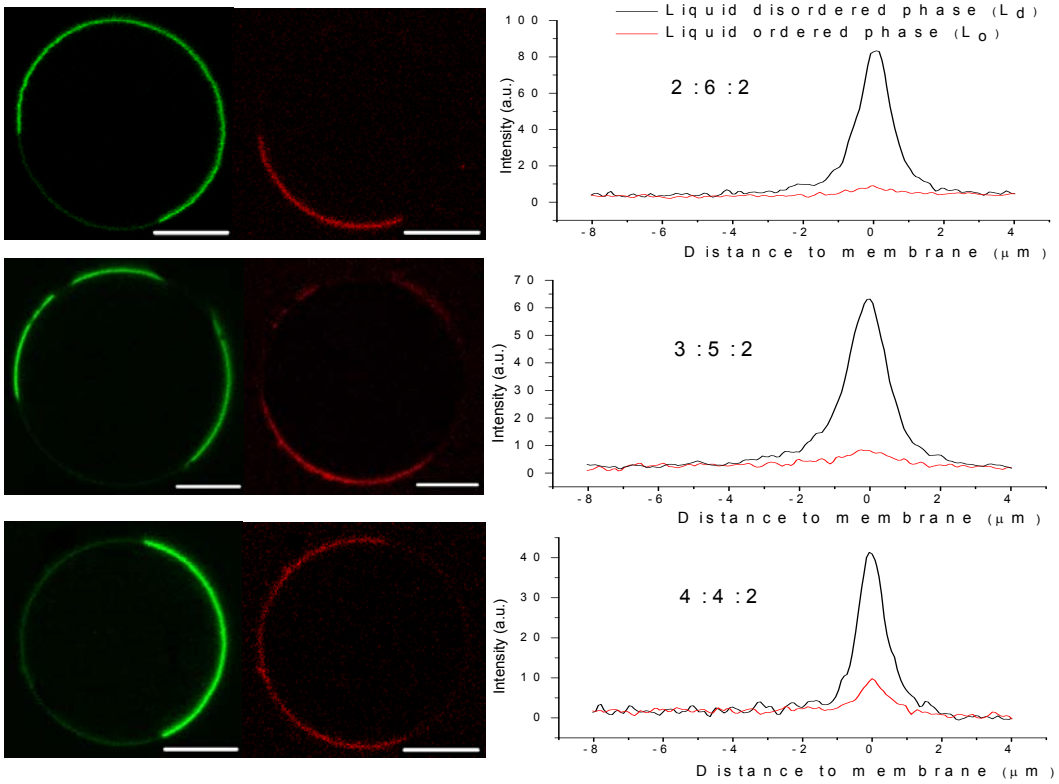

Figure 3.3.6 The left panel shows 2D snapshots of vesicles with compositions from top to bottom 2/6/2; 3/5/2; 4/4/2. On the left panel, the corresponding graphs provide examples for the intensity profiles of cyt c from the Ld (red curve) and Lo (black curve) phases on the vesicles with different lipid compositions. Scale bars correspond to 10μm.

Figure 3.3.7 shows a graph which describes the dependence of the cyt c partitioning ratio (Ld/Lo) in membranes with different lipid compositions from the two fluid phase coexistence region. Intensity calculation method is introduced and described in detail in chapter 2.10 in section Materials and Methods. Error bars were obtained with the method called error propagation.

Propagation of uncertainty or propagation of error is the effect of errors on the uncertainty of a function based on them. In our case, we take in account the errors separately from measured values of intensity of Ld and Lo when calculating the ratio between them.

The results suggest that the partitioning of cyt c into phase separated membranes depends on the specific lipid composition of the domains. The protein prefers adsorbing to domains with higher concentration of DOPG and the partitioning ratio between Ld /Lo phases decreases with increased PG concentration, giving us insight about the compositional differences of vesicles in different states. This in turn can be employed for characterizing the composition of the respective phases and in this way locate and define the exact orientation of tie lines in the region of two fluid phase coexistence.

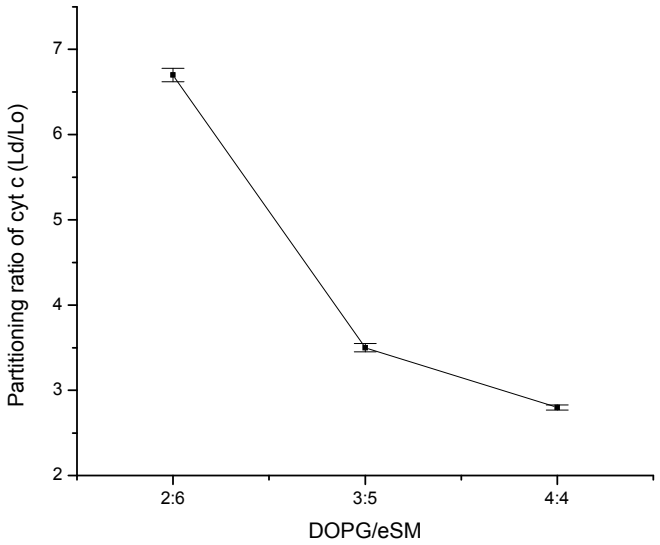

Figure 3.3.7 Dependence of cyt c partitioning between Ld and Lo phases into different lipid compositions of 2/6/2, 3/5/2 and 4/4/2 as given by the intensity ratio of the cyt c signal in the Ld and Lo domains. Error bars were calculated by standard deviation of the data using error propagation method.

3.4. Characterization of domain size changes upon binding of cytochrome c to DOPG/eSM/Chol membranes

As described in chapter 3.2, we characterized the change in the phase diagram of the ternary lipid mixture DOPG/eSM/Chol induced by interaction of cyt c with lipids. It was shown previously that in binary PC/PG mixtures, cyt c induces local demixing of PG and PC molecules [16]. In combination of resonance energy transfer measurements with Monte-Carlo simulations, the authors have shown that at lower PG concentrations, cyt c induces the formation of lateral domains enriched in anionic lipids, and that at high PG concentrations, the lipid distribution is close to random. The size of the formed domains is comparable to the protein size suggesting that lipid demixing takes place locally at the contact site of the protein with the lipids [16].

To detect the changes in the domain morphology directly upon contact with cyt c solutions, we followed the response of individual vesicles while exchanging the external media. This was done using a home made flow chamber described in detail in chapter 2.6 in section Materials and Methods. This approach allows us to follow and capture alterations of the domain size and vesicle morphology in the absence and presence of cyt c. In our experiments, we prepared vesicles with already characterized composition, namely the three lipid compositions from the two fluid phase coexistence region (2/6/2; 3/5/2; 4/4/2) and we used the same concentrations of the lipids, protein and the fluorescent dye as in the measurements for intensity calculations (chapter 3.3.1). For the observation, we chose vesicles only with two domains. Apart from being well equilibrated (the phase separation and domain coalescence is complete), for such vesicles calculation of the domain areas was simplified. The vesicles were labelled with PEG2000PECF. Figure 3.4.1 shows results, which suggest that the area of the Lo phase decreases in the presence of cyt c and this change diminishes with increasing PG concentration. Herewith, the vesicle size itself does not change after protein addition.

Our results are in a good agreement with theoretical models proposed by Sylvio May et al. [86], where authors have shown that lipid redistribution at the contact sites is more evident in lipid mixtures with lower concentration of anionic lipids compared to the mixtures with higher charge densities. Extend of the lipid redistribution depending on the different charge densities between protein and lipids were evaluated [86]. As already mentioned in section 3.2, domain area changes induced by cyt c occured in both leaflets simultaneously. There was “registration” of the domains in all cases.

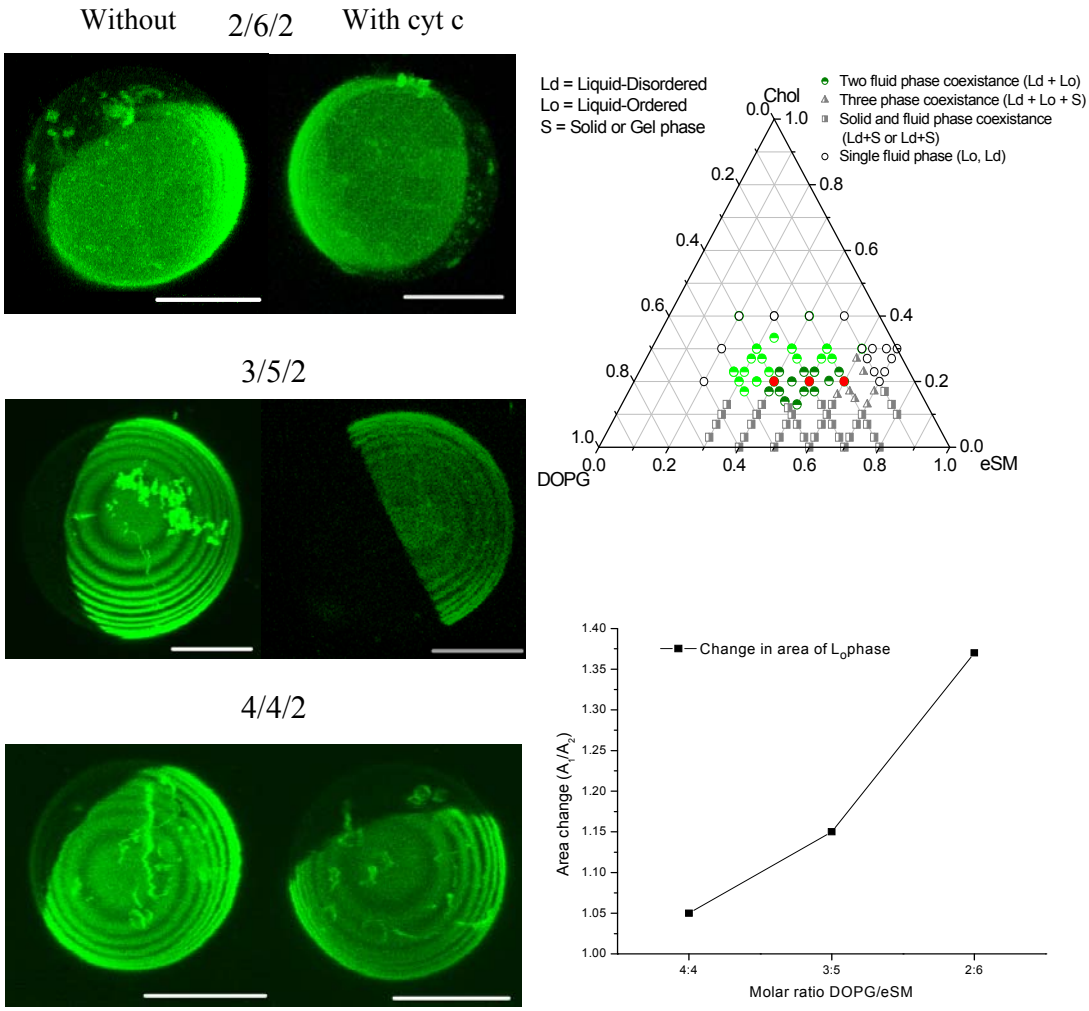

Figure 3.4.1 Change in the domain area upon addition of cyt c in two-phase vesicles with Lo and Ld domains. The three explored compositions are shown in the phase diagram (upper left). The right panel includes 3D snapshots of vesicle hemispheres made of three different lipid compositions before and 30 min after adding cyt c. On the graph (lower left) the relative area change of the Lo domain (green), A_1/A_2, is plotted for the three different lipid compositions explored, where A_1 and A_2 are the areas of the Lo domain before and after adding cyt c, respectively. Scale bars correspond to 10µm.

3.5. Thermodynamic characterization of cytochrome c binding to DOPG/eSM/Chol membranes

In parallel with confocal laser scanning microscopy, binding of cyt c to the charged multicomponent lipid membranes was studied thermodynamically with isothermal titration calorimetry. Previously, binding of cyt c to charged single-or two-component membranes was characterized widely with a number of different techniques. Differential scanning calorimetry (DSC) studies have shown enthalpy changes associated with the adsorption of protein to 1,2-ditetradecanoyl-*sn*-glycero-3-phospho-(1'-*rac*-glycerol) (DMPG) lipids. At high temperatures, the enthalpy changes were associated with lipid structural changes and at low temperature with protein-bound vesicle aggregation [87]. By nuclear magnetic resonance (NMR) [88, 89], resonance Raman spectroscopy (RR) [90] and circular dichrosim (CD) [91] it was shown that the binding of cyt c to anionic phospholipids induces changes in the confirmation of the protein. With CD and RR spectra, different heme configurations of cyt c bound to DOPG lipids have been observed [9]. The authors have shown that binding and partitioning of cyt c into DOPG lipid membranes highly depends not only on the lipid to protein ratio, but on the ionic strength of the solution as well. At low L/P ratios (<18) cyt c electrostaticaly binds to DOPG lipid membranes, whereas at higher L/P ratios (>18) the protein partially penetrates into the membrane [9].

T. Heimburg and L. Biltonen described in details the thermodynamics of cyt c binding to DMPG lipids at various temperatures characterized by ITC [87]. At low temperatures (7-20°), the binding isotherms suggest lipid structural changes upon protein binding. At higher temperatures (23-41°), the direction of the peaks in the binding isotherms, changing from endothermic to exothermic, suggests biphasic behavior of the process and aggregation of protein-bound vesicles. Isothermal titration calorimetry was implicated as well to study the thermodynamics of cyt c binding to DOPG lipid membranes [92]. Despite of the numerous studies, binding of cyt c have been characterized only for single charged or two component lipid mixture membranes. Here we investigated the thermodynamics of cyt c binding process to ternary lipid mixtures. One of the components, DOPG, carries one net negative charge mimicking the physiological environment of cyt c. Increasing the complexity of the membrane composition brings us closer to the natural lipid membranes which in turn gives opportunities for better describing cellular processes.

Isothermal titration calorimetry

Isothermal titration calorimetry was used to thermodynamically characterise the preferential binding of east cyt c with vesicles with different lipid composition. We aimed to study the interaction of cyt c to membranes with two different compositions from the homogenous single-phase region of DOPG/eSM/Chol phase diagram. These compositions are outside of the area in which 0.6 mM cyt c induces phase separation (shown on Figure 3.5.1 (d)). One of these compositions, 6/2/2, is in the Ld phase region and the other, 1/6/3, belongs to the Lo phase region. Binding of cyt c to these two membranes mimics the binding of cyt c to different domains in vesicles whose composition lies in the 2-fluid phase coexistence region. Our ultimate goal was to characterize the binding of cyt c to the Lo and Ld phase and eventually compare the stoichiometry of binding to the partitioning ratios obtained from confocal microscopy in GUVs.

Extruded vesicle suspension was stepwise titrated into the 0.3mM protein solution and the heats of binding from each injection recorded. The data revealed exothermic binding process with a strong heat absorption for the 1/6/3 composition and weaker for 6/2/2 lipid mixtures. We studied as well the binary mixture in single phase state with lipid composition of DOPG/eSM/Chol 0/6.6/3.3. The latter mixture allows comparison to 1/6/3 lipid compositional membranes excluding the effect of DOPG. In this way, we intended to separate the binding effect of cyt c to zwitterionic binary mixtures of eSM:Chol lipids from possible electrostatic interaction of the protein with DOPG.

Figure 3.5.1 shows the dependence of heat release on time and the integrated heat of each injection as a function of lipid to protein molar ratio for 6/2/2, 1/6/3 and 0/6.6/3.3 lipid vesicles interacting with 0.3mM cyt c in 1 mM EDTA and 2 mM HEPES buffer at pH 7.4. As it is seen from the graphs, the heat peaks are exothermic for all three compositions, but higher for 1/6/3 (Figure 3.5.1 (b)) and 0/6.6/3.3 (Figure 3.5.1 (c)) lipid mixtures in comparison to 6/2/2 (Figure 3.5.1 (a)).

The measurements were repeated several times to check for reproducibility. Along with each experiment, reference measurements were performed, for vesicles injected into the buffer as well as buffer injected into the protein. We have subtracted both reference measurements during the data analyzes, because the data values of the reference measurements were comparable to each other. Figure 3.5.2 represents the calorimetric data of integrated heat per injection plotted against the lipid to cyt c molar ratio. We have considered interaction of cyt c only to the outer leaflet of LUVs stipulated from the fact that cyt c is a hydrophilic protein with size comparable to the membrane thickness and it is not able to cross the bilayer and interact with the inner leaflet of the membrane.

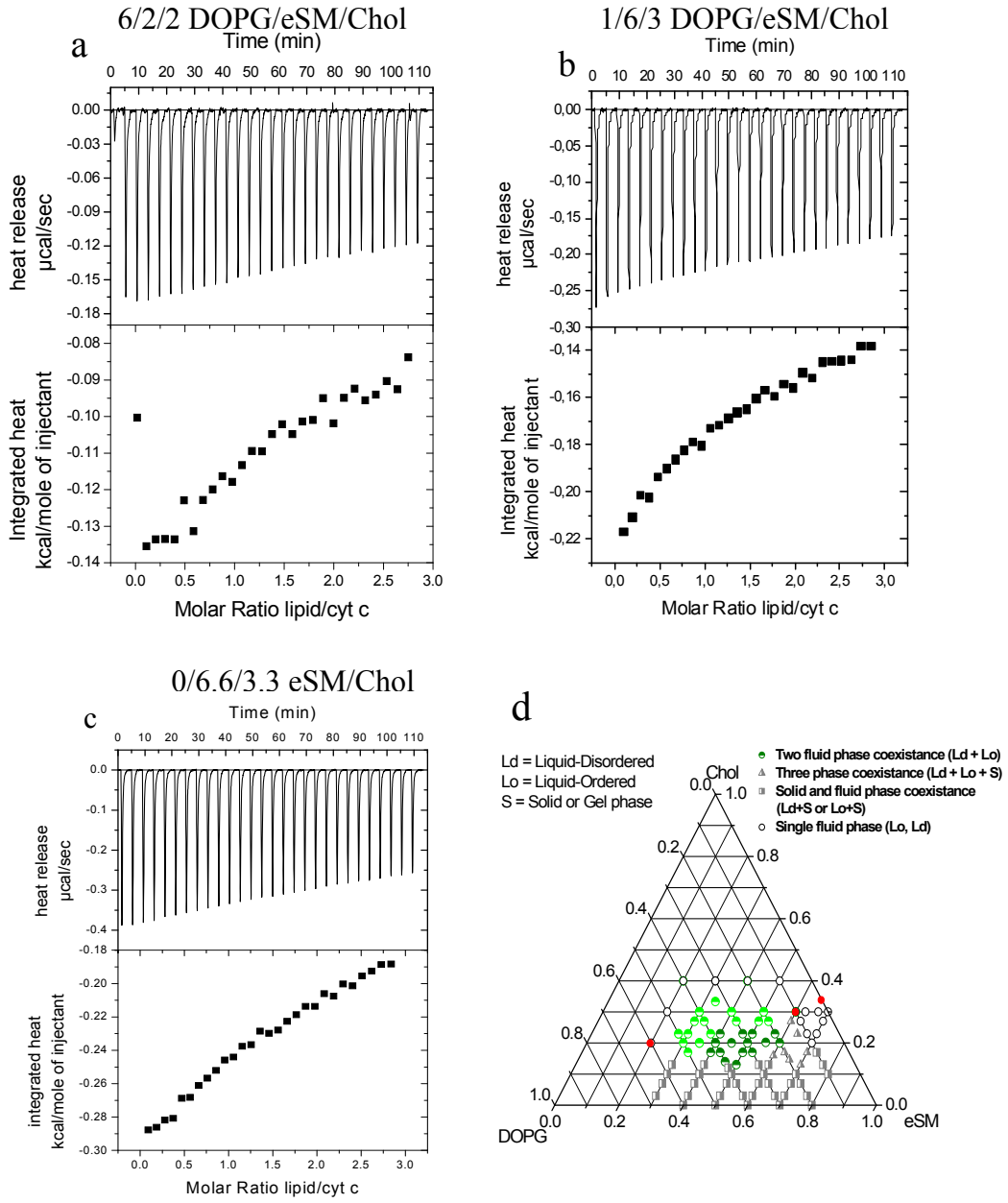

Figure 3.5.1 Calorimetric titration experiments, heat release plotted against time along with integrated heat plotted against the molar ratio of lipid to cyt c after each injection for (a) 6/2/2 DOPG/eSM/Chol, (b) 1/6/3 DOPG/eSM/Chol, and (c) 0/6.6/3.3 DOPG/eSM/Chol lipid compositions. The sample was constantly stirred at a 310 rpm stirring rate at 25 ˚C. (d) Phase diagram of DOPG/eSM/Chol in the presence of 0.6 mM cyt c denoting studied lipid compositions with red dots. In (c) lipid mixtures with 4mM concentration were injected into 0.3mM cyt c. Injections were divided in 28 steps separated by 2 min interval. The first injection was 2 µl and discarded from the data analyses, followed by 10 µl injections. The final concentration of lipid was 0.3 mM considering only the outer leaflet of the LUVs and 0.25 mM for the cyt c. All solutions were made in 1 mM EDTA and 2 mM HEPES buffer at pH 7.4.

When calculating the concentration of lipids in the outer leaflet, we have considered the curvature of the vesicle. We took in account the fact that the distance from the center for the inner leaflet is less than for the outer one. Considering thickness of the membrane (~ 4 μm), the final concentration of lipids from the outer leaflet of the vesicle was to be 51% of total lipid concentration.

The data for the interaction of cyt c with lipid compositions of 1/6/3, 6/2/2 and 0/6.6/3.3 were fitted with the single-site binding model introduced in section 2.7 in Materials and Methods. In this model, each protein molecule binds to a lipid cluster containing N lipid molecules with enthalpy ΔH, binding constant K and entropy ΔS (see chapter 2.7 in Materials and Methods section). The thermodynamic parameters determined during data analyzes for the studied compositions are summarized in Table 3.5.1. We have fixed ΔH to the extrapolated value and not used it as a fitting parameter. This is why in Table 3.5.1 for ΔH error values are zero. Gibbs free energy ΔG, entropic contribution of protein to membrane binding process was calculated as follows: $\Delta G = -RT \ln(55.5K)$, where R is the universal gas constant and T is the temperature.

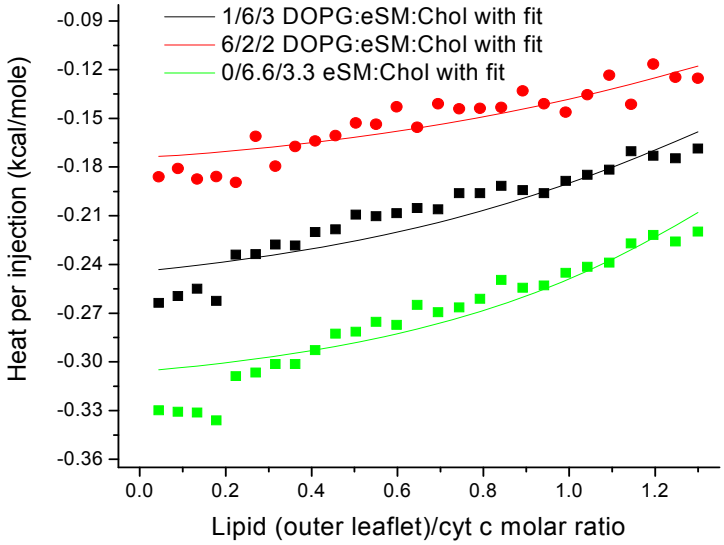

Figure 3.5.2 Integrated heat per injection plotted against lipid protein molar ratio for 1/6/3, 6/2/2 and 0/6.6/3.3 DOPG/eSM/Chol extruded vesicles fitted with the single-site binding model. DOPG/eSM/Chol extruded vesicles, with 4 mM lipid concentration were injected in cyt c solution with 0.3 mM concentration. Reference measurements, vesicles injected into buffer and buffer injected into cyt c, were subtracted from the data for all three compositions. The final concentration of lipid was 0.3 mM considering only the outer leaflet of the LUVs and 0.25 mM for cyt c. All solutions were prepared in 1 mM EDTA and 2 mM HEPES buffer at pH 7.4 and all experiments were done at 25˚C.

The factor 55.5 comes from the concentration of water, taking in account the fact that ΔG is defined for the molar ratios of components involved in the binding process. The entropy gain was then calculated from the Gibbs free energy: $T\Delta S = \Delta H - \Delta G$.

Vesicle composition DOPG/eSM/Chol	Stoichiometry N	Binding constant K (10^3 M^{-1})	Enthalpy change ΔH (kcal/mole)	Entropy change TΔS (kcal/mol)	Gibbs free energy ΔG (kcal/mole)
6/2/2	4.78±1.34	5.1±2.6	-0.19	6±1.7	-6.2±1.7
1/6/3	3.84±0.28	9.5±1.8	-0.26	6.2±1.4	-6.5±1.4
0/6.6/3.3	3.76±0.22	11.1±1.7	-0.33	6.3±1.6	-6.6±1.6

Table 3.5.1 Thermodynamic parameters for cyt c binding to 1/6/3, 6/2/2 and 0/6.6/3.3 DOPG/eSM/Chol vesicles at 25˚C.

As seen from Figure 3.5.2, the binding signal for the 1/6/3 lipid composition (composition closer to that of the Lo phase in vesicles with Lo and Ld domains) is higher compared to the 6/2/2 mixture (composition closer to that of the Ld phase). This result is in agreement with the data obtained previously by intensity measurements in Figure 3.3.6 showing preferential partitioning of cyt c to the Ld/Lo domains and the fact that the partitioning ratio for 2/6/2 with lower DOPG concentration is higher in comparison to the 4/4/2, with higher DOPG lipid composition (see chapter 3.3.2). Surprisingly, the binding isotherm for 0/6.6/3.3 lipid mixture with no charged DOPG lipids shows even higher binding signal compared to 1/6/3 and 6/2/2 mixtures, suggesting that the binding process of cyt c to the lipid membranes is not only of electrostatic origin, but it can either exhibit strong hydrophobic binding to the membrane core or interacts particularly strongly with eSM.

The results summarized in Table 3.5.1 indicate that binding of the protein is strongest to the DOPG-free membrane (0/6.6/3.3) as characterized by the highest value of the binding constant. The stoichiometry of binding, however, is similar within the error bars and close to 4 lipids per protein. The binding to all three membrane compositions is exothermic, i.e., characterized by negative enthalpic changes. This feature is usually associated with electrostatic nature of the interaction between the protein and the membrane. Even though the measured binding processes are exothermic, the largest contributions to the Gibbs free energy change are entropic (compare ΔG and $-T\Delta S$), suggesting significant structural reorganization in the hydration layers of the protein and the membrane.

We studied as well binding of cyt c to membranes with different lipid composition at various lipid protein concentrations. Interestingly, at higher (10 mM) lipid concentration, for the same lipid compositional vesicles, the binding peaks change direction and turn to be endothermic. Figure 3.5.3 below shows the ITC measurements for 10 mM 1/6/3 and 6/2/2 lipid compositional vesicles interacting with 0.1 mM cyt c.

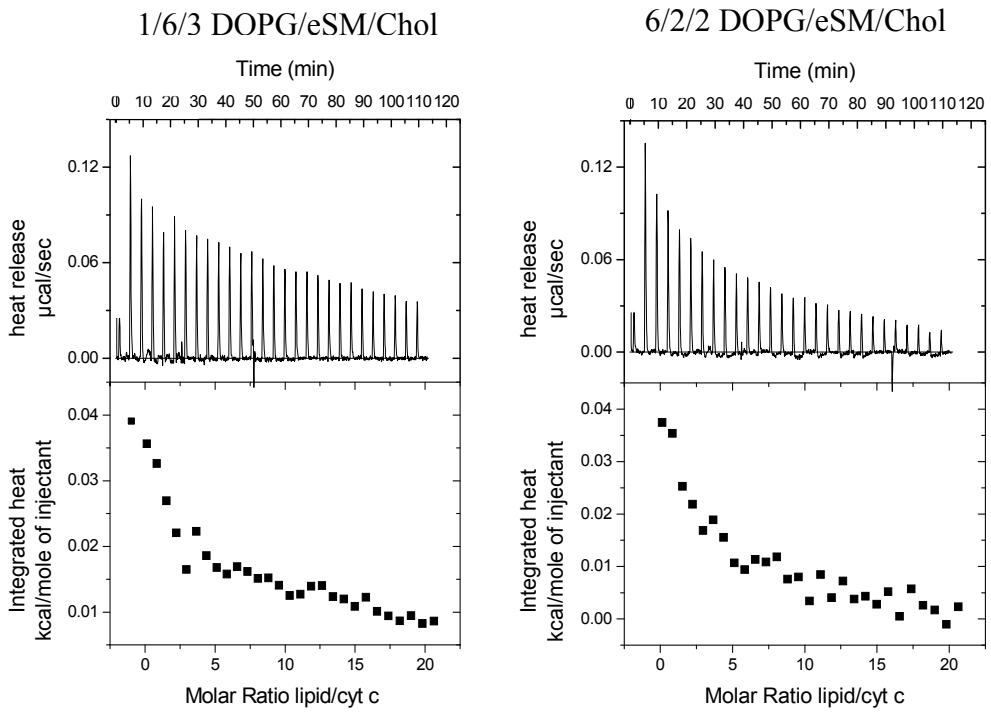

Figure 3.5.3 Calorimetric titration experiments, heat release plotted against time along with integrated heat plotted against the molar ratio of lipid to cyt c after each injection for 10 mM 6/2/2 and 1/6/3 DOPG/eSM/Chol vesicle compositions. The final concentration of lipid was 0.8 mM considering only the outer leaflet of the LUVs and 0.08 mM for the cyt c. All solutions were prepared in 1 mM EDTA and 2 mM HEPES buffer at pH 7.4 buffer and all experiments done at 25˚C.

Along with experiments, reference measurements were performed, for vesicles injected into the buffer as well as buffer injected into the protein. We have subtracted both reference measurements during the data analyses. Figure 3.5.4 shows the dependence of heat release on time and the integrated heat of each injection as a function of lipid to protein molar ratio for 10 mM 6/2/2 and 1/6/3 lipid vesicles interacting with 0.3mM cyt c in 1 mM EDTA and 2 mM HEPES buffer at pH 7.4. As it is seen from the graphs the heat peaks are endothermic for both compositions.

Such kind of changed signal direction has been reported previously for ITC measurements, when interaction of cyt c was studied with pure DMPG membranes as a function of lipid-to-protein ratio [87]. It might imply that the interaction of the protein with ternary lipid mixture is associated with the loosening of protein conformation and partial penetration into the membrane [92, 93].

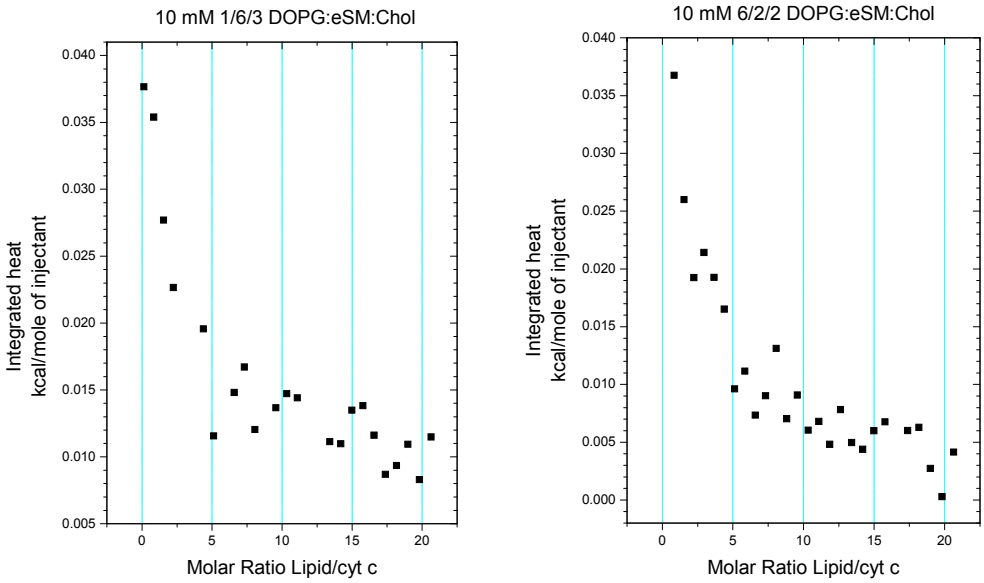

Figure 3.5.4 Integrated heat per injection plotted against lipid protein molar ratio for 1/6/3, and 6/2/2 DOPG/eSM/Chol extruded vesicles. DOPG/eSM/Chol extruded vesicles, with 10 mM lipid concentration were injected in cyt c solution with 0.1 mM concentration. Reference measurements, vesicles injected into buffer and buffer injected into cyt c, were subtracted from the data for both compositions. The final concentration of lipid was 0.8 mM considering only the outer leaflet of the LUVs and 0.08 mM for cyt c. All solutions were prepared in 1 mM EDTA and 2 mM HEPES buffer at pH 7.4 and all experiments were done at 25˚C.

3.6. Effect of cytochrome c adsorption on the surface charge and size of large unilamellar vesicles made of DOPG/eSM/Chol

The surface charge of DOPG/eSM/Chol LUVs were monitored with Zetasizer Nano, which measures average electrophoretic mobility of the vesicles and converts it to zeta potential (see chapter 2.9 in Materials and Methods section). The size distribution of the vesicles before and after an ITC measurement is checked with dynamic light scattering operated by the same instrument (see chapter 2.8 in Materials and Methods section).

Figure 3.6.1 displays results for the zeta potential and size distribution of LUVs composed of DOPG/eSM/Chol (0/6.6/3.3) and DOPG/eSM/Chol (1/6/3, 6/2/2) before and after adding 0.3 mM cyt c. As it is seen from the graph for the vesicles with lipid composition of eSM/Chol without the charged DOPG lipid component the difference in the zeta potential as well in the vesicle size with and without cyt c is negligible.

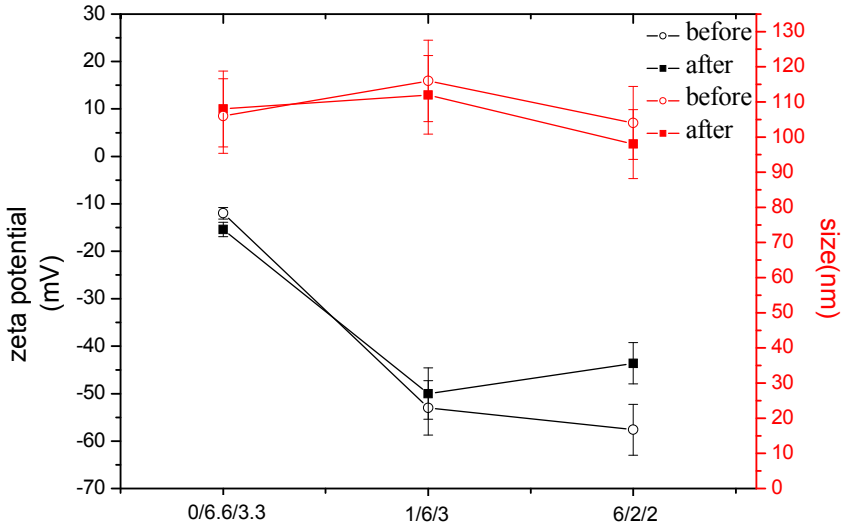

Figure 3.6.1 Y axis Zeta potential (left axis) and average size (right axis) of DOPG/eSM/Chol (0/6.6/3.3) and DOPG/eSM/Chol (1/6/3, 6/2/2) LUVs with total lipid concentration of 4 mM, before and after adding 0.3 mM cyt c. The final concentration of lipid was 0.3 mM considering only the outer leaflet of the LUVs and 0.25 mM for the cyt c. Error bars correspond to the standard deviation of the data collected from different samples. All solutions were prepared in 1 mM EDTA and 2 mM HEPES buffer at pH 7.4 buffer and all experiments done at 25˚C.

For the vesicles with 10% (1/6/3) after adding 0.3 mM cyt c the zeta potential change stays within the error bars. However, vesicles with 60% (6/2/2)

of charged DOPG lipids the zeta potential decreases slightly. No obvious decrease of the zeta potential in 1/6/3 lipid compositions compare to 6/2/2 probably is stipulated by differences in the content of negatively charged lipids. Electrostatic interaction of cyt c to membranes should be more prominent for the lipid compositions containing higher amount of charged lipids.

Judging by no changes in the size distribution shape after addition of cyt c, we could conclude that vesicle aggregation did not take place. Presumably, because of the small protein size, even total coverage of the vesicle with the protein did not affect or was not detected as a vesicle size change. To test for charge compensation and eventually saturation of the negative charge of the 1/6/3 and 6/2/2 vesicles upon adsorption of the positively charged cyt c, we studied the zeta potential of LUVs at different cyt c concentrations. Figure 3.6.2 shows the zeta potential of 1/6/3 and 6/2/2 LUVs at zero, 0.3 mM and 100 mM cyt c concentrations. As it is seen from the graph, the net negative charge of the vesicles decreases and at 100 mM cyt c concentration reaches -16 and -21 mV for the vesicles with 60% and 10% DOPG lipid content respectively. Decrease of the membrane negative charge indicates positively charged protein adsorption to the DOPG membrane. We did not check higher concentrations as they are not biologically relevant, but increasing the protein concentration, presumably would make the effective charge reach zero completely neutralizing the negative charge of the membrane.

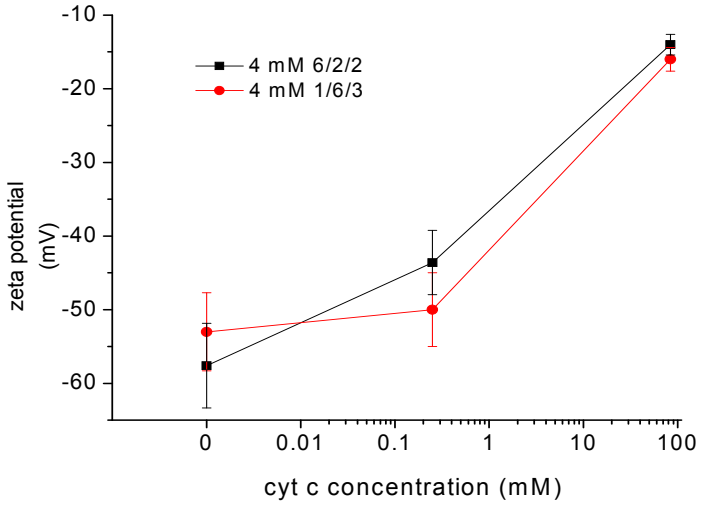

Figure 3.6.2 Zeta potential of DOPG/eSM/Chol (1/6/3, 6/2/2) LUVs in the presence of cyt c at zero, 0.3 mM and 100 mM concentrations. The concentration of lipid was 0.3 mM considering only the outer leaflet of the LUVs. For 0.3 mM protein the final concentration was 0.25 mM and for 100 mM protein 84 mM respectively. Error bars correspond to the 10% standard error of the data collected from different samples. All solutions were prepared in 1 mM EDTA and 2 mM HEPES buffer at pH 7.4 buffer and all experiments done at 25˚C.

3.7. Purification of DC-SIGN

This work has been done in the laboratory of the US partner, Prof. N. Thompson, at the University of Noth Carolina Chapel Hill.

Dendritic cells (DCs) are initiators and modulators of the immune response. While mature DCs prime T cells complete the immune response process, immature DCs capture antigens to form major histocompatibility peptide complexes (MHCs). The immature DCs express the C-type lectin DC-SIGN (CD209) receptor, which functions as an antigen capture and cell adhesion molecule. DC-SIGN molecules form discrete nanoscale domains and are thought to play an important role in viral, bacterial and yeast binding [94-101]. Therefore understanding the function and dynamics of DC-SIGN domains is of high importance. Recent studies have demonstrated that DC-SIGN forms microdomains, which are complex in their structure, but still it is not well-defined at present. It has been shown that these clusters partially colocalize with clathrin and other C-type lectins (dectin-1 and macrophage mannose receptor) [100]. This observation implies that the biochemical composition of DC-SIGN domains is heterogeneous, which may be important in efficient pathogen recognition and processing. In order to identify and determine if other molecules are co-purified through binding to DC-SIGN, we purified the protein using affinity chromatography method with DC-SIGN specific antibodies (described in details in chapter 2.3 of Materials and Methods). Developing a procedure for isolating DC-SIGN will also enable future measurements in which the mechanism of DC-SIGN forming clusters can be investigated in reconstitution studies. After purification of DC-SIGN we intended to study the incorporation of the protein into the multicomponent GUVs and study the preferential partitioning of DC-SIGN into different domains.

The hybridoma (DC6) antibody, specific for DC-SIGN, was purified from DC6 cell supernatants using a Protein G affinity column. After the supernatant was applied to the protein G affinity column, DC6 antibodies were eluted with the help of low pH buffer and collected in tubes containing high pH buffer for immediate pH neutralization and dialyzed against PBS buffer. The concentration of protein was determined by measuring the absorbance at 280nm. For visualization of the expected molecular weight of the purified DC6 protein we used SDS-PAGE and by Western-blot we confirmed that the appearing band was in fact representative of the expected protein (Figure 3.7.1).

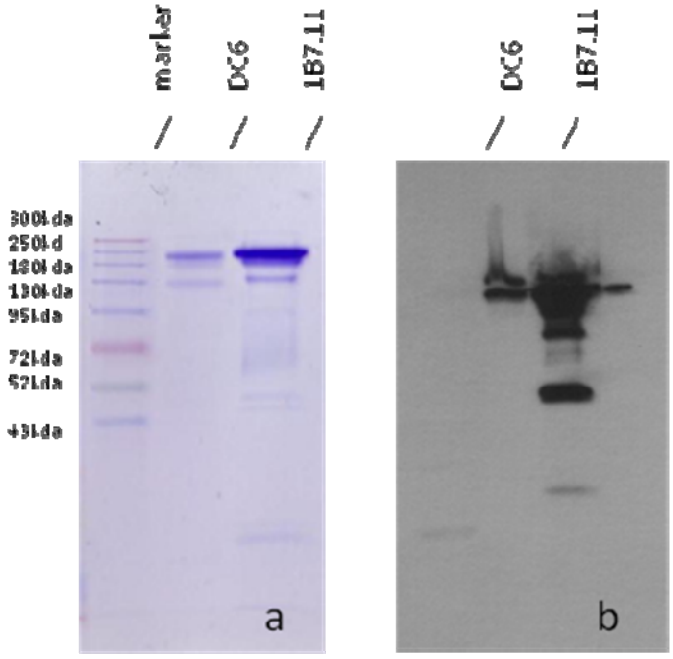

Figure 3.7.1 Non-reducing SDS-PAGE gel electrophoresis of DC6 antibodies purified by affinity chromatography and mouse IgG, 1B7.11, as a standard (a). Western-blot probing for DC6 using anti-mouse IgG-HRP (b).

As a next step we constructed a column from the purified DC6 antibodies for isolation of DC-SIGN from the lysates of cells that express this receptor. THP(NCl) DC-SIGN cells were grown up to 6x10^9 and lysed using a Dounce homogenizer. After couple of steps of centrifugation the clarified supernatant was applied to the DC6 affinity column. DC-SIGN was eluted using a low pH buffer containing the detergents octylglucoside to prevent aggregation of eluted protein and neutralized immediately with high pH Tris buffer. For visualization of the expected molecular weight (~47kDa) of the purified DC-SIGN protein we used silver staining and by Western-blot (see chapter 2.3, Materials and Methods) we confirmed that the appearing band was in fact representative of the expected protein (Figure 3.7.2).

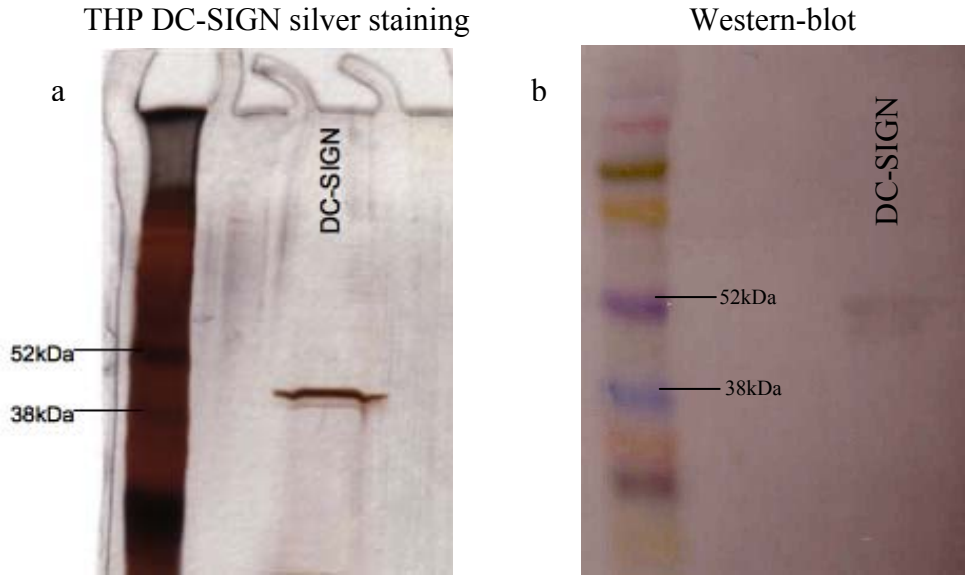

Figure 3.7.2 Silver staining of DC-SIGN protein purified by DC6 affinity chromatography (a) Western-blot for DC-SIGN using primary DCN46 mAb followed by secondary goat anti-mouse antibody conjugated with Alexafluoro 488 (b).

4. Summary and conclusions

Interactions of soluble proteins with membranes play a crucial role in biological processes including energy and signal transduction, regulation of biological activity, and transport processes. In general, soluble proteins exhibit a hydrophilic surface constituted mainly by polar and charged amino acid side chains. Thus, interactions with membranes are primarily electrostatic in nature and largely restricted to (temporarily) binding of the protein to the periphery of the membrane. However, many of these proteins can also interact with the hydrophobic core of the bilayer which may lead to a partial or a complete integration of the protein into the membrane which may occur transiently during the transmembrane transport. Hydrophobic interactions of soluble proteins with membranes are likely to be associated with substantial structural changes in both the protein and the lipid bilayer. However, up to now, the underlying mechanisms are far from being fully understood. Specifically, it is not known which parameters (i) control the interplay between electrostatic and hydrophobic binding and (ii) trigger the structural changes in soluble proteins that are required for the (partial) insertion into the hydrophobic core of bilayer.

To summarize the present work, we characterized the phase diagram of DOPG/eSM/Chol ternary mixture in a 2 mM HEPES/1 mM EDTA (pH 7.5) buffer. Compared to the phase diagram of the same ternary lipid mixtures described in a previous study [67], in the presence of buffer we accounted a number of differences. The two fluid Ld/Lo phase coexistence region was expanded towards the DOPG corner of the phase diagram and detailed studies on the lipid compositions from the Gibbs triangle revealed the existence of a Ld/Lo/So three phase region. We have used confocal microscopy and fluorescent dyes to resolve these changes in the phase diagram.

The effect of cyt c on the phase behavior of membranes of the lipid compositions representing different phases was studied. Adding 0.6 mM cyt c into vesicles influenced the membrane by rearranging of lipids and induced the phase separation and fluid phase domain formations for single liquid phase membranes. Overall, in the presence of cyt c the two fluid phase coexistence region was enlarged altering the membranes from single Ld phase, whereas cyt c did not induce detectable changes in the phase state of the membranes from Ld/So or Ld/Lo/So phases. New boundary lines on the phase diagram of the DOPG/eSM/Chol ternary mixture in the presence of 0.6 mM cyt c were drawn.

Apoptotic pathway of the cell involves movement of proapoptotic proteins from the cytosol to mitochondrial membranes [102, 103]. Several studies indicate that these non residential proteins of mitochondria induce cyt c release by channel formation or activation of permeability transition pore [104-106104-106]. This is followed by redistribution of lipids in the mitochondrial membrane favoring

microdomain formation, further escalating apoptotic signaling. Our results of the influence of cyt c on the phase state of ternary mixture lipids suggest that indeed cyt c to some extent induces lipid rearrangement and domain formation in homogenous one phase state membranes. With the relevance to biological membranes, the released of cyt c caused by cytosolic proteins or/and high calcium level, can influence the phase state, lipid redistribution and microdomain formation, which in turn plays a key role in further signaling apoptotic pathway.

Quantitative calculations of cyt c preferential partitioning ratios between two Ld/Lo phases were performed. It was found that in vesicles with Ld/Lo coexisting phases, cyt c partitions more into the Ld phase, which is rich in negatively charged DOPG lipids. The partitioning ratio of cyt c between the two fluid phases strongly depends on the lipid composition of vesicles and decreases with increasing DOPG concentration.

ITC was used to characterize thermodynamically the binding of cyt c to ternary lipid membranes from Ld or Lo phases. The experimental calorimetric titration data have been analyzed. At constant temperature of 25˚C and for certain range of protein concentration, smaller enthalpy change is observed for the binding of cyt c to membranes of lipid composition with higher DOPG (60%) concentration, whereas higher enthalpy change was recorded for vesicles with lower (10%) and no DOPG content. Nevertheless, the binding constant of the process KA was observed to be higher as well for lower DOPG (10%) concentration. Our results clearly indicate complex biphasic behavior of the binding process of cyt c to ternary lipid mixtures exhibiting not only electrostatic interaction, but strong hydrophobic binding of the heme group of the protein to the membrane core.

As a future study one can explore with ITC the various homogenous vesicles located in the vicinity of the enlarged area of the two fluid phase coexistence region (Figure 3.2.1). Calculation of thermodynamic parameters of cyt c binding process, in particular stochiometry ratios can be extracted between the lipid compositions close to Ld and Lo phases. The latest can be compared to the ratios of cyt c between Lo and Ld phases obtained from fluorescent intensity studies (see chapter 3.3). Comparable ratios calculated from two different studies will lead in resolving and locating the tie-lines on the characterized phase diagram of DOPG/eSM/Chol ternary mixture (see chapter 3.1).

References

[1] K. Simons, D. Toomre, Lipid rafts and signal transduction, Nat. Rev. Mol. Cell Biol., 1 (2000) 31-39.

[2] R.E. Dickerson, Cytochrome-C and the Evolution of Energy-Metabolism, Sci Am, 242 (1980) 137.

[3] P. Williams, L. Coates, F. Mohammed, R. Gill, P. Erskine, D. Bourgeois, S.P. Wood, C. Anthony, J.B. Cooper, The 1.6A X-ray structure of the unusual c-type cytochrome, cytochrome cL, from the methylotrophic bacterium Methylobacterium extorquens, Journal of molecular biology, 357 (2006) 151-162.

[4] G.W. Bushnell, G.V. Louie, G.D. Brayer, High-resolution three-dimensional structure of horse heart cytochrome c, Journal of molecular biology, 214 (1990) 585-595.

[5] H.A. Harbury, P.A. Loach, Interaction of Nitrogenous Ligands with Heme Peptides from Mammalian Cytochrome-C, J Biol Chem, 235 (1960) 3646-3653.

[6] T.J.T. Pinheiro, H. Cheng, S.H. Seeholzer, H. Roder, Direct evidence for the cooperative unfolding of cytochrome c in lipid membranes from H-H-2 exchange kinetics, Journal of molecular biology, 303 (2000) 617-626.

[7] G.W. Pettigrew, G.R. Moore, Cytochromes c : biological aspects, Springer-Verlag, Berlin ; New York, 1987.

[8] X.S. Liu, C.N. Kim, J. Yang, R. Jemmerson, X.D. Wang, Induction of apoptotic program in cell-free extracts: Requirement for dATP and cytochrome c, Cell, 86 (1996) 147-157.

[9] S. Oellerich, S. Lecomte, M. Paternostre, T. Heimburg, P. Hildebrandt, Peripheral and integral binding of cytochrome c to phospholipids vesicles, J Phys Chem B, 108 (2004) 3871-3878.

[10] Y. Hudecek, P. Hildebrandt, D. Marsh, T. Heimburg, Spectroscopic studies of cytochrome c interaction with lipid membranes - The coupling of cytochrome c function with surface absorption and integration, in: Spectroscopy of Biological Molecules: Modern Trends, 1997, pp. 297-300.

[11] M.J. Zuckermann, T. Heimburg, Insertion and pore formation driven by adsorption of proteins onto lipid bilayer membrane-water interfaces, Biophysical journal, 81 (2001) 2458-2472.

[12] P.A. Beales, C.L. Bergstrom, N. Geerts, J.T. Groves, T.K. Vanderlick, Single Vesicle Observations of the Cardiolipin-Cytochrome c Interaction: Induction of Membrane Morphology Changes, Langmuir, 27 (2011) 6107-6115.

[13] A. Rietveld, P. Sijens, A.J. Verkleij, B. Dekruijff, Interaction of cytochrome c and its precursor apocytochrome c with various phospholipids, EMBO J., 2 (1983) 907-913.

[14] D.M. Haverstick, M. Glaser, Influence of Proteins on the Reorganization of Phospholipid-Bilayers into Large Domains, Biophysical journal, 55 (1989) 677-682.

[15] T. Heimburg, B. Angerstein, D. Marsh, Binding of peripheral proteins to mixed lipid membranes: Effect of lipid demixing upon binding, Biophysical journal, 76 (1999) 2575-2586.

[16] G.P. Gorbenko, V.M. Trusova, J.G. Molotkovsky, P.K.J. Kinnunen, Cytochrome c induces lipid demixing in weakly charged phosphatidylcholine/phosphatidylglycerol model membranes as evidenced by resonance energy transfer, Bba-Biomembranes, 1788 (2009) 1358-1365.

[17] B.A.J. Alberts, Julian Lewis, Martin Raff, Keith Roberts, Peter Walter, Molecular Biology of the Cell, Garland Publishing Inc, New York, 1994.

[18] J.E. Chipuk, L. Bouchier-Hayes, D.R. Green, Mitochondrial outer membrane permeabilization during apoptosis: the innocent bystander scenario, Cell Death Differ, 13 (2006) 1396-1402.

[19] M. Tafani, N.O. Karpinich, K.A. Hurster, J.G. Pastorino, T. Schneider, M.A. Russo, J.L. Farber, Cytochrome c release upon Fas receptor activation depends on translocation of full-length Bid and the induction of the mitochondrial permeability transition, J Biol Chem, 277 (2002) 10073-10082.

[20] L. Stryer, Biochemistry, W.H. Freeman and Company, New York, 1988.

[21] A.L. Lehinger, Principles of Biochemistry, Worth Publishers, New York, 1982.

[22] G.W.P.a.G.R. Moore, Cytochromes C — Biological Aspects, in: A. RICH (Ed.), Berlin, Heidelberg, 1987.

[23] in, www.invitrogen.com.

[24] H.S. VanWalraven, H. Strotmann, O. Schwarz, B. Rumberg, The H+/ATP coupling ratio of the ATP synthase from thiol-modulated chloroplasts and two cyanobacterial strains is four, Febs Lett, 379 (1996) 309-313.

[25] M. Yoshida, E. Muneyuki, T. Hisabori, ATP synthase--a marvellous rotary engine of the cell, Nature reviews. Molecular cell biology, 2 (2001) 669-677.

[26] B.J. Alberts, Alexander; Lewis, Julian; Raff, Martin; Roberts, Keith; Walter, Peter "Chapter 18 Apoptosis: Programmed Cell Death Eliminates Unwanted Cells" Molecular Biology of the Cell 2008.

[27] J.A. Karam, Apoptosis in Carcinogenesis and Chemotherapy, 2009.

[28] L.-H.H. Ting-Jun FAN1, Ri-Shan CONG, and Jin LIANG, Caspase family proteases and apoptosis, Acta Biochimica et Biophysica Sinica, 37(11) (2005) 719–727.

[29] S.G. Popov, R. Villasmil, J. Bernardi, E. Grene, J. Cardwell, A. Wu, D. Alibek, C. Bailey, K. Alibek, Lethal toxin of Bacillus anthracis causes apoptosis of macrophages, Biochemical and biophysical research communications, 293 (2002) 349-355.

[30] B. B, "Nitric oxide: NO apoptosis or turning it ON?", 10 (8): 864–9. (Brüne B).

[31] C. Cotran; Kumar, Robbins Pathologic Basis of Disease, W.B Saunders Company, Philadelphia, 1998.

[32] M.P. Mattson, S.L. Chan, Calcium orchestrates apoptosis, Nature cell biology, 5 (2003) 1041-1043.

[33] X. Liu, C.N. Kim, J. Yang, R. Jemmerson, X. Wang, Induction of apoptotic program in cell-free extracts: requirement for dATP and cytochrome c, Cell, 86 (1996) 147-157.

[34] S.M.-C. Laurent M. Dejean, Kathleen W. Kinnally, "Is MAC the knife that cuts cytochrome c from mitochondria during apoptosis?", 2006.

[35] D. Acehan, X. Jiang, D.G. Morgan, J.E. Heuser, X. Wang, C.W. Akey, Three-dimensional structure of the apoptosome: implications for assembly, procaspase-9 binding, and activation, Molecular cell, 9 (2002) 423-432.

[36] M. Capano, M. Crompton, Biphasic translocation of Bax to mitochondria, Biochem. J., 367 (2002) 169-178.

[37] A.J. Garcia-Saez, I. Mingarro, E. Perez-Paya, J. Salgado, Membrane-insertion fragments of Bcl-x(L), Bax, and Bid, Biochemistry, 43 (2004) 10930-10943.

[38] O. Terrones, B. Antonsson, H. Yamaguchi, H.G. Wang, J.H. Liu, R.M. Lee, A. Herrmann, G. Basanez, Lipidic pore formation by the concerted

action of proapoptotic BAX and tBID, J. Biol. Chem., 279 (2004) 30081-30091.

[39] E. Martinez-Abundis, F. Correa, N. Pavon, C. Zazueta, Bax distribution into mitochondrial detergent-resistant microdomains is related to ceramide and cholesterol content in postischemic hearts, FEBS J., 276 (2009) 5579-5588.

[40] T. Garofalo, A. Giammarioli, R. Misasi, A. Tinari, V. Manganelli, L. Gambardella, A. Pavan, W. Malorni, M. Sorice, Lipid microdomains contribute to apoptosis-associated modifications of mitochondria in T cells, Cell Death Differ., 12 (2005) 1378-1389.

[41] L. Ciarlo, V. Manganelli, T. Garofalo, P. Matarrese, A. Tinari, R. Misasi, W. Malorni, M. Sorice, Association of fission proteins with mitochondrial raft-like domains, Cell Death Differ., 17 (2010) 1047-1058.

[42] K. Simons, D. Toomre, Lipid rafts and signal transduction, Nature reviews. Molecular cell biology, 1 (2000) 31-39.

[43] K. Simons, E. Ikonen, Cell biology - How cells handle cholesterol, Science, 290 (2000) 1721-1726.

[44] M. Edidin, The state of lipid rafts: from model membranes to cells, Annual review of biophysics and biomolecular structure, 32 (2003) 257-283.

[45] T. Garofalo, R. Misasi, V. Mattei, A.M. Giammarioli, W. Malorni, G.M. Pontieri, A. Pavan, M. Sorice, Association of the death-inducing signaling complex with microdomains after triggering through CD95/Fas - Evidence for caspase-8-ganglioside interaction in T cells, J Biol Chem, 278 (2003) 8309-8315.

[46] J. Fullekrug, K. Simons, Lipid rafts and apical membrane traffic, Ann Ny Acad Sci, 1014 (2004) 164-169.

[47] D. Holowka, J.A. Gosse, A.T. Hammond, X. Han, P. Sengupta, N.L. Smith, A. Wagenknecht-Wiesner, M. Wu, R.M. Young, B. Baird, Lipid segregation and IgE receptor signaling: a decade of progress, Biochimica et biophysica acta, 1746 (2005) 252-259.

[48] D. Meder, M.J. Moreno, P. Verkade, W.L. Vaz, K. Simons, Phase coexistence and connectivity in the apical membrane of polarized epithelial cells, Proceedings of the National Academy of Sciences of the United States of America, 103 (2006) 329-334.

[49] P.V. Escriba, Membrane-lipid therapy: a new approach in molecular medicine, Trends Mol. Med., 12 (2006) 34-43.

[50] P.V. Escriba, J.M. Gonzalez-Ros, F.M. Goni, P.K.J. Kinnunen, L. Vigh, L. Sanchez-Magraner, A.M. Fernandez, X. Busquets, I. Horvath, G. Barcelo-Coblijn, Membranes: a meeting point for lipids, proteins and therapies, J. Cell. Mol. Med., 12 (2008) 829-875.

[51] S. Munro, Lipid rafts: elusive or illusive?, Cell, 115 (2003) 377-388.

[52] R. Dimova, S. Aranda, N. Bezlyepkina, V. Nikolov, K.A. Riske, R. Lipowsky, A practical guide to giant vesicles. Probing the membrane nanoregime via optical microscopy, J. Phys.: Condens. Matter, 18 (2006) S1151-S1176.

[53] C. Dietrich, L.A. Bagatolli, Z.N. Volovyk, N.L. Thompson, M. Levi, K. Jacobson, E. Gratton, Lipid rafts reconstituted in model membranes, Biophys. J., 80 (2001) 1417-1428.

[54] R. Lipowsky, R. Dimova, Domains in membranes and vesicles, J Phys-Condens Mat, 15 (2003) S31-S45.

[55] S.L. Veatch, S.L. Keller, Separation of liquid phases in giant vesicles of ternary mixtures of phospholipids and cholesterol, Biophys. J., 85 (2003) 3074-3083.

[56] T. Baumgart, G. Hunt, E.R. Farkas, W.W. Webb, G.W. Feigenson, Fluorescence probe partitioning between L-o/L-d phases in lipid membranes, Bba-Biomembranes, 1768 (2007) 2182-2194.

[57] C.C. Vequi-Suplicy, K.A. Riske, R.L. Knorr, R. Dimova, Vesicles with charged domains, Biochimica et Biophysica Acta (BBA) - Biomembranes, 1798 (2010) 1338-1347.

[58] J. Kilkus, R. Goswami, F.D. Testai, G. Dawson, Ceramide in rafts (detergent-insoluble fraction) mediates cell death in neurotumor cell lines, J Neurosci Res, 72 (2003) 65-75.

[59] I. Gkantiragas, B. Brugger, E. Stuven, D. Kaloyanova, X.Y. Li, K. Lohr, F. Lottspeich, F.T. Wieland, J.B. Helms, Sphingomyelin-enriched microdomains at the Golgi complex, Mol Biol Cell, 12 (2001) 1819-1833.

[60] S. Kaushik, A.C. Massey, A.M. Cuervo, Lysosome membrane lipid microdomains: novel regulators of chaperone-mediated autophagy, Embo J, 25 (2006) 3921-3933.

[61] D. Ardail, J.P. Privat, M. Egretcharlier, C. Levrat, F. Lerme, P. Louisot, Mitochondrial Contact Sites - Lipid-Composition and Dynamics, J Biol Chem, 265 (1990) 18797-18802.

[62] L. DD., Novel applications of liposomes, Trends biotechnology July 16(7):307-21 (1998).

[63] J. Israelachvili, Intermolecular & Surface Forces, Academic Press Limited, 1991.

[64] L. Bagatolli, P.B.S. Kumar, Phase behavior of multicomponent membranes: Experimental and computational techniques, Soft Matter, 5 (2009) 3234-3248.

[65] K. Simons, E. Ikonen, Functional rafts in cell membranes, Nature, 387 (1997) 569-572.

[66] M.I. Angelova, D.S. Dimitrov, Liposome electroformation, Faraday Discussions of the Chemical Society, 81 (1986) 303-311.

[67] C.C. Vequi-Suplicy, K.A. Riske, R.L. Knorr, R. Dimova, Vesicles with charged domains, Biochimica et biophysica acta, 1798 (2010) 1338-1347.

[68] N. Kahya, D. Scherfeld, K. Bacia, B. Poolman, P. Schwille, Probing lipid mobility of raft-exhibiting model membranes by fluorescence correlation spectroscopy, J Biol Chem, 278 (2003) 28109-28115.

[69] A.S. Cans, M. Andes-Koback, C.D. Keating, Positioning lipid membrane domains in giant vesicles by micro-organization of aqueous cytoplasm mimic, J Am Chem Soc, 130 (2008) 7400-7406.

[70] H. Towbin, T. Staehelin, J. Gordon, Electrophoretic transfer of proteins from polyacrylamide gels to nitrocellulose sheets: procedure and some applications. 1979, Biotechnology, 24 (1992) 145-149.

[71] J. Renart, J. Reiser, G.R. Stark, Transfer of proteins from gels to diazobenzyloxymethyl-paper and detection with antisera: a method for studying antibody specificity and antigen structure, Proceedings of the National Academy of Sciences of the United States of America, 76 (1979) 3116-3120.

[72] N.S. Claxton, Fellers, T. J., and Davidson, M. W. (1979). LASER SCANNING CONFOCAL MICROSCOPY. Microscopy 1979, 9-11.

[73] I. Jelesarov, H.R. Bosshard, Isothermal titration calorimetry and differential scanning calorimetry as complementary tools to investigate the energetics of biomolecular recognition, J Mol Recognit, 12 (1999) 3-18.

[74] D.L.S.D.P. Bruce J. Berne and R. Pecora, New York (2000).

[75] Z.A.U.M.D.M.o. http://malvern.com, in.

[76] B.G. Hawkins, B.J. Kirby, Electrothermal flow effects in insulating (electrodeless) dielectrophoresis systems, Electrophoresis, 31 (2010) 3622-3633.

[77] S.T. Hess, M.V. Gudheti, M. Mlodzianoski, T. Baumgart, Shape analysis of giant vesicles with fluid phase coexistence by laser scanning microscopy to determine curvature, bending elasticity, and line tension, Methods in molecular biology, 400 (2007) 367-387.

[78] A. Pralle, P. Keller, E.L. Florin, K. Simons, J.K.H. Horber, Sphingolipid-cholesterol rafts diffuse as small entities in the plasma membrane of mammalian cells, J Cell Biol, 148 (2000) 997-1007.

[79] K. Jacobson, D. Papahadjopoulos, Phase transitions and phase separations in phospholipid membranes induced by changes in temperature, pH, and concentration of bivalent cations, Biochemistry-Us, 14 (1975) 152-161.

[80] B.J. van Beek-Harmsen, W.J. van der Laarse, Immunohistochemical determination of cytosolic cytochrome c concentration in cardiomyocytes, J Histochem Cytochem, 53 (2005) 803-807.

[81] H.J. Forman, A. Azzi, On the virtual existence of superoxide anions in mitochondria: Thoughts regarding its role in pathophysiology, Faseb J, 11 (1997) 374-375.

[82] W.D. Butt, D. Keilin, Absorption Spectra and Some Other Properties of Cytochrome C and of Its Compounds with Ligands, P Roy Soc Lond B Bio, 156 (1962) 429-&.

[83] R. Nunnikhoven, Amino Acid Composition and Some Other Properties of Yeast Cytochrome-C in Comparison with Horse-Heart Cytochrome-C, Biochimica et biophysica acta, 28 (1958) 108-119.

[84] F. Sherman, J.W. Stewart, Margolia.E, J. Parker, W. Campbell, Structural Gene for Yeast Cytochrome C, Proceedings of the National Academy of Sciences of the United States of America, 55 (1966) 1498-&.

[85] K. Takahashi, T. Nakajima, S. Kanaki, Histopathological studies on the liver, kidney and thymus of chick embryos administered with hydroxymethylpyrimidine, The Journal of vitaminology, 5 (1959) 178-187.

[86] S. May, D. Harries, A. Ben-Shaul, Lipid demixing and protein-protein interactions in the adsorption of charged proteins on mixed membranes, Biophysical journal, 79 (2000) 1747-1760.

[87] T. Heimburg, R.L. Biltonen, Thermotropic Behavior of Dimyristoylphosphatidylglycerol and Its Interaction with Cytochrome-C, Biochemistry-Us, 33 (1994) 9477-9488.

[88] P.J.R. Spooner, A. Watts, Reversible Unfolding of Cytochrome-C Upon Interaction with Cardiolipin Bilayers .1. Evidence from Deuterium Nmr Measurements, Biochemistry-Us, 30 (1991) 3871-3879.

[89] B. Soussi, A.C. Bylund-Fellenius, T. Schersten, J. Angstrom, 1H-n.m.r. evaluation of the ferricytochrome c-cardiolipin interaction. Effect of superoxide radicals, The Biochemical journal, 265 (1990) 227-232.

[90] P. Hildebrandt, T. Heimburg, D. Marsh, Quantitative Conformational-Analysis of Cytochrome-C Bound to Phospholipid-Vesicles Studied by Resonance Raman-Spectroscopy, Eur Biophys J, 18 (1990) 193-201.

[91] H.H.J. Dejongh, J.A. Killian, B. Dekruijff, A Water Lipid Interface Induces a Highly Dynamic Folded State in Apocytochrome-C and Cytochrome-C, Which May Represent a Common Folding Intermediate, Biochemistry-Us, 31 (1992) 1636-1643.

[92] F.L. Zhang, E.S. Rowe, Calorimetric Studies of the Interactions of Cytochrome-C with Dioleoylphosphatidylglycerol Extruded Vesicles - Ionic-Strength Effects, Bba-Biomembranes, 1193 (1994) 219-225.

[93] A. Muga, H.H. Mantsch, W.K. Surewicz, Membrane-Binding Induces Destabilization of Cytochrome-C Structure, Biochemistry-Us, 30 (1991) 7219-7224.

[94] E.P. McGreal, J.L. Miller, S. Gordon, Ligand recognition by antigen-presenting cell C-type lectin receptors, Curr Opin Immunol, 17 (2005) 18-24.

[95] U.S. Khoo, K.Y.K. Chan, V.S.F. Chan, C.L.S. Lin, DC-SIGN and L-SIGN: the SIGNs for infection, J Mol Med-Jmm, 86 (2008) 861-874.

[96] P.Y. Lozach, L. Burleigh, I. Staropoli, A. Amara, The C type lectins DC-SIGN and L-SIGN: receptors for viral glycoproteins, Methods in molecular biology, 379 (2007) 51-68.

[97] P.Y. Lozach, A. Amara, B. Bartosch, J.L. Virelizier, F. Arenzana-Seisdedos, F.L. Cosset, R. Altmeyer, C-type lectins L-SIGN and DC-SIGN capture and transmit infectious hepatitis C virus pseudotype particles, J Biol Chem, 279 (2004) 32035-32045.

[98] T.B.H. Geijtenbeek, D.S. Kwon, R. Torensma, S.J. van Vliet, G.C.F. van Duijnhoven, J. Middel, I.L.M.H.A. Cornelissen, H.S.L.M. Nottet, V.N. KewalRamani, D.R. Littman, C.G. Figdor, Y. van Kooyk, DC-SIGN, a

dendritic cell-specific HIV-1-binding protein that enhances trans-infection of T cells, Cell, 100 (2000) 587-597.

[99] J. den Dunnen, S.I. Gringhuis, T.B.H. Geijtenbeek, Innate signaling by the C-type lectin DC-SIGN dictates immune responses, Cancer Immunol Immun, 58 (2009) 1149-1157.

[100] M.S. Itano, A.K. Neumann, P. Liu, F. Zhang, E. Gratton, W.J. Parak, N.L. Thompson, K. Jacobson, DC-SIGN and influenza hemagglutinin dynamics in plasma membrane microdomains are markedly different, Biophysical journal, 100 (2011) 2662-2670.

[101] A.K. Neumann, N.L. Thompson, K. Jacobson, Distribution and lateral mobility of DC-SIGN on immature dendritic cells--implications for pathogen uptake, Journal of cell science, 121 (2008) 634-643.

[102] M. Capano, M. Crompton, Biphasic translocation of Bax to mitochondria, The Biochemical journal, 367 (2002) 169-178.

[103] A.J. Garcia-Saez, I. Mingarro, E. Perez-Paya, J. Salgado, Membrane-insertion fragments of Bcl-xL, Bax, and Bid, Biochemistry-Us, 43 (2004) 10930-10943.

[104] M. Narita, S. Shimizu, T. Ito, T. Chittenden, R.J. Lutz, H. Matsuda, Y. Tsujimoto, Bax interacts with the permeability transition pore to induce permeability transition and cytochrome c release in isolated mitochondria, Proceedings of the National Academy of Sciences of the United States of America, 95 (1998) 14681-14686.

[105] T. Kuwana, M.R. Mackey, G. Perkins, M.H. Ellisman, M. Latterich, R. Schneiter, D.R. Green, D.D. Newmeyer, Bid, Bax, and lipids cooperate to form supramolecular openings in the outer mitochondrial membrane, Cell, 111 (2002) 331-342.

[106] O. Terrones, B. Antonsson, H. Yamaguchi, H.G. Wang, J. Liu, R.M. Lee, A. Herrmann, G. Basanez, Lipidic pore formation by the concerted action of proapoptotic BAX and tBID, J Biol Chem, 279 (2004) 30081-30091.

5. Apendix

List of symbols

C……. number of components
P…….. number of phases
F…….. number of degree of freedom
r……... the radius of the sphere
a…….. radius of the base of the cap is *h*, then the
A……. surface area
h…….. height of the cap
$\Delta q_{i\ app}$…….. apparent heat change
V_{cell}…….. calorimetric cell volume
ΔH_{app} …….. apparent molar enthalpy of association
$q_{i,dil}$…….. heat of ligand dilution
$\Delta[L_i]_{bound}$ ……. concentration of the bound ligand
Δq_i ……. effective heat change
N……. number of independent binding sites
X_i……. degree of saturation
D……. diffusion coefficient
R……. gas constant
T …… absolute temperature
N …… Avogadro's number
Z …… viscosity of the solution
r …… radius of the diffusing particle
υ …… velocity of the dispersed particle
E ……... applied electric field
μ_e ……... electrophoretic mobility
ε ……. dielectric constant
z …… zeta potential
η …… viscosity of solution
f(ka) ……. Henry function
ka …….. ratio of particle radius to the double layer thickness
ΔG …….. Gibbs free energy
ΔS …….. entropy change
ΔH …….. enthalpy change
Ld …….. liquid disordered phase
Lo …….. liquid ordered phase
So ……... solid ordered phase

List of figures

List of tables